Developments on Electrodynamic Levitation of Rotors

POLITECNICO DI TORINO

SCUOLA DI DOTTORATO

PhD in Mechatronics – XXIV cycle

PhD dissertation

Developments on Electrodynamic Levitation of Rotors

Joaquim Girardello Detoni

Supervisor
Nicola Amati

Doctoral Course Coordinator
Prof. Giancarlo Genta

29 February 2012

Acknowledgements

I am grateful to the whole staff of the Mechatronics Laboratory of Politecnico di Torino (LIM) for their support during the three years of graduate school. Their friendship and professional collaboration allowed for a great deal of personal and professional improvements.

I would like to express my most grateful acknowledgements to my supervisor Ing. Nicola Amati. His guidance during the research and his demonstrations of personal interest for the well being of the graduate students inspire admiration. His enormous help after my arrival in Italy at the beginning of the graduate school will never be forgotten. I am particularly grateful to Ing. Fabrizio Impinna, a great colleague in research on electrodynamic bearings and thoughtful friend. His untiring attitude towards our objectives in the research contributed a lot to this work, and will certainly contribute to the future developments on electrodynamic bearings. I gratefully acknowledge the director of LIM, Prof. Andrea Tonoli for his generous and creative comments and observations that broadened the limits of our knowledge.

Furthermore, I would like to thank Prof. Antero Arkkio for receiving me as visiting researcher at the electromechanics laboratory at the Aalto University in Finland. The months spent there helped me gaining a broader view on how high level research can be conducted. I am also thankful to Javier Martinez for his great help with the finite element simulations and the nice time spent together in the lonely lands of the Otaniemi campus.

Most of all, I would like to gratefully dedicate this work to my father, mother, and brothers who have always been my stronghold after I left my country to follow this journey in Italy.

Abstract

Magnetic bearings are systems capable of supporting rotors in absence of mechanical contact. Among many advantages with respect to ball and roller bearings are the possibilities of operating at extremely high rotational speeds and free of maintenance. Nevertheless, classical active magnetic bearings (AMB) are costly systems and may suffer from reliability problems. The most common types of passive magnetic bearings (PMB) based on the use of permanent magnet and reluctance forces are robust and relatively cheap but are affected by an intrinsic stability problem related to negative stiffness. The alternative of superconducting bearings has to deal with the difficulties for guaranteeing low temperatures for the superconducting materials to work; this represents a barrier for this technology.

In the last decades an alternative for obtaining stable passive magnetic levitation has been searched, leading to the development of electrodynamic bearings. These systems, capable of realizing electrodynamic suspension for rotors using regular materials at room temperature, may be an alternative for the suspension of high rotational speed machines in the near future. The technological solutions proposed are still unable of devising a system capable of demonstrating the feasibility of this concept.

Introduced in this context, this doctoral dissertation aims at developing models and design procedures to bring electrodynamic levitation of rotors closer to industrial applications. To this end, a large portion of the work is devoted to develop a unified model for representing the electromechanical interaction between rotor and stator generated by electrodynamic bearings of different types, namely homopolar and heteropolar configurations. The electromechanical model is developed taking advantage of the complex coordinate representation, typical in rotordynamics, in order to enable easy integration of the bearing's model with different rotordynamic models. An experimental validation of the model is carried out for homopolar configurations.

The study of the dynamics of rotors on electrodynamic bearings is probably one of the most important aspects that must be dealt with before the bearings can reach the technological development needed to become industrially available. Bearing this in mind, the dynamics of a Jeffcott rotor and that of a four degree of freedom rotor

are studied devoting special attention to the study of stability demonstrating the presence of unstable cylindrical and conical modes. The unbalance and frequency responses of the rotor on electrodynamic bearings are used to evidence the advantages and drawbacks between homopolar and heteropolar configurations. The studies are conduced using the state space formalism to obtain easy to manipulate system models.

The modelling of the suspension evidences the strong coupling between the subsystems, showing that the influence of each subsystem on the rotordynamic stability is not obvious, thus complicating the design of the whole suspension. Considering an iterative design approach, the design of a test rig is presented. It is designed to test the validity of the models and the feasibility of radial electrodynamic suspension. A the mechanical layout of the test rig is developed to deal with the stability aspects introduced by the use of electrodynamic bearings.

Contents

Chapter 1

Introduction

1.1 Motivation

Electrodynamic stabilised levitation of high-speed rotors is now reaching the borderline between academic interest and industrial application. Systems capable of realising this principle are commonly referred to as electrodynamic bearings (EDBs). The EDBs's unique characteristic of producing positive stiffness by passive means, without violating the Earnshaw stability criterion, has attracted the interest of many researchers during the last decades. Among EDBs's most interesting features is the possibility of obtaining stable levitation using standard conductive materials at room-temperature, and in absence of control systems, power electronics, and sensors. Because stable levitation can be achieved by passive means, electrodynamic bearings can be an advantageous alternative to active magnetic bearings.

The working principle of EDBs relies on exploiting repulsive forces generated by eddy currents to achieve levitation. The eddy currents can be of two different types: transformer eddy currents generated by time varying magnetic fields, or motional eddy currents generated by the interaction between a conductor and a constant magnetic field in presence of relative motion. Both types can be used to levitate a rotor; schematic representations of possible configurations of EDBs implementing these principles, and that have been studied and presented in literature, are shown in Fig. 2.1 and Fig. 2.2.

Using transformer type eddy currents to levitate a rotor has represented the beginning of the research on electrodynamic bearings. The concept is relatively simple to understand, but the large amount of energy dissipated to realize the suspension has limited the interest for this solution. On the other hand, the promising characteristics led to the development of EDBs that exploit motional eddy currents. In this case the relative motion between conductor and magnetic field induces eddy currents inside the conductor, thereby generating magnetic forces that can be used

to achieve levitation. Consider a disc conductor connected to a rotor with an axi-symmetric magnetic field fixed to the stator. The combination of rotor's spin and whirl may generate a non-symmetric electric field inside the conductor inducing currents, which in turn affects the forces on the rotor. The mechanical effect depends on the rotation speed. If the speed is low, the electromagnetic forces are tangential and aligned with the velocity. At high speeds, these forces become radial and proportional to the displacement of the rotor, thus stabilizing. It is worth emphasising that high and low speeds are related to the electric pole of the eddy currents arising in the conductor.

Although the working principle of EDBs may seem simple and straightforward, leading to very promising characteristics, the design of a rotor running exclusively on electrodynamic radial bearings is a challenging task. However eddy current forces are generally stabilizing, in the case of a rotating system this is not always true. The electromagnetic interaction between rotor and stator gives place to an intrinsically unstable whirling mode that must be dealt with. These rotordynamic instabilities have been presented and studied analytically by many researchers, however, very few of them have shown experimental evidence on this matter. An even smaller group has presented experimental proof os stable levitation of a rotor supported by EDBs, and, to the present day, no clear guideline on how to prevent the unstable behaviour of the suspension in practical terms is present in literature.

1.2 Aim of the work

The main purpose of this study is to design and develop a prototype for passive magnetic levitation of the radial degrees of freedom of a rotating shaft. The secondary goal is to develop and validate analytical models that can help the development of technology for the electrodynamic suspension of high speed rotating machinery.

1.3 Scientific contribution

The scientific contribution of this study is summarized below:

1. Development of a generalized modelling approach for electrodynamic bearings that allow appreciating differences and similarities between homopolar and heteropolar electrodynamic bearings.

2. Analysis of the behaviour of stiff rotors on electrodynamic bearings, shedding light onto certain aspects of these systems never examined before.

3. Numerical verification of the electromagnetic properties of improved performance electrodynamic bearings.

4. Experimental verification of the electromechanical properties of improved performance electrodynamic bearings.

This work was designed to be a step towards the final goal of developing a test rig to demonstrate the feasibility of EDBs, thus all these contributions were needed to achieve the final goal. In the following chapters these steps will be presented and explained in detail.

1.4 Dissertation outline

The present doctoral dissertation is divided in eight chapters.

Chapter 1 The first chapter gives the motivation based on a brief overview of the state of the art on electrodynamic bearings. Furthermore, the dissertation's objectives and structure are described.

Chapter 2 In the second chapter a review of the existing literature dealing with the electrodynamic levitation of rotors is presented. The main findings brought to light by other researchers are underlined.

Chapter 3 Chapter 3 presents the development of the unified model of the electromechanical interaction between a rotating conductor and a stationary magnetic field. The modelling in terms of complex coordinates is presented.

Chapter 4 The validation of the models developed in chapter 3 is presented. The quasi-stationary operating condition is described as a means for the validation of the analytical models and the expression obtained analytically is compared to experimental data for model validation. The test rig developed to perform the experimental study is described in detail.

Chapter 5 The models developed in chapter 3 are used to study the rotordynamics of a Jeffcott rotor supported by homopolar and heteropolar electrodynamic bearings. The difficulties in ensuring whirling stability of electrodynamic suspensions are evidenced. The differences between the dynamic behaviour of suspensions using homopolar or heteropolar EDBs are brought to light comparing the rotor's unbalance and frequency responses. In the last part of the chapter the EDB model is used to study the effects of anisotropy of the stator on the stability of the rotor.

Chapter 6 The models developed in chapter 3 are used to develop the model of a 4DOF rotor supported by EDBs. The models are used to study the role of gyroscopic effect on the stability of the rotor.

Chapter 7 The design of the prototype developed to achieve stable passive magnetic radial levitation is presented. The design of the main subsystems of the magnetic suspension is described in detail. At the end of the chapter the final layout of the test rig is described, and the mechanical parts shown.

Chapter 8 The main findings of the work are summarized and the conclusions presented. Possibilities for future research are discussed.

Chapter 2

Review of literature

The subject of magnetic suspension for high speed rotors has attracted the interest of researchers for many decades. In the last few years there has been a relatively strong interest on the research dedicated to electrodynamic bearings (this work is also part of this trend), but a survey on the literature dedicated exclusively to electrodynamic levitation of rotor's degrees of freedom has not yet been presented. Aiming at this fact, the present chapter is devoted to investigate the developments on electrodynamic levitation of rotors in the last three decades.

2.1 Radial electrodynamic bearings

The most interesting application of electrodynamic bearings is to produce passive radial suspension for high speed rotors. In most recent configurations, the passive and autonomous nature could largely increase the use of magnetic suspensions in commercial applications.

First interest on this type of passive suspension can be found in the work of Basore [1]. He presented a detailed study of passive suspensions for high speed flywheels; a large quantity of information about the design of flywheels is introduced, and a passive suspension scheme proposed. In the proposed suspension scheme the main levitation force is provided by reluctance bearings. The bearing's magnetic field is homopolar and generated by permanent magnets. This same magnetic field is used to devise the electrodynamic bearings. Different arrangements of homopolar electrodynamic bearings are also discussed; additionally, Basore proposes the use of a heteropolar magnetic field combined to null flux coils in radial bearings.

In Basore's study the EDB provides a stabilizing radial force when a displacement between rotor and stator is introduced, but the destabilizing tangential forces are neglected. The analysis of the bearing's forces is conducted considering constant displacement between rotor and stator, where the spin speed is also kept constant.

This condition is known as quasi stationary operating condition. Although it proves useful when predicting the bearing's performance, it is not suitable for dynamic conditions, where the rotor is animated by non-synchronous whirl or non-periodic motion about the stator's axis. Hence, the design approach described by Basore does not prove effective when addressing difficulties regarding dynamic stability of the suspension.

Unstable behaviour of a rotor on electrodynamic bearings is found in the work of Nikolajsen [2]. No theoretical developments are presented to describe the phenomenon, but a brief description of some experiments is given. The prototype used for the experiments is based on the electromagnetic river concept [3], and consists in wrapping around a linear induction motor to provide radial stiffness, axial stiffness, and drive torque to the rotor. As mentioned by Ting and Tichy [4], the behaviour described in the experiments of Nikolajsen is coherent with the dynamics of a rotor on EDBs, where electromagnets supplied with AC currents generate the main magnetic field. They proved that in this case the bearing's damping may become negative, thus destabilizing. In a later study Nikolajsen [5] analysed the feasibility of applying this concept in flywheels for spatial applications, but the large amount of energy dissipated as Joule heating in the rotating conductors proved to be a barrier to the development of this technology.

Connor and Tichy [6] presented theoretical developments using the journal bearing configuration shown in Fig. 2.1a; this configuration is similar to that proposed by Nikolajsen. They derived an analytical solution for the two dimensional electromagnetic fields in a heteropolar bearing to analyse the behaviour of its properties in terms of losses, force amplitude, and attitude angle. The attitude angle represents the phase angle between the direction of displacement of the rotor and that of the reaction force. Realizing the promising characteristics, but noting the relatively low stiffness and high losses, Tichy and Connor [7] studied the effects of geometry on the load capacity of the bearing. The exhausting mathematical treatment and somewhat confusing presentation renders the results difficult to be interpreted. Ting and Tichy [4] and Simone and Tichy [8] re-proposed the solution of the magnetic field to predict the mechanical properties of the bearing. Direct and cross-coupled stiffness and damping are evaluated evidencing the possible occurrence of negative damping, thus proving the destabilizing contribution of electrodynamic bearings to the rotordynamics.

Energy dissipation in the rotor has represented an obstacle for the application of AC heteropolar electrodynamic bearings in the suspension of regular size rotors. Siegwart *et al.* [9] propose to solve the problem of excess heating by using micro scale rotors. They discussed the use of eddy current bearings for the levitation of a small aluminium cylinder on full electrodynamic suspension (radial and axial), and the motoring magnetic field is supplied by the same electromagnets used for levitation. Relatively low rotor temperatures (60°C to 100°C) are reported in working

conditions, whereas rotordynamic stability is not discussed, but very low damping of the suspension is mentioned as a critical factor.

Given the difficulties in solving the Joule heating problems with AC bearings, the interest on this type of configuration has faded. Following the ideas of Basore [1], Post and his co-workers conducted a long lasting research on EDBs at the Lawrence Livermore National Laboratory (LLNL) studying a configuration that virtually eliminates thermal problems. Post and Ryutov [10] proposed the use of rotating permanent magnets in cylindrical Halbach arrays and stationary Litz wire conductors; the arrangement proposed is shown in Fig. 2.1b. Placing the conductors in the stator allows simpler fabrication, more robust layout, and easier cooling. The use of 'window frame' circuits with even-order Halbach arrays ensures flux cancellation at centred position [10, 11], thus eliminating unwanted energy losses and strongly reducing the excess heating problem.

Nevertheless, Post's heteropolar configuration has a drawback with respect to the AC configuration; it cannot give any supporting force at zero rotational speed[1]. Furthermore, the rotordynamic stability is a problem that must be dealt with similarly to the previous case. The concerns with stability of rotor's whirl modes has been present since the beginning of Post and Ryutov works [10]. The modelling of the suspension, coupling a simplified electromechanical model of the EDB with a Jeffcott rotor model is used to establish the conditions needed for stable levitation. The introduction of non-rotating electromagnetic damping associated to the relative speed of motion between rotor and stator is identified as a possible solution for stability. An innovative solution (in this context) for the stabilization, relying on the use of anisotropic electromechanical properties of the EDBs, is also proposed. The necessary conditions to obtain stable levitation using this technique are derived using a slightly modified suspension model. The stability bounds identified by Post *et al.* [10–12] seem to be incorrect due to an oversimplification of the electromechanical model. The proposed bearing model can be interpreted considering the analogy between electrical and mechanical systems, where Post *et al.*consider the interaction between a magnet and a conductor with relative motion as a parallel spring-damper system. This modelling is known to be incorrect in this context [13].

In a later work Post and Bender [14] presented an experimental study on a flywheel system supported by heteropolar electrodynamic bearings. A small collection of experimental results obtained under quasi stationary conditions is presented showing the behaviour of the bearing's transverse stiffness, axial stiffnesses, and the influence of the lateral displacement on the voltage induced inside the coils. Also

[1]This represents a drawback shared by all configurations that use the relative motion between permanent magnets and conductors instead of AC electromagnets to provide the levitation force.

the electromagnetic dampers used to introduce non-rotating damping between rotor and stator are tested, but generally, no relevant conclusion can be taken as the results obtained in quasi stationary conditions tend to dim the real difficulty to be encountered when working in dynamic conditions.

Like Post and Ryutov [11], Eichenberg *et al.* [15] modelled the bearing's electromechanical interaction starting from the analytical solution of the magnetic flux density generated by the Halbach array in a rotating reference frame. This solution is used to integrate the magnetic flux linkage in the stationary conductors taking into account of generic displacements between rotor and stator. The currents and forces are calculated in quasi stationary conditions, considering a fixed position of the rotor and neglecting its lateral speed. The expressions obtained for force and current are compared to experimental results for model validation. The test rig used to produce the experimental data resembles more an electromagnetic brake than a radial bearing because only one pole piece of the stator is built, and the null flux scheme cannot be implemented. The experimental results are nonetheless interesting, showing good agreement between model and experimental data for force and rotational loss measurements. Furthermore, the results prove clearly the severe limitation in the lift and drag forces caused by the introduction of external inductively loaded circuits in series with the stator coils.

Another possible configuration that allows eliminating unwanted eddy current losses and has been visited by many researchers is the homopolar electrodynamic bearing configuration. Two possible layouts are shown in Fig. 2.2. A fundamental difference between heteropolar and homopolar configurations is that while the heteropolar scheme allows placing the conductors on the stator, the homopolar scheme requires a rotating conductor. In the first case unwanted losses at centred position are avoided with the null flux scheme whereas in the latter they are avoided by the axisymmetry of the magnetic field.

First experiments on homopolar electrodynamic bearings where presented by Murakami and Satoh [16]. An axial flux configuration such as shown in Fig. 2.2a was studied, where the homopolar flux crosses the rotating conductor parallel to the axis of rotation. Discs with different diameters were tested and effect of displacement between rotating conductor and magnetic field was shown to be linear. The effect of rotating speed at constant displacement was also investigated for a relatively limited range of speed, thus limiting the conclusions that can be taken. On the same period Bermudez *et al.* [17] presented an analogous study on the characteristics of a radial flux homopolar bearing; the configuration used by Bermudez is similar to that of Fig. 2.2b.

Filatov and Maslen [18] proposed a homopolar electrodynamic bearing using conducting loops presenting a modelling approach and describing the realization of experiments where stable electrodynamic levitation is achieved. In a later work from Filatov [19] the configuration studied is called by the author as 'null-E' magnetic

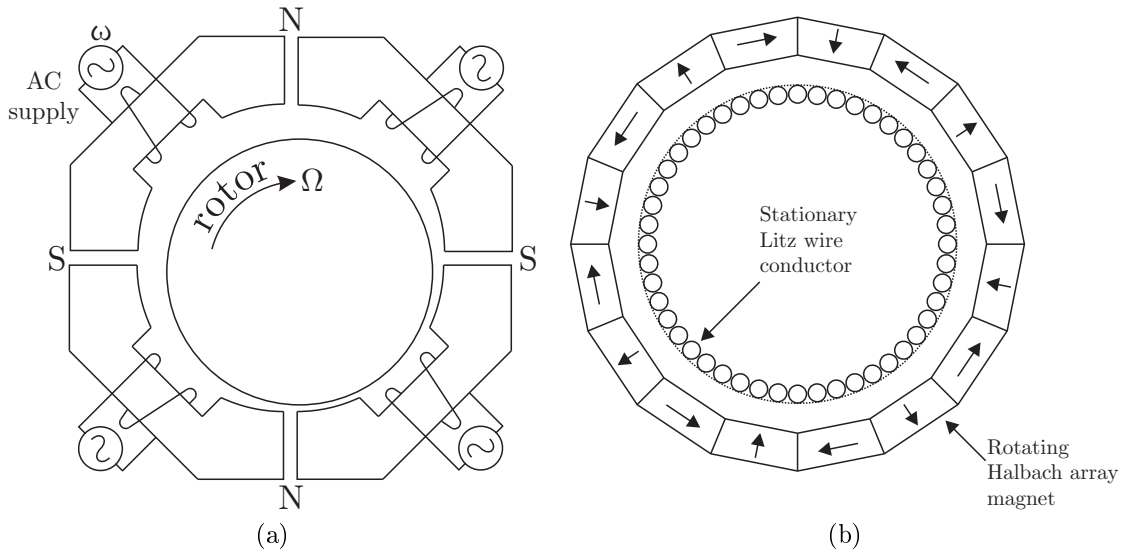

Figure 2.1. Different configurations of heteropolar electrodynamic bearings. (a) Scheme of a heteropolar AC electrodynamic bearing proposed by Nikolajsen and Tichy. (b) Post's heteropolar configuration.

bearing because the null flux condition is not satisfied in the homopolar case, but since the flux linkage is constant, the induced electric field E is null. To the author's knowledge, Filatov and Maslen were the only capable of achieving stable levitation using a suspension based on electrodynamic radial bearings. They described the tests performed stressing the fact that very low rotational loss is introduced by the EDB, but the results and data described are very difficult to recast in their own models. In succeeding works Filatov *et al.* [20–22] revisited the analyses, where they present an initial modelling of the electromechanical interaction between rotor and stator caused by the electrodynamic bearing. The authors introduce and develop the problem of unstable behaviour of the suspension when no external non rotating damping is introduced, but the conclusions are incorrect due to oversimplification. The models do not consider correctly the electrical dynamics of the currents inside the coils because they assume that the phase angle (attitude angle) between rotor displacement and bearing's force depend only on the ratio between rotational speed and electrical time constant. This is true exclusively when working at fixed displacement, and lateral speeds are null. The assumption of low lateral speeds is incorrect as the frequency of the lateral motion is likely to be of the same order of magnitude of the RL electric pole frequency (and possibly higher). Another aspect presented in the work is the use of inductive loaded electric circuits shunted with the coils to reduce the stabilization threshold speed. This is correct for what concerns the stability, but, as noted by Filatov an Maslen [18], the inductive loaded circuits also

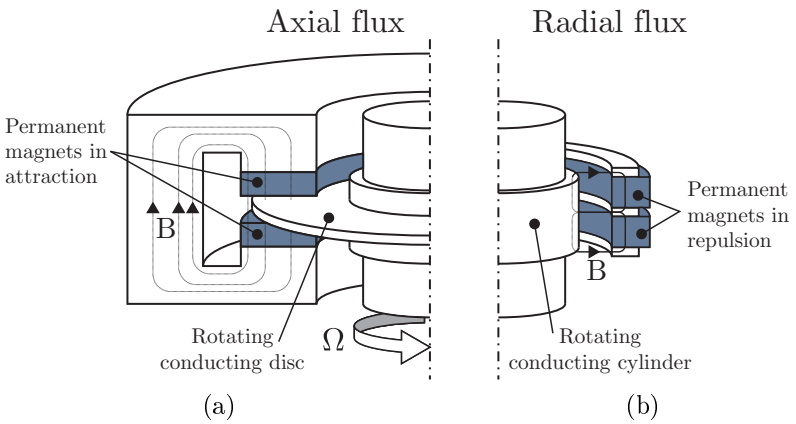

Figure 2.2. Possible configurations of homopolar electrodynamic bearings. (a) Axial flux configuration, (b) radial flux configuration

reduce the radial stiffness of the bearing.

A continuation of these works is presented by Davey *et al.* [23]. They presented the design of a flywheel using homopolar bearings, substituting the conducting loops with a solid conductor disc. The main aspect dealt with is the introduction of lateral non rotating damping needed to stabilize the whirl modes of the rotor; two different configurations of electromagnetic dampers are proposed to optimize the non-rotating damping. This work is continued by Filatov *et al.* [24], where the electromechanical properties of the electrodynamic bearing are estimated using finite element models. The same models of the suspension proposed in the previous works are used to establish stability bounds, thus leading to incorrect results.

On the modelling of the electromechanical interaction between rotor and stator on homopolar bearings, the work of Kluyskens *et al.* [25] presented clear considerations on the role of the rotating conductor on rotor's stability. The rotating damping is clearly identified as the cause of instability, and stability bounds for a Jeffcott rotor in presence of rotating damping and stiffness are defined. An electromechanical model devised to describe the dynamics of a rotor on eddy current bearings is presented. The analysis of the stability are developed using the Rout-Hurwitz criterion to establish stability conditions for the suspension similarly to what proposed by Filatov and Maslen [18]. Also in this case, the incomplete solution of the electrical dynamics of the eddy currents inside the conductors falses the results, leading to incorrect stability bounds. The proposed model is nevertheless valid under quasi stationary conditions at relatively low frequencies, and the results of finite element simulations are compared to analytical results evidencing this characteristic. The electromechanical models are refined [26] to consider the skin effect inside solid conductors using frequency variable impedance models presented later [27].

Noting a recurrent inaccuracy in the electromechanical models presented in the literature [1, 14, 15, 25], in the last few years Amati *et al.* [28] presented a new modelling approach to correctly account for the electromechanical interaction between rotating conductor and stationary magnetic field for homopolar electrodynamic bearings. The model is derived considering the equivalence between the state equations of a voice coil model and that of a spring-damper in series. The choice of referring to the mechanical analogue instead of the electrical system is adopted because the reference frames can be established in a more intuitive basis, which is a key point when dealing with rotating machines. This allows easily writing the system's equations in complex coordinates, rendering straightforward its use in connection with rotordynamic models. Furthermore, the stability of a Jeffcott rotor on homopolar electrodynamic bearings is studied. The validation of the proposed models is presented by Tonoli *et al.* [29]. In this latter work a large collection of experimental data is used to validate the models under both quasi stationary and dynamic conditions, showing very good agreement. Moreover, a new stabilization technique on the electrodynamic suspension context is presented. This technique proposes the introduction of stiffness and damping between the stator of the electrodynamic bearing and the case of the machine, allowing a simplification of rotor's layout compared to solutions proposed previously [12, 18] with a possible reduction of the stabilization speed threshold.

As the modelling techniques for motion induced eddy currents with finite elements improved in accuracy, allowing to consider different conductor shapes, also the design of electrodynamic bearings resorted to this instrument to improve the quality of the models. Currently the research on electrodynamic suspensions is often developed using analytical models to study the rotordynamics, while finite element simulations of the electromagnetic fields serve to evaluate the mechanical properties of the bearing itself. Especially when dealing with electrodynamic bearings using solid conductors in the rotor, the finite element simulations are essential since they represent the most reliable way to predict and optimize the bearing's performance prior to the realization of prototypes.

The first finite element analysis of an electrodynamic bearing is found in the work of Iskierka [32]. He presented a two dimensional time-harmonic solution of an aluminium tube rotating at constant eccentricity in an heteropolar magnetic field generated by electromagnets. The results in terms of lift and tangential forces for different excitation frequencies of the stator coils are shown making a comparison between symmetric and non-symmetric current density distributions on the stator. The analyses put in evidence the possible advantages of using a non-symmetrical current density distribution.

The most important reference in the finite element modelling of electrodynamic bearings is doubtless the work presented by Lembke [30,33]. A very complete survey on the modelling of homopolar radial electrodynamic bearings is presented shedding

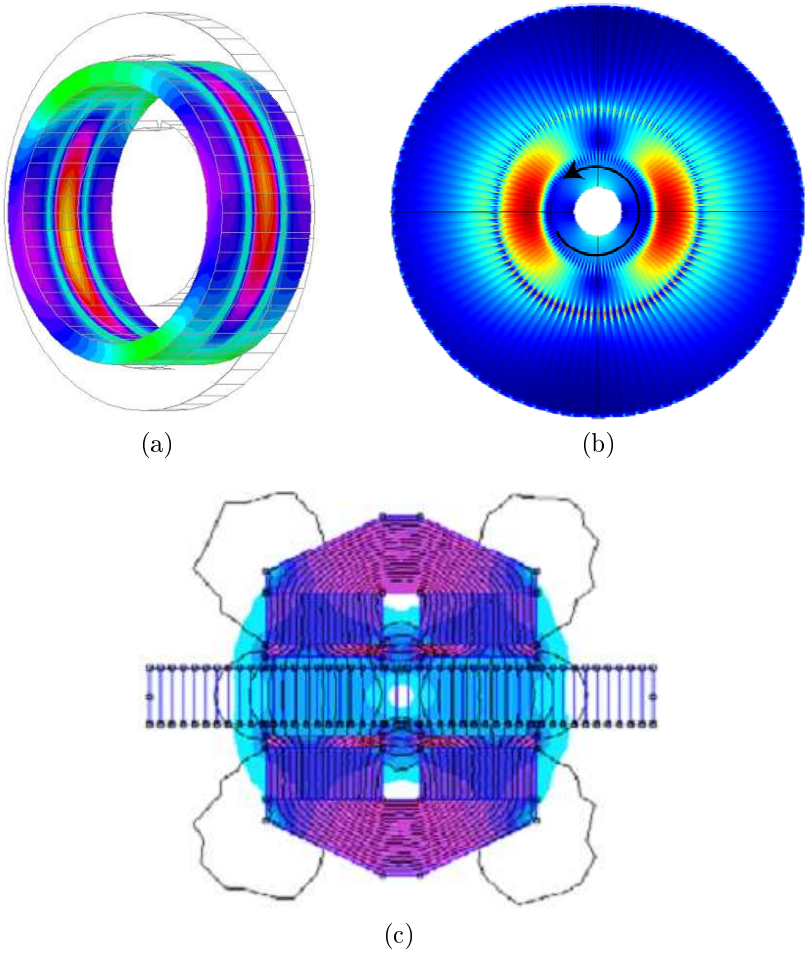

(a) (b)

(c)

Figure 2.3. Finite element results for homopolar EDBs presented in literature. (a) Lembke [30], (b) Kluskens *et al.* [31], (c) Filatov *et al.* [24]

light onto many aspects never discussed in previous works. Most of the analyses are developed under quasi stationary conditions and an optimization of the bearing's performance is conducted, but rotor's stability is not taken into account during the optimization, thus the feasibility of the proposed suspension is not demonstrated.

A different approach to the finite element modelling of homopolar bearings was proposed by Filatov *et al.* [24], where a simplified two dimensional time-harmonic model is used to estimate the stiffness and damping properties of the bearing. Because the flux distribution is three dimensional in the homopolar case, this approach leads to less accurate results, but nevertheless valid for fast feasibility analysis.

Following the indications given in the work of Lembke, Genta *et al.* [34] and

Amati *et al.* [35] developed sensitivity analyses of the bearing's properties to variations in the geometry using finite element computations. Kluyskens *et al.* [31] used finite element results to study the effects of eddy current forces in semi-passive bearings having a configuration similar to that of a homopolar electrodynamic bearing, presenting experimental measurements for model validation.

Usually, the finite element analyses of bearings based on eddy currents are performed under quasi stationary conditions. This means that the rotor's position is fixed with respect to the stator, and the forces generated between rotor and stator are calculated for different values of rotating speed. If the moving conductor has invariant cross section at right angles to the direction of motion the modelling is strongly simplified and the solution can be obtained in three dimensions with a fixed mesh, without resorting to time-stepping methods [36,37]. This condition is usually satisfied for homopolar configurations. An alternative to this method is to use two dimensional time-harmonic analysis, but less accurate results are obtained in this case. An illustration of the typical results obtained with two and three dimensional finite element simulations of homopolar electrodynamic bearings is shown in Fig. 2.3.

2.2 Axial electrodynamic bearings

The use of null flux coils for magnetic levitation minimizing drag forces was first devised to provide lift force for the levitation of high speed trains [38]. The same concept can be applied for the realization of axial bearings for high speed rotors using electrodynamic forces [39].

Besides the promising characteristics of this configuration, to the author's knowledge, there is very little literature in the subject. Post *et al.* [10] presented the configuration based on stationary conductors and rotating magnets using Halbach arrays and considering the same design equations proposed for radial bearings in that work. The research on the topic has evolved mainly relying on experimental analysis [40–42].

In the case of axial electrodynamic bearings, the use of finite element simulations to calculate the forces generated by the currents induced in the null flux coils is much more complex than in the radial bearings case. Due to the shape of the conductors the analysis require three dimensional time-stepping simulations. To the author's knowledge no results using this procedure were presented for axial EDBs. The results of finite element simulations of the stationary magnetic field generated by the permanent magnets, and coupled with analytical models to predict the bearing's performance, was presented by Thompson [43] and Storm [44].

The modelling of the axial dynamics of the rotor mass was presented by Tonoli *et al.* [45], and a test rig similar to that proposed by Sandtner and Bleuler [40] was

devised to produce experimental data used to validate the models under quasi stationary conditions. The models are used to study the axial stability. The proposed models were revised by Impinna *et al.* [46], and possible instability of the axial suspension is evidenced, but the conditions needed to stabilize this unstable mode are easily satisfied. Experimental results showing passive stable levitation are presented and discussed.

Part I

Modelling and experimental validation

Chapter 3

Electromechanical model

In the present chapter a model of electrodynamic bearing is presented. The objective is to develop a model that allows studying the rotordynamics of any kind of rotor supported by EDBs. To study the dynamics of a rotor supported by electrodynamic bearings we define the system under analysis. Figure 3.1 presents two types of electrodynamic bearings. Figure 3.1a shows a schematic representation of a heteropolar electrodynamic bearing such as that studied in [10,11] while Fig. 3.1b shows a scheme of a homopolar electrodynamic bearing. In the first case, the magnetic field lines close in the same plane of the main flux B_s while in the second the field closure happens outside the plane as shown in Fig. 3.1c. Two sets of short circuited coils (1,1' and 2,2') are installed on the rotor on orthogonal planes. This is the simplest configuration representative of the dynamic behaviour of the system as it allows taking into account the vector nature of the electrical quantities arising in the rotor.

The geometries considered and depicted in the figure were chosen to put in evidence the similarities between the two cases. All geometrical configurations of heteropolar EDBs based on the null-flux scheme and all homopolar configurations mentioned in the previous chapter are considered to be possible under the same modelling procedure.

The models are developed under the following assumptions:

- The electric parameters of the coils are the same, and they are both shorted. The case of a generic passive shunt can be dealt with by considering the appropriate value of the impedance in series with the winding.

- The magnetic circuit is isotropic and independent from the angular position of the rotor.

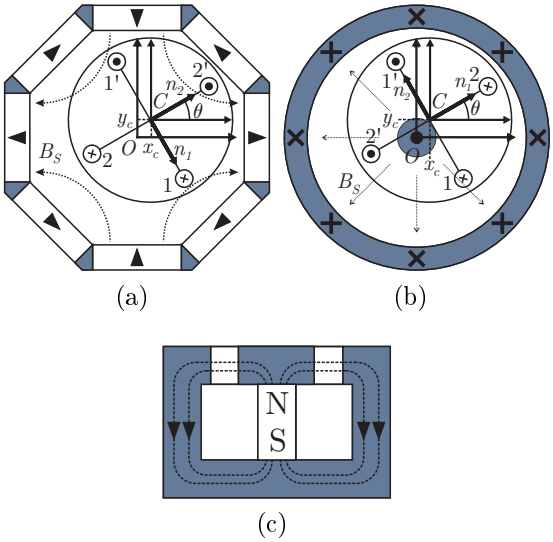

Figure 3.1. Schematic representation of a) heteropolar and b) homopolar electrodynamic bearing configurations. c) Closure of field lines outside the plane for the homopolar case.

- The flux density due to the stator is constant as if generated by permanent magnets. Additionally, the magnetic field of the stator is fixed in space[1].
- The cross section of each winding has a negligible area, hence all conductors are affected by the same magnetic field.
- Lateral displacements of the rotor are much smaller than the radius of the coils ($x_c, y_c \ll r_c$).
- The rotor angular speed Ω is an input to the system.
- The coordinates x_c and y_c are the Lagrangian coordinates giving the position of point C, i.e., the geometric centre of the rotor, with respect to point O, i.e., the centre of the magnetic field.

The arbitrary orientation of the currents shown in the figure does not affect the results. An appropriate choice, however, enables writing the system's equations in terms of complex coordinates, resulting in simpler and more compact equations [47,48]. The most appropriate choice ensures positive flux linkages for positive

[1]The expressions describing a system with rotating magnets are analogue, requiring a simple modification in the reference frames of the final equations.

displacements of point C in the xy plane. Furthermore, unit vectors $n_{1,2}$ perpendicular to the plane of windings 1 and 2 have their orientation obtained from the positive coil currents by the right-hand rule. Rotor angle θ is measured from the x axis in counter-clockwise direction.

3.1 Potentials and Fluxes

The rotor is allowed to move in the xy plane and the magnetic flux linked by the rotor's coils is affected by this motion. Expressions for the flux linkages as a function of the rotor's position and angle can be derived from the analysis of the analytical solution of the magnetic vector potential and flux density in the air surrounding the coils. The different shape of the magnetic field in the air for the homopolar and heteropolar cases requires the use of different solution strategies for each case.

3.1.1 Heteropolar configuration

The heteropolar magnetic field is generated by Halbach arrays of permanent magnets; it is assumed to be sinusoidal just outside the border of the permanent magnets. The two dimensional field distribution allows to formulate the partial differential equation giving the flux distribution in terms of the component of the magnetic vector potential $\mathbf{A}_z$ perpendicular to the plane of the flux distribution. The magnetic flux density $\mathbf{B}$ in the plane can be derived from the solution for the vector potential. Furthermore, according to the assumption that the Halbach arrays generate a sinusoidal field, using the properties of the vector potential formulation, it is possible to formulate a boundary value problem for a generic number of magnetic pole pairs p. The problem is then defined as:

$$\begin{aligned} \nabla^2 \mathbf{A}_z &= 0 \\ \mathbf{A}_z(r_0) &= A_0 \sin p\theta. \end{aligned} \tag{3.1}$$

The second line gives the value of the magnetic vector potential at the boundary. The magnetic flux density can then be obtained as:

$$\mathbf{B} = \nabla \times \mathbf{A}_z. \tag{3.2}$$

Due to the circular geometry, this problem is more conveniently formulated in polar coordinates. Equation (3.1) can be solved using the variable separation method and the flux densities in polar coordinates are obtained from Eq. (3.2) as

$$\begin{aligned} \mathbf{A}_z(r,\theta) &= A_0 \left(\frac{r}{r_0}\right)^p \sin(p\theta) \\ \mathbf{B}(r,\theta) &= A_0 \frac{r^{p-1}}{r_0^p} p \begin{Bmatrix} \cos p\theta \\ -\sin p\theta \end{Bmatrix}. \end{aligned} \tag{3.3}$$

For the study it is useful to define the components of $\mathbf{B}$ in Cartesian coordinates. It is simple to define a transformation matrix between polar and Cartesian coordinates as:

$$\mathbf{B}_{x,y}(r,\theta) = \begin{bmatrix} \cos\theta & -\sin\theta \\ \sin\theta & \cos\theta \end{bmatrix} \mathbf{B}_{r,\theta}(r,\theta). \tag{3.4}$$

Note that only the components of the solution are mapped from polar to Cartesian coordinates. The variables of the equation remain the in the polar frame. Using Eq. (3.4) it is possible to represent the flux density in the air region surrounding the rotor as:

$$\mathbf{B}_{x,y}(r,\theta) = A_0 \frac{r^{p-1}}{r_0^p} p \begin{Bmatrix} \cos((p-1)\theta) \\ -\sin((p-1)\theta) \end{Bmatrix}. \tag{3.5}$$

Figure 3.2a shows the graphical representation of Eq. (3.5) for $p = 2$. In the figure the cones give the flux direction and the lines represent the contour of the flux density.

3.1.2 Homopolar configuration

The homopolar flux can be generated, for example, as shown in Fig. 3.1c. The lateral movement of the rotor breaks the axial symmetry of the problem and it becomes three-dimensional. This does not allow using the vector potential formulation in a similar way as for the heteropolar case presented in Eq. (3.1). Fortunately, the flux distribution in the region of interest is of great simplicity and the expression can be derived with the help of some simple physical considerations.

The main consideration is that the flux in the region of interest is radial. The flux must respect the Gauss's law for magnetic fields and consequently the problem is formulated as follows:

$$\begin{aligned} \nabla \cdot \mathbf{B} &= 0 \\ \mathbf{B}_r(r_0) &= B_0. \end{aligned} \tag{3.6}$$

The x and y components of the flux density can be expressed as:

$$\mathbf{B}_{x,y}(r,\theta) = B_0 \frac{r_0}{r} \tag{3.7}$$

As in the previous case it is convenient to have the flux expressed in Cartesian coordinates. Using Eq. (3.4), the flux density surrounding the rotor is:

$$\mathbf{B}_{x,y}(r,\theta) = B_0 \frac{r_0}{r} \begin{Bmatrix} \cos\theta \\ \sin\theta \end{Bmatrix} \tag{3.8}$$

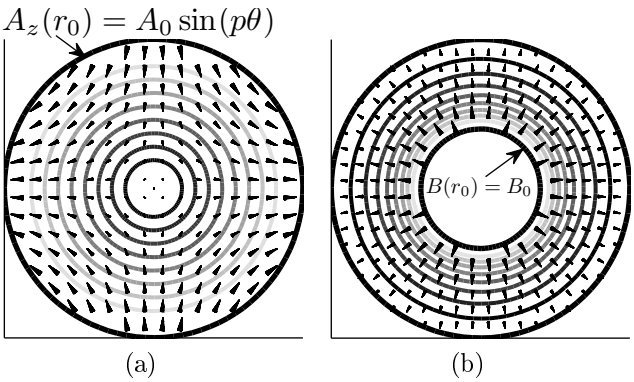

Figure 3.2. Graphical representation of the magnetic flux density in the air surrounding the rotor. a) Heteropolar b) Homopolar.

A graphical representation of the solution to the differential equation given by Eq. (3.8) is shown in Fig. 3.2b.

3.2 Flux linkages

The first step of the proposed modelling is to evaluate the magnetic flux linked by the rotor's coils as a function of the rotor's angular position and lateral displacement in the Cartesian frame of reference. The system under analysis and the geometrical quantities used in this operation are defined in Fig. 3.3 .

The magnetic flux λ generated by the stator and linked by the rotor can be obtained from the magnetic flux density as:

$$\lambda_i = \int \mathbf{B} \cdot \mathbf{n}_i d\Omega, \tag{3.9}$$

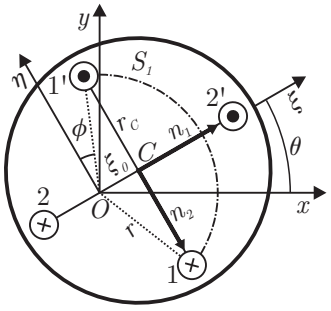

Figure 3.3. Sketch of the rotor with the variables for the flux calculation.

where $\mathbf{n}_i$ represents the unit vector normal to the generic surface Ω. If for simplicity we consider the field to be constant along the z axis perpendicular to the plane of the figure for the entire length h of the rotor, the surface integration simplifies into a line integration along the line S.

$$\lambda_i = h \int \mathbf{B} \cdot \mathbf{n}_i dS_i. \tag{3.10}$$

If the magnetic flux $\mathbf{B}$ in the plane can be represented in terms of the vector potential $\mathbf{A}_z$ following Eq. 3.2, then according to the Stoke's theorem [49], it is possible to demonstrate that the flux across this surface can be calculated as:

$$\lambda_i = h(\mathbf{A}_{z_{i'}} - \mathbf{A}_{z_i}). \tag{3.11}$$

To define an expression for the total magnetic flux λ_1 and λ_2 linked by the rotor's windings due to the magnetic field of the stator one can define a reference frame (O,ξ,η) that rotates together with the rotor with angle θ. First a virtual displacement between the points O and C in ξ direction is applied, and Eq. (3.10) is computed for generic values of the rotor angle θ. The same operation is repeated for a virtual displacement of the rotor in η direction. The integrals are computed in arbitrary surfaces S_1 and S_2 that are chosen to be sectors of cylinders for convenience. The procedure is developed for both heteropolar and homopolar configurations. Due to the different mathematical representation chosen for the homopolar and heteropolar configurations of EDBs, the integration of the flux linkage has to be performed separately for each case.

To perform this operation we recall one of the assumptions made in chapter 3. It is assumed that the lateral displacements of the rotor are much smaller than the radius of the coil's. Making reference to Fig. 3.3 this represents that:

$$\begin{aligned} r &\approx r_c \\ \cos\phi &\approx 1 \\ \sin\phi &\approx \phi \\ \phi &\approx \frac{\xi_0}{r}. \end{aligned} \tag{3.12}$$

3.2.1 Heteropolar

The heteropolar model is derived considering an even number of pole pairs p. This consideration doesn't reduce the validity of the model.

Virtual displacement ξ_0

Coil 1 The magnetic flux linked by each coil is obtained by operating the procedure described using Eq. (3.11) instead of Eq. (3.10). Imposing a fixed position ξ_0 in the rotating frame and evaluating the flux linked by coil 1 we obtain:

$$\begin{aligned}\mathbf{A}_{z_{1'}} &= A_0 \left(\frac{r}{r_0}\right)^p \sin(p(\theta + (\frac{\pi}{2} - \phi))) \\ \mathbf{A}_{z_1} &= A_0 \left(\frac{r}{r_0}\right)^p \sin(p(\theta - (\frac{\pi}{2} - \phi))).\end{aligned} \tag{3.13}$$

Knowing that p is an even number the expression of the flux linkage is:

$$\lambda_{1_\xi} = h(\mathbf{A}_{z_{1'}} - \mathbf{A}_{z_1}) = -(-1)^{\frac{p}{2}} 2hA_0 \left(\frac{r}{r_0}\right)^p \cos p\theta \, \sin p\phi. \tag{3.14}$$

According to the linearization hypothesis this expression can be written as:

$$\lambda_{1_\xi} = -(-1)^{\frac{p}{2}} \xi_0 2\, p\, h\, A_0 \frac{r^{p-1}}{r_0^p} \cos p\theta. \tag{3.15}$$

Considering the coefficient:

$$\Lambda_0 = 2\, p\, h\, A_0 \frac{r^{p-1}}{r_0^p}, \tag{3.16}$$

the expression for the flux linked by coil 1 due to a displacement of the rotor in ξ direction is

$$\lambda_{1_\xi} = -(-1)^{\frac{p}{2}} \Lambda_0 \xi_0 \cos p\theta. \tag{3.17}$$

Coil 2 The vector potential at the terminals of coil 2'2 due to a displacement ξ_0 are:

$$\begin{aligned}\mathbf{A}_{z_{2'}} &= A_0 \left(\frac{r + \xi_0}{r_0}\right)^p \sin p\theta \\ \mathbf{A}_{z_2} &= A_0 \left(\frac{r - \xi_0}{r_0}\right)^p \sin p\theta.\end{aligned} \tag{3.18}$$

According to Eq. (3.11) the flux linkage is:

$$\lambda_{2_\xi} = \frac{A_0}{r_0^p} \sin p\theta \, ((r + \xi_0)^p - (r - \xi_0)^p) \tag{3.19}$$

We notice the presence of the binomials of power p. These can be expanded unsing the binomial theorem in the form:

$$(x+y)^n = \sum_{k=0}^{n} \binom{n}{k} x^{n-k} y^k. \tag{3.20}$$

Combining the two binomials the existence of cases for different values of pole pairs p can be obtained. The cases are:

$$(r+\xi_0)^p - (r-\xi_0)^p = \begin{cases} 0 & \text{for } k = \text{even} \\ 2r^{p-k}\xi_0^p \binom{p}{k} & \text{for } k = \text{odd} \end{cases} \tag{3.21}$$

In agreement with the linearization hypothesis assumed previously, we are interested only in the terms with ξ_o^k for $k = 0, \quad 1$. The resulting expression for the flux linkage of coil 2 is:

$$\lambda_{2_\xi} = \xi_0 \, 2 \, p \, h \, A_0 \frac{r^{p-1}}{r_0^p} \sin p\theta. \tag{3.22}$$

Considering the definition of Eq. (3.16), the final expression is:

$$\lambda_{2_\xi} = \Lambda_0 \xi_0 \sin p\theta. \tag{3.23}$$

Virtual displacement η_0

The procedure to obtain an expression for the flux linkages due to a virtual displacement η_0 along the η direction of the rotating reference frame is the same as described previously for ξ direction. In this case only the final expressions will be presented for each coil. They are:

$$\lambda_{1_\eta} = (-1)^{\frac{p}{2}} \Lambda_0 \eta_0 \sin p\theta \tag{3.24}$$

$$\lambda_{2_\eta} = \Lambda_0 \eta_0 \cos p\theta. \tag{3.25}$$

The complete expression for the flux linkage can be written in matrix form as:

$$\begin{Bmatrix} \lambda_1 \\ \lambda_2 \end{Bmatrix}_{\text{HE}} = \Lambda_0 \begin{bmatrix} -(-1)^{\frac{p}{2}} \cos p\theta & (-1)^{\frac{p}{2}} \sin p\theta \\ \sin p\theta & \cos p\theta \end{bmatrix} \begin{Bmatrix} \xi_c \\ \eta_c \end{Bmatrix}. \tag{3.26}$$

It's possible to note how the sign of the elements of the first row of the matrix has to be defined as consequence of the number of pole pairs. This shows how an appropriate choice of current orientation inside the coil allows to have the flux in terms of a rotation matrix. Later in the chapter we will see how this choice will enable the representation in terms of complex coordinates, simplifying the notation.

At this point it is important to recall that the expression for the heteropolar flux given by Eq. (3.26) is derived for an even number of pole pairs ($p = 2, \quad 4, ...$). In this case there is flux cancelation when the rotor is at centred position minimizing the losses [11]. An odd number of pole pairs ($p = 1, \quad 3, ...$) breaks the symmetry eliminating the flux cancelation characteristic for the rotor's coils at centred position. This causes the system to behave as an electromagnetic brake/damper, mainly dissipating the energy associated to the rotation, thus there is no reason for applying it in the electrodynamic bearing context. For this reason this type of system is not dealt with in this dissertation; readers may refer to [48, 50, 51] for an extensive discussion on the topic.

3.2.2 Homopolar

In the homopolar configuration, the flux is obtained directly through the integration of Eq. (3.10) considering the flux distribution given by Eq. (3.7). As stated previously, the arbitrary surfaces of integration are chosen to be sectors of cylinder for convenience. The surfaces are evidenced in Fig. 3.3.

Virtual displacement ξ_0

Coil 1 The integration of Eq. (3.10) for a virtual displacement of the rotor in ξ direction is equal to:

$$\lambda_{1_\xi} = hr_0 \int_{-\frac{\xi_0}{r_c}}^{\frac{\xi_0}{r_c}} \frac{B_0}{r_c} r \mathrm{d}\theta = 2B_0 h \xi_0 \frac{r_0}{r_c}. \tag{3.27}$$

In this case it can be defined:

$$\Lambda_0 = 2B_0 h \frac{r_0}{r_c} \tag{3.28}$$

and the resulting expression for the flux is:

$$\lambda_{1_\xi} = \Lambda_0 \xi_0. \tag{3.29}$$

In Eq. (3.27) the surface normal is a unit vector pointing radially.

Coil 2 When coil 2 is subject to a displacement in the ξ direction it doesn't perceive any flux because the homopolar flux has zero tangential component. This means that:

$$\lambda_{2_\xi} = 0 \tag{3.30}$$

Virtual displacement η_0

Also in the homopolar configuration the procedure is repeated for a displacement of the rotor centre in η direction. The expressions for the fluxes in this case are:

$$\lambda_{1_\eta} = 0 \tag{3.31}$$

$$\lambda_{2_\eta} = \Lambda_0 \eta_0. \tag{3.32}$$

The final expression for the flux linkage by the two coils due to rotor motion in the homopolar configuration is:

$$\begin{Bmatrix} \lambda_1 \\ \lambda_2 \end{Bmatrix}_{\text{HO}} = \Lambda_0 \begin{Bmatrix} \xi_c \\ \eta_c \end{Bmatrix}. \tag{3.33}$$

This expression is written in a reference frame $\xi\eta$ that rotates synchronous with the rotor.

3.2.3 Flux in non-rotating Cartesian coordinates

In the previous paragraphs the expressions were obtained in terms of rotating coordinates. For the derivation of the rotor's equations of motion it is more convenient to have the expressions in terms of a non-rotating Cartesian reference frame positioned in the centre of the magnetic field. This reference frame does not have to be inertial as will be seen in the next chapter.

The transformation between rotating and non-rotating reference frames is given by:

$$\begin{Bmatrix} \xi_c \\ \eta_c \end{Bmatrix} = \begin{bmatrix} \cos\theta & \sin\theta \\ -\sin\theta & \cos\theta \end{bmatrix} \begin{Bmatrix} x_c \\ y_c \end{Bmatrix}. \tag{3.34}$$

The resulting expressions for the flux linkages as a function of the displacement of the rotor in non-rotating coordinates are:

$$\begin{Bmatrix} \lambda_1 \\ \lambda_2 \end{Bmatrix}_{\text{HE}} = \Lambda_0 \begin{bmatrix} \cos(p-1)\theta & -\sin(p-1)\theta \\ \sin(p-1)\theta & \cos(p-1)\theta \end{bmatrix} \begin{Bmatrix} x_c \\ y_c \end{Bmatrix} \tag{3.35}$$

$$\begin{Bmatrix} \lambda_1 \\ \lambda_2 \end{Bmatrix}_{\text{HO}} = \Lambda_0 \begin{bmatrix} \cos\theta & \sin\theta \\ -\sin\theta & \cos\theta \end{bmatrix} \begin{Bmatrix} x_c \\ y_c \end{Bmatrix}. \tag{3.36}$$

The coefficient Λ_0 is present in both equations, but in the mathematical developments presented previously it does not result to be identical (see Eq. (3.16) and Eq. (3.28)). As stated previously, this is a consequence of the different formulation needed to solve the magnetic field in the air for the two configurations. It is, nevertheless, a coefficient that groups together the magnetic and geometrical parameters defining the flux linkage dependence on lateral displacements and in both cases has units Wb m^{-1}. In practice this coefficient has to be identified either by means of finite element simulations or experimentally.

3.3 Forces

The forces acting on the rotor are a consequence of the interaction between the stator magnetic field and the rotor's currents in absence of ferromagnetic materials. For this reason they are of Lorentz nature and can be calculated as:

$$F = NL\mathbf{i} \times \mathbf{B}. \tag{3.37}$$

To obtain the expression for the total force acting on the rotor for any value of current and position of the rotor, a procedure similar to what described previously for the fluxes can be applied. The only difference is that in this case Eq. (3.37) must be calculated. Under the assumptions listed in the introduction of chapter 3, the expressions for the force for the heteropolar and homopolar bearings are:

$$\begin{Bmatrix} F_x \\ F_y \end{Bmatrix}_{\mathrm{HE}} = \Lambda_0 \begin{bmatrix} \cos(p-1)\theta & \sin(p-1)\theta \\ -\sin(p-1)\theta & \cos(p-1)\theta \end{bmatrix} \begin{Bmatrix} i_1 \\ i_2 \end{Bmatrix} \tag{3.38}$$

$$\begin{Bmatrix} F_x \\ F_y \end{Bmatrix}_{\mathrm{HO}} = \Lambda_0 \begin{bmatrix} \cos\theta & -\sin\theta \\ \sin\theta & \cos\theta \end{bmatrix} \begin{Bmatrix} i_1 \\ i_2 \end{Bmatrix}. \tag{3.39}$$

It is important to notice how the force, differently from the flux, is independent from the lateral position of the rotor, being a function of the rotor angle and coil's currents only. The coefficient Λ_0 is identical to that obtained for the fluxes in Eqs. (3.35) and (3.36).

3.4 Equations in complex notation

Equations (3.35) and (3.36) describe the magnetic flux linkage perceived by the rotor, and Eqs. (3.38) and (3.39) give the force acting on the rotor.

The equations show that the magnetic flux linked by the rotor's windings can be represented by a rotating vector. Similarly, the displacement of point C, the current in the coils and the force can be represented as vectors. These vectors can be written as complex numbers. The advantage is a more compact notation to represent the system's equations.

The vector quantities written as complex numbers can be interpreted as:

$$\begin{aligned} q_c &= x_c + \mathrm{j}y_c \\ \lambda &= \lambda_1 + \mathrm{j}\lambda_2 \\ i &= i_1 + \mathrm{j}i_2 \\ F_q &= F_x + \mathrm{j}F_y \end{aligned} \tag{3.40}$$

where $\mathrm{j} = \sqrt{-1}$. Written as functions of the complex variables, Eqs. (3.35), (3.36), (3.38) and (3.39) are:

$$\lambda_{\mathrm{HE}} = q_c \Lambda_0 \mathrm{e}^{\mathrm{j}(p-1)\theta} \tag{3.41}$$

$$\lambda_{\mathrm{HO}} = q_c \Lambda_0 \mathrm{e}^{-\mathrm{j}\theta} \tag{3.42}$$

$$F_{\mathrm{HE}} = i\Lambda_0 \mathrm{e}^{-\mathrm{j}(p-1)\theta} \tag{3.43}$$

$$F_{\mathrm{HO}} = i\Lambda_0 \mathrm{e}^{\mathrm{j}\theta}. \tag{3.44}$$

Equations (3.41) and (3.42) may be seen as two cases of bearings characterized by different number of pole pairs in circumferential direction. The heteropolar has p pole pairs (p inversions of the magnetic field in the air gap) while the homopolar has none (no inversions of the field in the air gap, i.e., $p = 0$). In both cases there is flux cancellation when the rotor is centred. It is possible to see that even if the heteropolar and homopolar solutions do not come from the same mathematical treatment, they can be unified. The expressions can be merged into a set of equations representing both cases as:

$$\begin{aligned} \lambda &= q_c \Lambda_0 \mathrm{e}^{\mathrm{j}(p-1)\theta} \\ F_q &= i\Lambda_0 \mathrm{e}^{-\mathrm{j}(p-1)\theta}. \end{aligned} \tag{3.45}$$

Considering this equation, it is possible to proceed the analytic treatment of electrodynamic bearings in an unified way for both homopolar and heteropolar configurations. Analysing one case or the other becomes a simple parametric problem.

3.5 Dynamic behaviour

To describe the dynamics of the eddy currents inside the coils and also the dynamic effects of electrodynamic bearings on rotors supported by them, we make the assumption that the rotor rotates at constant angular speed Ω ($\theta = \Omega t$). Assuming constant, or slowly varying, rotating speed is commonly done in rotordynamics [47] and does not reduce the validity of the model.

At this point it is possible to write an equation that describes the behaviour of the current in the electric circuit of the coils. Figure 3.4 presents the electric circuit where the terms R_c and L_c are the resistance and inductance of the coil. For some applications it may be interesting to connect inductive loaded circuits in series with the coil [10, 11, 18, 19, 21]. For this reason the terms of a generic passive shunt R_{add} and L_{add} are introduced in the model. The mutual inductance between the coils has been neglected. The orthogonality between the two coils justifies this assumption.

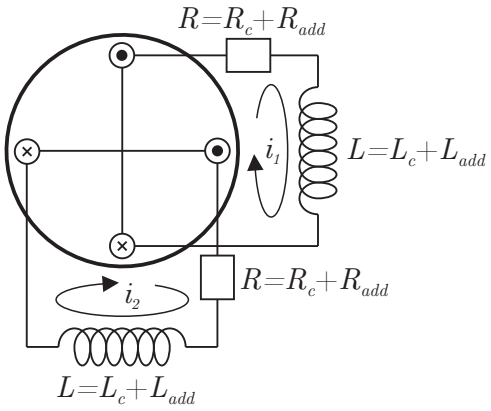

Figure 3.4. Electric circuit of the rotor's short circuited coils.

3.5.1 Eddy currents and bearing's forces

Taking the definition of the complex variables in Eq. (3.40) into account, the state equation describing the dynamics of the eddy currents inside the coils can be written as:

$$\frac{\mathrm{d}i}{\mathrm{d}t} = \frac{\dot{\lambda}}{L} - \frac{R}{L}i. \tag{3.46}$$

The equation describing the dynamics of the current inside the coils is obtained applying the Kirchoff's voltage law.

Combining Eq. (3.45) and (3.46) it is possible to obtain the final state equation describing the electromechanical interaction created by the electrodynamic bearing. Putting in evidence the mechanical inputs (q_c, Ω) and outputs (F_q), the state and output equations become:

$$\begin{aligned} \frac{\mathrm{d}i}{\mathrm{d}t} &= \frac{\Lambda_0}{L}(\dot{q}_c + \mathrm{j}(p-1)q_c\Omega)\mathrm{e}^{\mathrm{j}(p-1)\Omega t} - \frac{R}{L}i \\ F_q &= i\Lambda_0\mathrm{e}^{-\mathrm{j}(p-1)\Omega t}. \end{aligned} \tag{3.47}$$

Although linear, this equation has time varying coefficients. To study the dynamics using typical LTI (Linear Time-Invariant) analysis tools it is necessary to obtain an equation with time invariant coefficients. The information of interest from Eq. (3.47) are the bearing's forces. Bearing this in mind, it is possible to exchange the state and the output variables. Force F_q becomes then the state and current i the output. The second equation of Eq. (3.47) is used as a coordinate transformation to obtain the following constant coefficient equation:

$$\begin{aligned} \dot{F}_q &= \frac{\Lambda_0^2}{L}\left(\dot{q}_c + \mathrm{j}(p-1)q_c\Omega\right) - F_q\left(\frac{R}{L} + \mathrm{j}(p-1)\Omega\right) \\ i &= \frac{F_q}{\Lambda_0}\mathrm{e}^{\mathrm{j}(p-1)\Omega t}. \end{aligned} \tag{3.48}$$

This set of equations will be used for modelling the electrodynamic bearing in all the following analyses.

Chapter 4

Experimental validation through quasi-stationary tests

This chapter describes the experimental work carried out to validate the electrodynamic bearing models presented in the previous chapter. The validation is performed by comparing the model's results with experimental data obtained under a controlled operating condition. An axial flux homopolar electrodynamic bearing is used to perform the validation.

4.1 Modelling of the experiment

When dealing with homopolar electrodynamic bearings usually it is necessary to use solid conductors and the concepts of resistance and inductance are difficult to apply directly. Hence, the model's coefficients are more easily interpreted and dealt with referring to their mechanical equivalents [28] as:

$$\begin{aligned} k &= \frac{\Lambda_0^2}{L} \\ c &= \frac{\Lambda_0^2}{R} \\ \omega_{RL} &= \frac{R}{L} = \frac{k}{c}. \end{aligned} \tag{4.1}$$

In the mechanical equivalent representation the parameters are interpreted as:

- k represents the bearing's mechanical stiffness at infinite rotational speed.
- c represents the bearing's equivalent viscous damping at zero rotational speed.

- ω_{RL} is the electric pole frequency.

It is obvious that the mechanical coefficients given by Eq. (4.1) can be substituted directly in the EDB's dynamic model given by Eq. (3.48) without any loss of validity, and the studies presented previously remain valid.

To perform the experiments that serve to validate the models described previously it is necessary to identify a working condition that can be reproduced experimentally and does not require neglecting any parameter. One possible condition is the quasi stationary (or quasi static) condition. With reference to Fig. 3.1b, the test in quasi stationary conditions requires the introduction of a fixed, known value of eccentricity between points O and C. The rotor must be put into rotation at different values of spin speed that remains constant during each measurement. From the modelling point of view this imposes the following constraints to the solution:

$$\begin{aligned} q_c &= q_0 \\ \dot{q}_c &= 0. \end{aligned} \tag{4.2}$$

Applying these constraints to Eq. (3.48), the force produced by the electrodynamic homopolar electrodynamic bearing in quasi stationary conditions is equal to:

$$F_q = \frac{\Lambda_0^2}{L}\left(\frac{1}{1+\left(\frac{R/L}{\Omega}\right)^2} - \mathrm{j}\frac{\Omega}{\frac{R}{L}\left(1+\left(\frac{\Omega}{R/L}\right)^2\right)}\right). \tag{4.3}$$

The solution is in accordance with the notation used during the derivation of the model, hence, the real and imaginary parts of the solution represent the components of the force in x and y directions, respectively.

A non-linear curve fitting tool can be used to fit Eq. (4.3) to values of force measured experimentally, serving both as a model validation tool and as a tool for identification of parameters.

4.2 Test rig for quasi stationary characterization

The tests are addressed to produce experimental evidence of the correctness of the assumptions used to develop the models. A second objective is to verify the procedure for the identification of the model's coefficients by means of curve fitting.

The requirements for the realization of the experimental tests are:

- Measure the radial forces developed by the electrodynamic bearing at fixed, known eccentricity.

- Measure the spin speed of the rotor.

To this end the test rig shown in Fig. 4.2 was designed. The test rig is composed of three main parts: (a) the mechanical structure, (b) the magnetic circuit, forming the stator of the electrodynamic bearing, and (c) the rotating parts. The parts of the test rig are numbered in the balloons in Figs. 4.2a and 4.2b.

The structural part is composed by two aluminium plates (5) rigidly connected between each other with 4 vertical beams (15). A micrometric positioning stage (11) is fixed to the upper aluminium plate. A DC electric motor is fixed to the positioning stage using a two piece structure similar to a bell housing (4). The maximum rotation speed of the electric motor is 10000 rpm.

The rotating parts are supported by two ball bearings. The shaft (2) that drives the rotating conductor of the electrodynamic bearing (9) is connected to the electric motor by means of a flexible coupling (3). The magnetic circuit of the electrodynamic bearing is composed of three iron parts (8) forming the back iron and two permanent magnets (7). It is connected to the test rig structure by means of four flexible steel beams (6). Two load cells (10) positioned orthogonal to each other are used to constrain the position of the EDB's stator and to measure real and imaginary components of the force produced by the EDB. An optical encoder (12) is attached to the upper end of the shaft providing the spin speed signal.

The main geometrical parameters characterizing the electrodynamic bearing used for the tests are illustrated in Fig. 4.1. With respect to this figure, the values of the dimensions and physical quantities characterizing the whole system are grouped in Tab. 4.1.

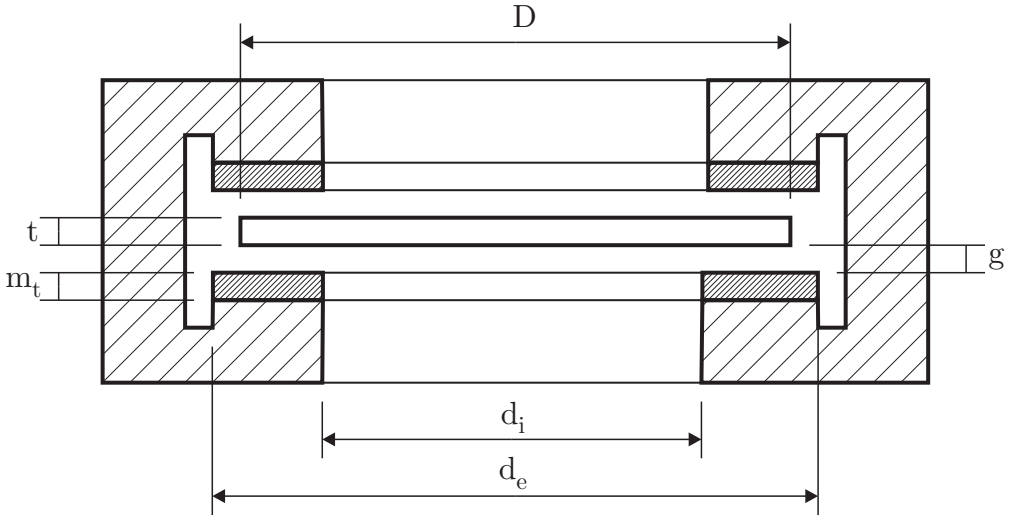

Figure 4.1. Reference model with quotations of the fundamental geometric parameters of the electrodynamic bearing used in the experimental tests.

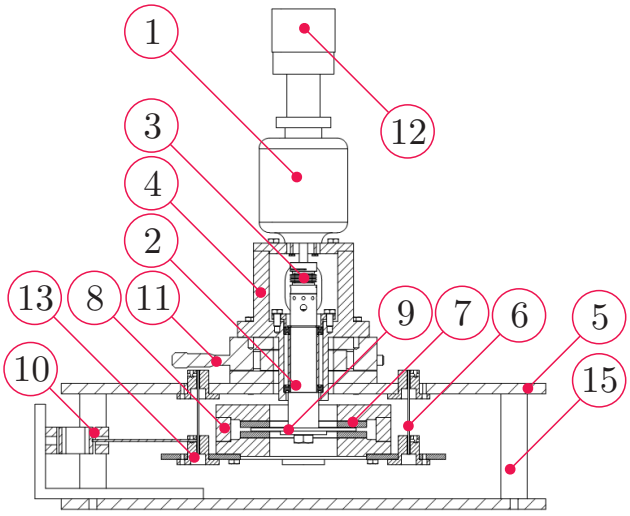

(a)

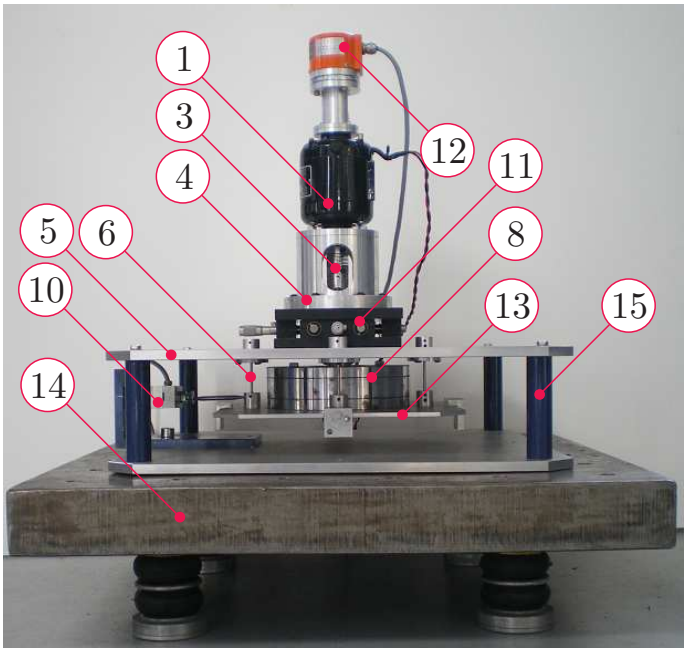

(b)

Figure 4.2. Test rig for the measurement of the quasi-static characteristic of the bearing. a) Cross section view. b) Picture of test rig.

Table 4.1. Main parameters of the test rig for quasi stationary characterization.

Parameter		Value	Unit
Geometry of the permanent magnets		Ring	-
Material of the permanent magnets		NdFeB	-
Residual magnetization		1.09	T
Permanent magnets' external diameter	d_e	120	mm
Permanent magnets' internal diameter	d_i	64	mm
Permanent magnets' thickness	m_t	5.5	mm
Conducting discs' external diameter	D	110	mm
Conducting discs' thickness	t	3	mm
Air gap	g	1	mm

4.3 Experimental analysis.

The realization of experimental tests requires an accurate observation of the phenomena involved, trying to isolate as much as possible the effects of interest. Usually it is very difficult to predict all the details that influence the final results, and a fine tuning of the experiments can only be found following with rigour a testing procedure. The testing procedure for the electrodynamic bearing's characterization under quasi stationary conditions requires performing the following steps before and during each test:

1. Connection of the EDB's rotor to the lower end of the shaft and connection of the EDB's stator using four flexible steel beams (6).

2. Introduction of the load cells in between the EDB's stator and a rigid inertial basing.

3. Calibration of the measurement chain to account for the stiffness in parallel introduced by the four steel beams (6).

4. Definition of the centred position (referring to Fig. 3.1b, $O = C$). This is done by putting the rotor into rotation at a relatively high rotational speed and then acting on the micrometric positioning stage until the forces measured by the load cells are brought close to zero. In practical terms the zero can be reached within a tenth of a Newton.

5. Imposition of the eccentricity q_0 by acting in one of the micrometres. In the tests presented $q_0 = 0.5$ mm.

6. Accelerate the rotor to different values of rotational speed and measure the values of forces produced by the bearing. Since the electrical dynamics of the

eddy currents is usually much faster than the mechanical dynamics, the measurements can be performed in a run up test without any loss of information.

The data obtained performing this procedure is acquired using a LMS digital signal analyser. A filtering and down sampling operation is performed in post processing phase to render the data clearer and easier to manipulate.

The tests are performed for three different types of conducting materials, namely brass, aluminium, and copper. The geometry of the sample discs is equal in the three cases and is defined in Tab. 4.1 with respect to Fig. 4.1. The results obtained are shown in Fig. 4.3. Figure 4.3a shows the results obtained using a brass disc, Fig. 4.3b shows the results for an aluminium disc, and Fig. 4.3c shows the results for a copper disc.

The agreement between the experimental results for the bearing's forces and the analytical model is very good in all three cases, confirming the validity of the model. The values of the mechanical equivalent parameters describing each test (brass, aluminium, and copper) are summarized in Tab. 4.2. The values of these parameters are the results of curve fitting between Eq. (4.3) and the experimental data for each case. A confirmation of the goodness of the parameter estimation can be obtained comparing the values of k and c for the different materials. As expected the stiffness remains virtually the same in all three cases. This is due to the fact that the parameter k is not affected by the conductivity of the material but depends only on the magnetic characteristics of the magnetic circuit and the shape of the eddy current path. Since the geometry of the conductor and magnetic circuit is the same in all cases, the k must remain constant. On the other hand, the damping is strongly affected by the material's conductivity and increases for increasing values of conductivity, thus the copper disc is expected to have higher damping than the aluminium and brass discs.

Table 4.2. Main parameters of the test rig for quasi stationary characterization.

Material	k [N m^{-1}]	c [N s m^{-1}]
Brass	35541	19.5
Aluminium	36018	35
Copper	35722	67.1

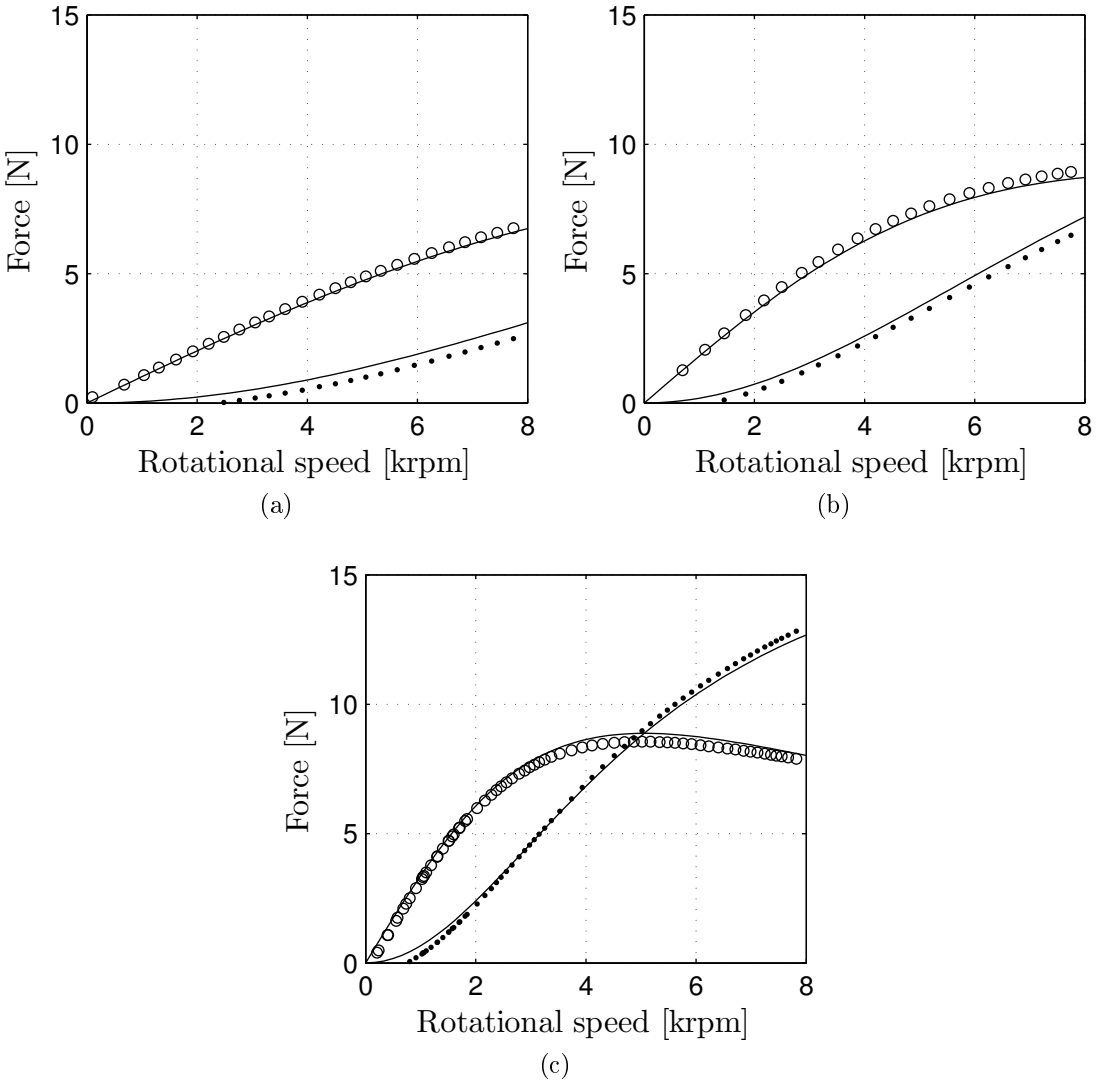

Figure 4.3. Comparison between experimentally measured forces and analytical model for different conducting materials in the EDB's rotor. a) Brass, b) aluminium, and c) copper. Measured imaginary component of force ($\circ$), measured real component ($\cdots$), analytical model ($-$)

Part II

Dynamics of rotors on electrodynamic bearings

Chapter 5

Jeffcott rotor

By the nature of the phenomena, studying the dynamics of a rotor on magnetic bearings requires one to consider that the centre of the rotor is moving relative to the stator. In the specific case of the electrodynamic bearing, this means that the centre of the conductor (point C) is moving relative to the magnetic field (point O). Equation (3.48) takes this into account. The new state variable F_q can be used to find the coupling with the dynamic equation of the rotor mass m. In this way it is possible to study the rotordynamic implications of supporting rotors with different types of electrodynamic bearings.

The simplest model that can be used to study the dynamic behaviour of a rotor is the Jeffcott rotor model. It consists of a point mass attached to a massless shaft. This model represents an oversimplification as it neglects many aspects present in real world rotors but, nevertheless it allows to gain insight into important phenomena specially in the case of rotors supported by electrodynamic bearings.

In this section we will study the stability of the Jeffcott rotor model supported exclusively by EDBs. The stability of a linear system is determined by the eigenvalues of this system. Briefly, the system is stable if the real part of all the eigenvalues is negative [52]. This means that the system will exhibit a bounded output for respective bounded inputs. In the rotordynamics context this means that the rotor will respond to any disturbance forces with orbits of bounded radius.

For the demonstration of the concepts some graphs are used. The values of the EDB's parameters and rotor's mass used to produce the diagrams are given in Tab. 5.1.

Table 5.1. Parameters describing the dynamics of a Jeffcott rotor on EDBs.

Parameter	Symbol	Value	Unit
Rotor's mass	m	2.025	kg
Flux linkage constant	Λ_0	10	Wb m^{-1}
Bearing's resistance	R	0.286	Ω
Bearing's inductance	L	0.33	mH

5.1 Undamped Jeffcott rotor

The equation of motion of the Jeffcott rotor supported by EDBs is

$$m\ddot{q}_c + F_q = F_{\text{ext}}, \tag{5.1}$$

where F_q is the force introduced in the system by the electrodynamic bearing and F_{ext} is a generic disturbance force acting in the rotor's mass. Note that the force introduced by the bearing is seen as a reaction by the rotor mass.

The electrodynamic bearing of Eq. (3.48) and the rotor of Eq. (5.1) are interacting subsystems. The rotor block responds to forces and moments with velocities and displacements. The bearing responds to the rotor's outputs with forces. As a consequence, to study the dynamic behaviour of the rotor running on EDBs, Eq. (3.48) and (5.1) must be solved together. Given the linear time invariant form of the equations, a state-space model can be built for this purpose. The state-space model has the form:

$$\begin{Bmatrix} \ddot{q}_c \\ \dot{q}_c \\ \dot{F}_q \end{Bmatrix} = \mathbf{A} \begin{Bmatrix} \dot{q}_c \\ q_c \\ F_q \end{Bmatrix} + \mathbf{B} \left\{ F_{\text{ext}} \right\}. \tag{5.2}$$

The dynamic matrix $\mathbf{A}$ is

$$\mathbf{A} = \begin{bmatrix} 0 & 0 & -\frac{1}{m} \\ 1 & 0 & 0 \\ \frac{\Lambda_0^2}{L} & \mathrm{j}\frac{\Lambda_0^2}{L}(p-1)\Omega & -\left(\frac{R}{L} + \mathrm{j}(p-1)\Omega\right) \end{bmatrix} \tag{5.3}$$

and the input gain matrix $\mathbf{B}$ is equal to

$$\mathbf{B} = \begin{bmatrix} \frac{1}{m} \\ 0 \\ 0 \end{bmatrix}.$$

The state-space modelling allows studying the rotordynamic stability, frequency response, unbalance response, and enables developing other tools to study the dynamics of the suspension in a fast and easy way. The analysis of different systems can be performed as simple parametric studies.

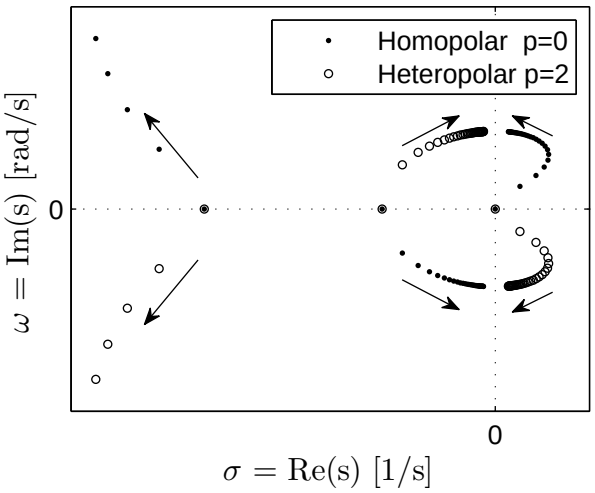

Figure 5.1. Root loci plot of the Jeffcott rotor supported by electrodynamic bearings for increasing values of rotating speed.

To study the rotor's stability we calculate the eigenvalues of the dynamic matrix **A** of the suspension's model (rotor supported by EDB) and analyse the evolution of the system's poles in a root loci plot. Figure 5.1 shows the root loci plot obtained by calculating the eigenvalues of Eq. (5.3) for increasing values of rotating speed Ω. Note that the figure shows the evolution of the poles for the homopolar case and for the heteropolar with $p = 2$.

It can be seen how the system presents a root that is in the right hand part of the complex plane for any value of rotating speed different from zero. This is true for both homopolar and heteropolar cases, representing that the Jeffcott rotor supported by EDBs is unstable for any value of rotating speed if the system is not modified. The reason for this unstable behaviour has been identified to be the presence of rotating damping in the system. The eddy currents induced in the conducting part of the electrodynamic bearing dissipate energy associated to the motion of the rotating part. Rotating damping forces are known to destabilize the free whirling motion of rotors for speeds above the first critical. In particular, if the rotating damping is of viscous type, the instability threshold of the undamped system (no external non rotating damping) is equal to the first critical speed [47].

Intuitively one can think that the instability arises from the fact that the system is always operating in supercritical regime because the electrodynamic supports are unable to give radial stiffness at zero rotating speed. Actually this statement is only partially valid since the behaviour of the electrodynamic bearing cannot be correctly represented by a rotating viscous damper. The frequency dependence of the bearing's forces must be taken into account, modifying the overall behaviour. In the next sections we will use the suspension model to study its dynamic response

and analyse different stabilization techniques previously presented in the literature [10, 29].

5.2 Damped Jeffcott rotor

The most straightforward way to introduce non rotating damping in the system is to do it by means of an electromagnetic damper associating non rotating damping to the rotor translational degree of freedom q_c. This stabilization technique has been proposed almost from the beginning of the interests in electrodynamic suspension of rotors. From the modelling point of view it consists simply in introducing a viscous damping element associated to the rotor translational degree of freedom q_c. As a result non-rotating damping is introduced in the model of Eq. (5.1) and the new equation of motion of the rotor's mass is:

$$m\ddot{q}_c + c\dot{q}_c + F_q = F_{\text{ext}}. \tag{5.4}$$

The dynamic matrix of the state-space model is also updated

$$\mathbf{A} = \begin{bmatrix} -\frac{c}{m} & 0 & -\frac{1}{m} \\ 1 & 0 & 0 \\ \frac{\Lambda_0^2}{L} & \mathrm{j}\frac{\Lambda_0^2}{L}(p-1)\Omega & -\left(\frac{R}{L} + \mathrm{j}(p-1)\Omega\right) \end{bmatrix}. \tag{5.5}$$

Figure 5.2 shows the influence of the non-rotating damping on the system's poles. It is readily seen that the presence of damping allows stabilizing the dynamic behaviour above a certain value of rotating speed Ω_S. This value represents a stability threshold, being the system unstable for spin speeds below it and stable for speeds above it. Another conclusion that arises from this diagram is that the bearing's rotating damping contribution reduces for higher values of spin speed, when the stabilizing stiffness contribution becomes dominant.

It can also be pointed out that increasing the number of pole pairs of the heteropolar configuration is beneficial for the stability. The presence of more magnetic pole pairs increases the frequency perceived by the electrical circuit. The resulting effect is that the spin speed for which the damped rotor becomes stable is decreased. This characteristic can be observed in Fig. 5.3 where the real part of the unstable root is plotted versus the spin speed. The spin speed for which the graph crosses the zero represents the stability threshold for that configuration.

5.2.1 Unbalance response

The static unbalance introduces a force whose amplitude is a quadratic function of the spin speed and can become quite large for high speed rotors [47]. Conventional ball and roller bearings, that can be modelled as stiff spring-damper elements,

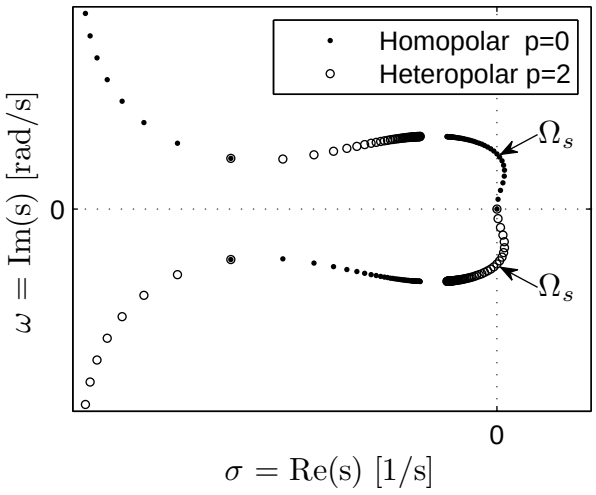

Figure 5.2. Root loci plot of the damped Jeffcott rotor.

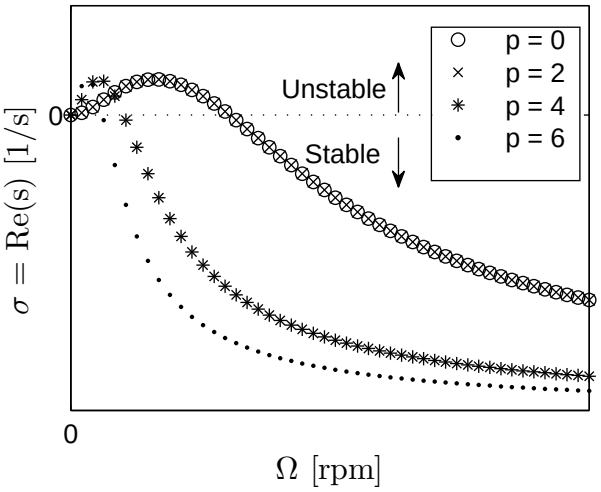

Figure 5.3. Influence of the number of magnetic pole pairs on stabilization threshold speed.

constrain the rotor to spin around its geometrical axis, transmitting the unbalance force to the housing of the machine. This may lead to large vibrations or even to bearing failure.

Unbalance compensation has been an important research topic in the magnetic bearing community almost from the beginning. In case of active magnetic bearings, the presence of a feedback loop opens opportunities for managing unbalance that were almost unthinkable with conventional bearings. Several algorithms have been proposed to actively identify and compensate the effects of the unbalance [53, 54].

By converse, very little effort has been focused on the unbalance effects in case of rotors supported by passive magnetic bearings.

Similarly to conventional bearings, passive magnetic bearings using reluctance forces or permanent magnet forces cannot deal with unbalance and may as well resent of vibrations due to residual unbalance, specially during acceleration phases.

Electrodynamic bearings react to unbalance forces in different ways according to the number of magnetic pole pairs. It is shown in Fig. 5.4a how the unbalance response of the rotor running on homopolar bearings presents no amplification due to resonance. On the other hand, Fig. 5.4b shows that a rotor on heteropolar bearings presents an unbalance response that, besides the stability issue, is similar to the response of a rotor on flexible supports.

It can be demonstrated that the absence of a resonance peak in the unbalance response of the homopolar case is not due to the external damping added to stabilize the system, but is an intrinsic characteristic of the homopolar bearing. Considering that the force generated by the unbalance of the rotor introduces a synchronous forcing function with the form:

$$F_{\text{unb}} = m\varepsilon\Omega^2 \mathrm{e}^{\mathrm{j}\Omega t}; \tag{5.6}$$

the response of the rotor to such a force is a synchronous whirl

$$q_c = q_0 \mathrm{e}^{\mathrm{j}\Omega t}. \tag{5.7}$$

Substituting Eq. (5.7) in Eq. (3.45) we get that the flux linked by the coils as a function of the rotor angle is

$$\lambda = q_0 \Lambda_0, \tag{5.8}$$

which is constant for every rotor angle. This means that the back electromotive force in the coils $bemf = -\dot{\lambda}$ is equal to zero. From Eq. (3.46) this results in no current in the coils and, therefore, no force due to unbalance. This is not true for any heteropolar configuration.

The unbalance response of the homopolar electrodynamic bearing results to be equal to the residual unbalance in the whole working range, which means that the rotor always spins around its inertia axis (self-centred). As a consequence, no force due to rotor's unbalance is produced by the bearing and transmitted to the housing, thus the rotor should rotate smoothly. On the other hand, analysing the reaction forces produced by the heteropolar bearing it is possible to notice how it reacts as a normal flexible support, perceiving all external disturbances and reacting to it.

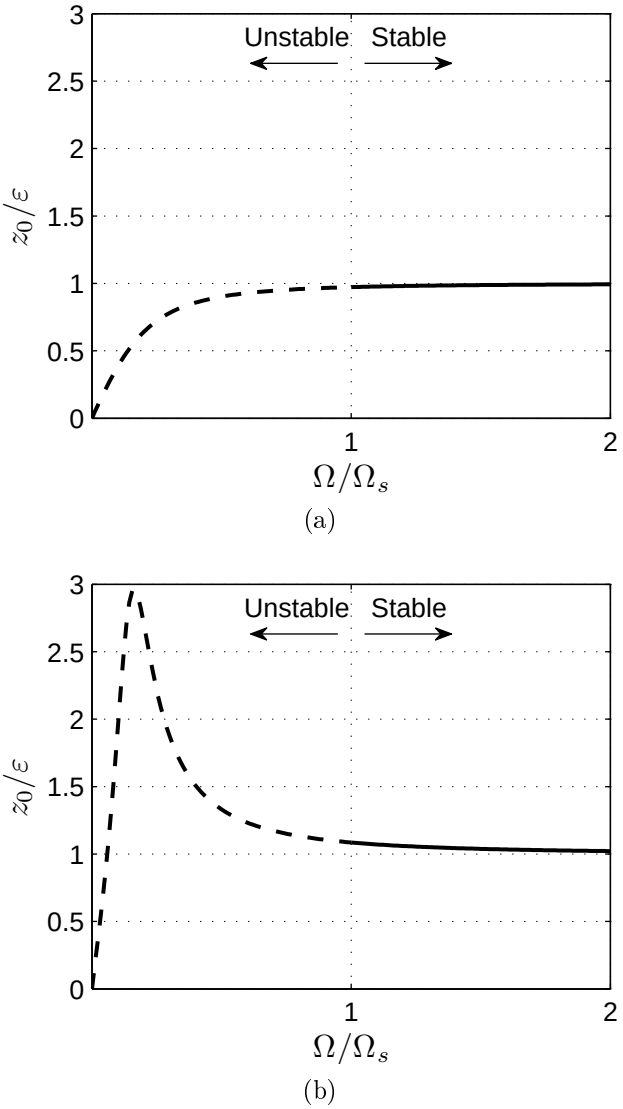

Figure 5.4. Unbalance response of a rotor running on a) homopolar and b) heteropolar electrodynamic bearings.

5.2.2 Frequency response

The behaviour of electrodynamic bearings subject to unbalance forces can also be evidenced by the transfer response function between input rotor's forces and output forces transmitted to the housing. This function is shown in Fig. 5.5. The graph is plotted with respect to a non-dimensional frequency equal to the forcing frequency ω divided by the spin speed Ω.

It can be noticed how the force produced by the homopolar bearing has the

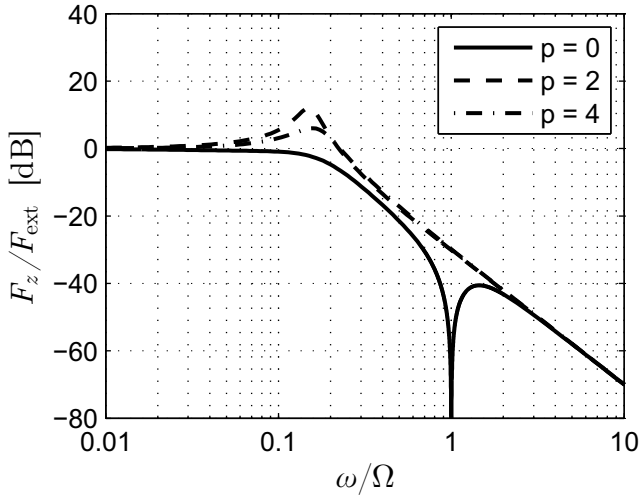

Figure 5.5. Frequency response function between the electrodynamic support forces and the rotor forces.

behaviour of a narrow notch filter for a force excitation synchronous with the rotating speed ($\omega/\Omega = 1$). As in the previous section, it reinforces the fact that the homopolar bearing cannot perceive synchronous forces and consequently these are filtered and not transmitted to the housing. This is an advantage of this particular type of passive bearing with respect to active magnetic bearings. Similar behaviour is pursued in the active magnetic bearing context by means of complex control strategies that require platforms with high processing performance.

The heteropolar bearing behaves again as a regular elastic support reacting to every input frequency.

5.3 Jeffcott rotor on elastic basing

An alternative to the previous solution that allows introducing non-rotating damping in an effective way is to introduce a stabilizing element between the stator of the EDB and a rigid base. This element can be devised in different ways, but in any case must be capable of introducing both stiffness and damping. This solution has been applied successfully to damp rotor induced vibrations, being the most evident case that of a common laundry machine.

Within the EDB's context this system was analysed by Tonoli *et al.* [29]. It was shown that the stability boundaries of a Jeffcott rotor on this kind of support can be reduced with respect to those of the case described in Sec. 5.2. It also avoids increasing the rotor's mass and complexity by eliminating the permanent magnets dedicated to the damping in the former configuration. Instead, damping

is introduced between two non-rotating elements, thus enabling the use of regular damping systems such as viscoelastic materials or squeeze film dampers. However, the choice of appropriate values of stiffness and damping of the stabilizing element is not obvious, requiring the solution of an optimization problem.

From the modelling point of view, this case is interpreted as shown in Fig. 5.6. In the figure the xy frame is inertial as if attached to an infinitely stiff base while $x'y'$ is a translating frame attached to the stator mass. The axes of the two systems remain parallel to each other. It must be noticed that in this case there are three interacting subsystems, namely, the rotor, the EDB and the stator. With respect to the figure, the associated complex degrees of freedom are:

- The displacement of the rotor geometric centre C in the inertial frame.

$$q = x + \mathrm{j}y \tag{5.9}$$

- The displacement of the stator mass m_s represented by the point S in the inertial frame.

$$q_s = x_s + \mathrm{j}y_s \tag{5.10}$$

- The relative displacement between the displacement between points C and S.

$$q_c = q - q_s \tag{5.11}$$

The equations of the rotor mass and EDB are given by Eq. (5.1) and Eq. (3.48) respectively. The displacements and speeds considered in the EDB's equations are the relative ones (q_c and $\dot{q}_c$). The stator mass dynamics is described by the following equation:

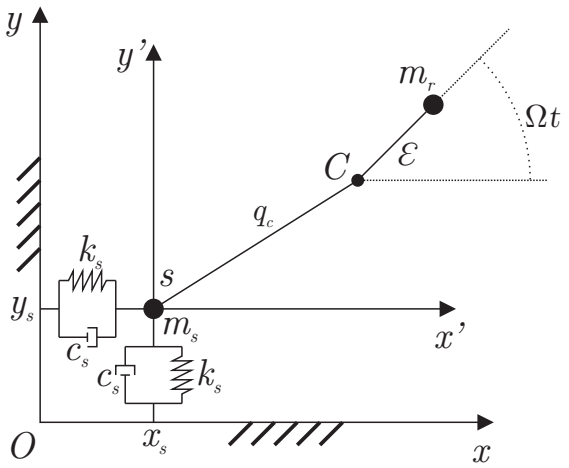

Figure 5.6. Model of the Jeffcott rotor on elastic supports.

$$m_s\ddot{q}_s + c_S\dot{q}_s + k_s q_s - F_q = 0. \tag{5.12}$$

The presence of the negative sign on the bearing force F_q means that the stator mass sees this force as an external force while the rotor mass perceives it as a reaction force (see Eq. (5.1)).

The state space model of this system can be written as:

$$\begin{Bmatrix} \ddot{q} \\ \ddot{q}_s \\ \dot{q} \\ \dot{q}_s \\ \dot{F}_q \end{Bmatrix} = \mathbf{A} \begin{Bmatrix} \dot{q} \\ \dot{q}_s \\ q \\ q_s \\ F_q \end{Bmatrix} + \mathbf{B} \left\{ F_{\text{ext}} \right\}. \tag{5.13}$$

The dynamic matrix $\mathbf{A}$ for the state-space model of this system is:

$$\mathbf{A} = \begin{bmatrix} 0 & 0 & 0 & 0 & -\frac{1}{m_r} \\ 0 & -\frac{c_s}{m_s} & 0 & -\frac{k_s}{m_s} & \frac{1}{m_s} \\ 1 & 0 & 0 & 0 & 0 \\ 0 & 1 & 0 & 0 & 0 \\ \frac{\Lambda_0^2}{L} & -\frac{\Lambda_0^2}{L} & \mathrm{j}\frac{\Lambda_0^2}{L}(p-1)\Omega & -\mathrm{j}\frac{\Lambda_0^2}{L}(p-1)\Omega & -\left(\frac{R}{L} + \mathrm{j}(p-1)\Omega\right) \end{bmatrix} \tag{5.14}$$

and the input gain matrix $\mathbf{B}$ is equal to

$$\mathbf{B} = \begin{bmatrix} \frac{1}{m_r} \\ 0 \\ 0 \\ 0 \\ 0 \end{bmatrix}.$$

The root loci of this system considering the same bearing's characteristics of the previous case is shown in Fig. 5.7. The values of stiffness k_s and damping c_s are 240 kN/m and 510 N s/m. The choice of these values must be done performing an optimization to minimize the stabilization threshold speed. To have an objective view of the problem one can resort to a plot showing the response of the stabilization threshold speed in terms of different values of k_s and c_s. Figure 5.8 shows a countour plot of the stabilization threshold speed. The presence of a minimum is clear in the figure leaving to the designer the task of optimizing the system's properties to minimize the stabilization threshold speed guaranteeing that the region surrounding the minimum lies within a region of physically feasible property values. This operation is described for the design of a prototype system in chapter 7.

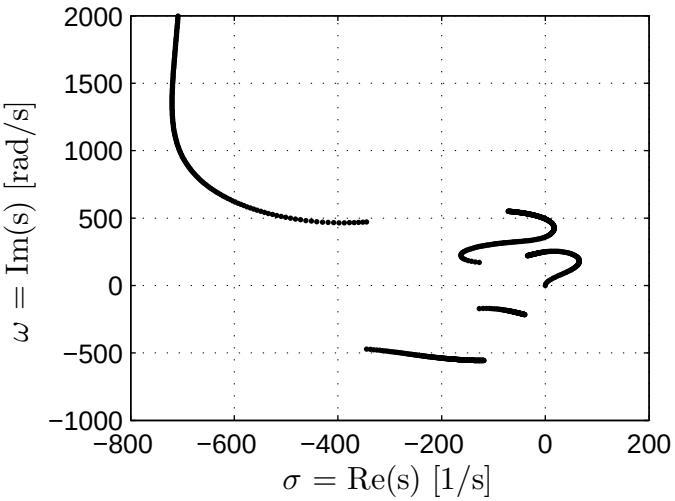

Figure 5.7. Root loci plot showing the evolution of the system's poles for increasing values of spin speed Ω.

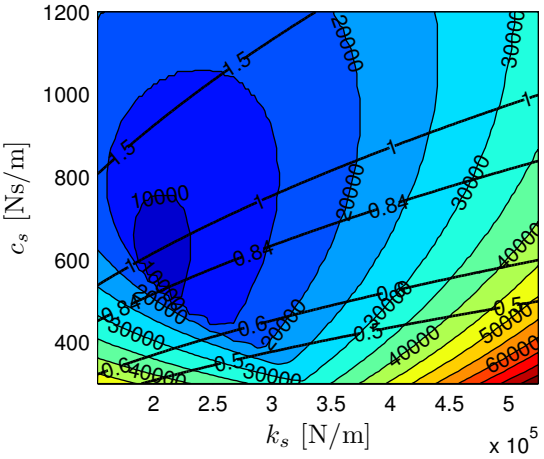

Figure 5.8. Example of mapping of the stabilization threshold speed in terms of the mechanical properties of the elastic element connecting EDB's stator and inertial base.

5.4 Anisotropy of heteropolar bearings

In the preceding sections, both rotor and stator were assumed to be axial symmetric. Considering the difficulty in insuring stability of the whirling motion of the rotor, a stabilizing technique for transverse whirl modes introducing anisotropy into the bearing stiffness can be considered [11]. For solving this problem it is necessary to open the state space model in complex coordinates given by Eq. (5.5) into it's representation in real coordinates as:

$$\begin{Bmatrix} \ddot{x}_c \\ \ddot{y}_c \\ \dot{x}_c \\ \dot{y}_c \\ \dot{F}_x \\ \dot{F}_y \end{Bmatrix} = \mathbf{A} \begin{Bmatrix} \dot{x}_c \\ \dot{y}_c \\ x_c \\ y_c \\ F_x \\ F_y \end{Bmatrix} + \mathbf{B} \left\{ F_{\text{ext}} \right\}, \tag{5.15}$$

where the dynamic matrix is:

$$\mathbf{A} = \begin{bmatrix} -\frac{c}{m} & 0 & 0 & 0 & -\frac{1}{m} & 0 \\ 0 & -\frac{c}{m} & 0 & 0 & 0 & -\frac{1}{m} \\ 1 & 0 & 0 & 0 & 0 & 0 \\ 0 & 1 & 0 & 0 & 0 & 0 \\ \frac{\Lambda_{0_x}^2}{L_x} & 0 & 0 & (p-1)\frac{\Lambda_{0_x}^2}{L_x}\Omega & -\frac{R_x}{L_x} & -(p-1)\Omega \\ 0 & \frac{\Lambda_{0_y}^2}{L_y} & -(p-1)\frac{\Lambda_{0_y}^2}{L_y}\Omega & 0 & (p-1)\Omega & -\frac{R_y}{L_y} \end{bmatrix}. \tag{5.16}$$

Calculating the eigenvalues of the dynamic matrix for different values of spin speeds it is possible to find the stabilization threshold speed. If different values of the ratio between the properties in x direction and those in y direction, and finding the stabilization threshold speed in every case, it is possible to study how the anisotropy of these properties influence the stabilization speed. Figure 5.9 shows the graphs obtained performing this operation for different values of non-rotating damping between rotor and stator. It can be noticed that the anisotropy has a strong influence on the stabilization speed. In fact, one of the worst cases is exactly when the properties of the bearing are isotropic; this is evidenced by the peak in the stabilization threshold speed. The non-rotating damping has the effect of reducing the stabilization speed in the whole range. One aspect to be noticed is that for very large values of anisotropy combined to large values of bearing's stiffness, the stabilization threshold reduces strongly towards zero also for low values of non-rotating damping.

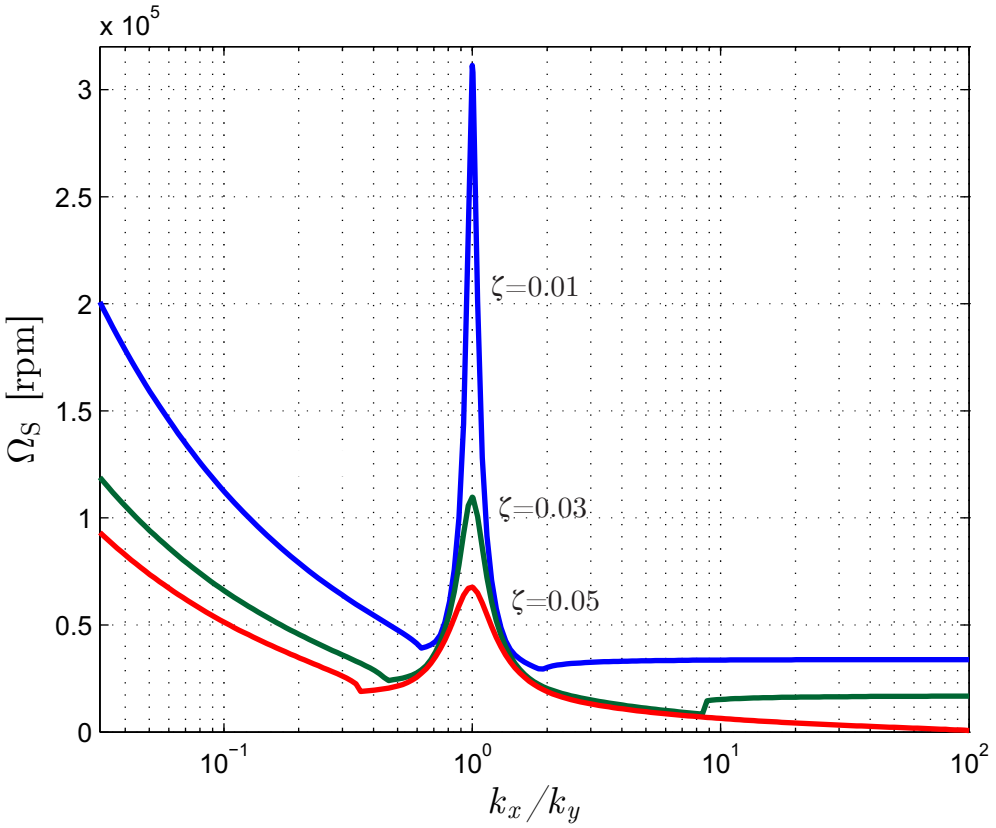

Figure 5.9. Stabilization speed of the rotor on heteropolar EDB with anisotropic properties of the bearing.

5.5 Anisotropy of stator-casing connections

The homopolar concept was first devised to eliminate unnecessary eddy current losses generated by AC electrodynamic bearings [30]. The concept itself presupposes axial symmetry of both rotor and stator, hence the introduction of anisotropy of the bearing is not possible. On the other hand, considering the configuration presented in Sec. 5.3, it is possible to imagine a system where the stiffness and damping of the connections between the stator of the EDB and the basing are different in each direction.

Similarly to the previous case, this system is more conveniently represented in real coordinates. The representation in complex coordinates is possible as well [47] but creates difficulties for the state-space modelling.

In the first paragraph the homopolar concept was cited to motivate this section however, as a consequence of the unified modelling, the effect of anisotropy can be appreciated in both homopolar and heteropolar configurations. The state-space

model can be written as:

$$\begin{Bmatrix} \ddot{x}_c \\ \ddot{y}_c \\ \ddot{x} \\ \ddot{y} \\ \dot{x}_c \\ \dot{y}_c \\ \dot{x} \\ \dot{y} \\ \dot{F}_x \\ \dot{F}_y \end{Bmatrix} = \mathbf{A} \begin{Bmatrix} \dot{x}_c \\ \dot{y}_c \\ \dot{x} \\ \dot{y} \\ x_c \\ y_c \\ x \\ y \\ F_x \\ F_y \end{Bmatrix} + \mathbf{B} \left\{ F_{\text{ext}} \right\}. \tag{5.17}$$

where the dynamic matrix is:

$$\mathbf{A} = \begin{bmatrix} 0 & 0 & 0 & 0 & 0 & 0 & 0 & 0 & -\frac{1}{m} & 0 \\ 0 & 0 & 0 & 0 & 0 & 0 & 0 & 0 & 0 & -\frac{1}{m} \\ 0 & 0 & -\frac{c_x}{m_s} & 0 & 0 & 0 & -\frac{k_x}{m_s} & 0 & \frac{1}{m_s} & 0 \\ 0 & 0 & 0 & -\frac{c_y}{m_s} & 0 & 0 & 0 & -\frac{k_y}{m_s} & 0 & \frac{1}{m_s} \\ 1 & 0 & 0 & 0 & 0 & 0 & 0 & 0 & 0 & 0 \\ 0 & 1 & 0 & 0 & 0 & 0 & 0 & 0 & 0 & 0 \\ 0 & 0 & 1 & 0 & 0 & 0 & 0 & 0 & 0 & 0 \\ 0 & 0 & 0 & 1 & 0 & 0 & 0 & 0 & 0 & 0 \\ \frac{\Lambda_0^2}{L} & 0 & -\frac{\Lambda_0^2}{L} & 0 & 0 & \frac{\Lambda_0^2}{L}\Omega & 0 & -\frac{\Lambda_0^2}{L}\Omega & -\frac{R}{L} & -\Omega \\ 0 & \frac{\Lambda_0^2}{L} & 0 & -\frac{\Lambda_0^2}{L} & -\frac{\Lambda_0^2}{L}\Omega & 0 & \frac{\Lambda_0^2}{L}\Omega & 0 & \Omega & -\frac{R}{L} \end{bmatrix} \tag{5.18}$$

From the stability viewpoint, the inputs of the system are irrelevant [52] and the input gain matrix doesn't have to be defined.

The possibility of taking advantage of anisotropy of the connections to reduce the stabilization threshold speed, the stabilization speed can be calculated for different values of the anisotropy ratio ($\alpha = k_x/k_y$). Considering constant values of the rotor and stator masses, m and m_s respectively, and the system scheme of Fig. 5.6, the effect of anisotropy is studied in terms of the damping ratio ζ. Figure 5.10 shows how anisotropy and damping ratios affect the stabilization speed. For systems having low damping ratios, the anisotropy can have a beneficial role, reducing the stabilization speed threshold. The increase in the damping ratio eliminates the positive effects anisotropy in the elastic connections, but effectively reduces the stabilization threshold.

The anisotropy in this case has a different effect with respect to that illustrated in Fig. 5.9. The increase in the anisotropy ratio with a respective increase in the stiffness of one direction results to increase the stabilization threshold speed. This diagram is case dependent but in general it is expected that the anisotropy will have

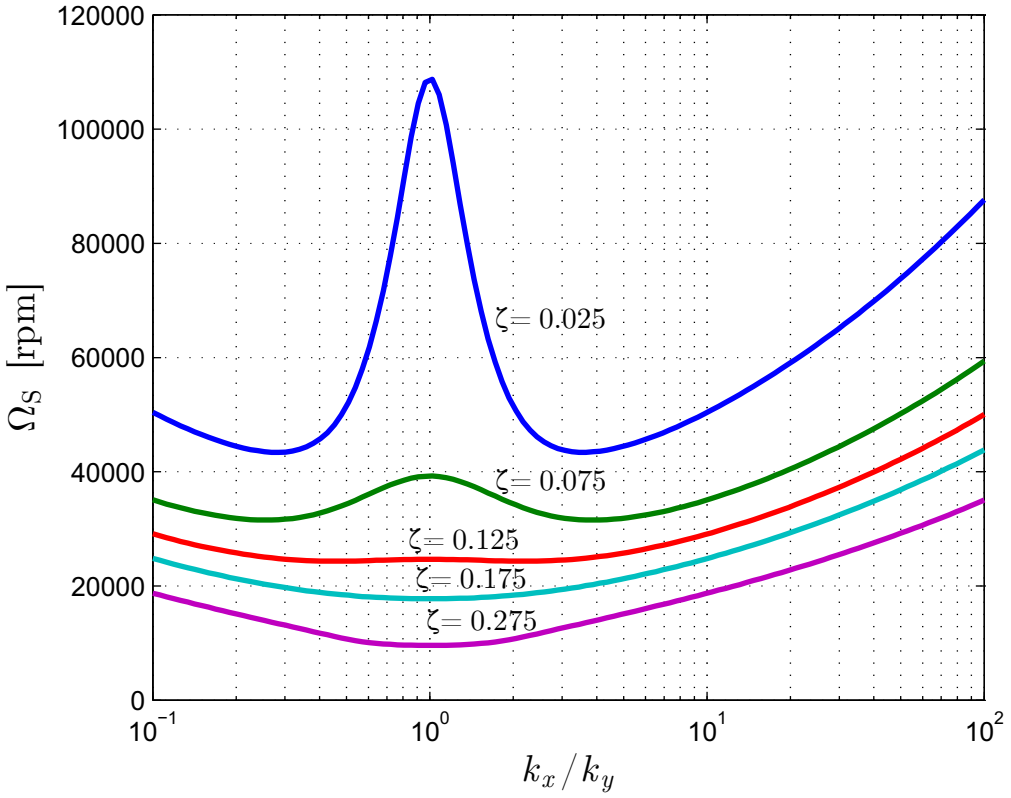

Figure 5.10. Stabilization speed of the rotor on homopolar EDB with anisotropic connections between bearing stator and basing.

a positive contribution only when the value of damping is low [47]. Furthermore, within physically feasible margins, it is always more advantageous to increase the value of damping than to use anisotropy effects because the stabilization threshold speed is more sensitive to the first than to the latter.

Chapter 6

4 DOF model

In the previous chapter the dynamic behaviour of a Jeffcott rotor supported by electrodynamic bearings has been studied. As stated there, this rotor model represents an oversimplification. The four degree of freedom (4DOF) model represents a more realistic model since the tilting degree of freedom of the rotor's centre of mass is taken into account. In the present chapter the aspects related to stability of the suspension are addressed considering a 4DOF rotor model. This analysis should put in evidence some critical aspects related to the system's stability that have never been studied in previous works.

The system under analysis is composed by three subsystems that interact with each other by exchanging forces, namely rotor, electrodynamic bearing, and the EDB's stator connected to the basing through elastic elements. A schematic representation is shown in Fig. 6.1.

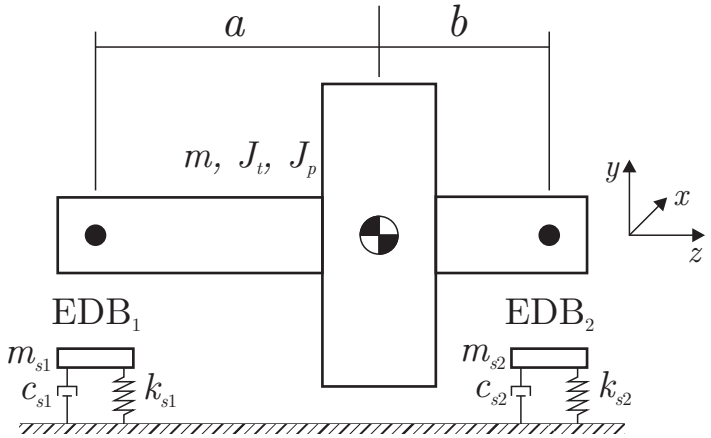

Figure 6.1. Model of a four degree of freedom rotor supported by electrodynamic bearings on elastic basing.

To correctly model the tilting degree of freedom, the position of the supports must be considered. For this matter, in the following section we define a set of operations that transform the motion of the rotor's centre of mass into motion at the bearings and also the reactions at the bearings into reactions at the rotor's centre of mass.

6.1 Transformation matrices

Representing the interaction between the rotor and the electrodynamic bearings requires the definition of a transformation between inputs and outputs of rotor's centre of mass and bearing's centre and vice versa. The bearing responds to displacements and speeds with forces that are applied at the bearing's centre, but act on rotor's centre of mass. Similarly, the lateral and rotational motions of the centre of mass generate an equivalent lateral motion at the bearing's centre[1]. Two different arrangements of rotor and EDBs are analysed to define these relations, they are:

1. Rotor's centre of mass located between the two bearings.
2. The two bearings located at the same side of the rotor's centre of mass.

The transformation matrices are defined in terms of real quantities and subsequently the complex notation is introduced to reduce their order.

6.1.1 Rotor's centre of mass between bearings

Considering a rotor supported by two generic bearings located at the two ends of the shaft, the transformations are presented in figures 6.2 and 6.3.

Figures 6.2a and 6.2b represent the transformations of forces generated by the bearings at the ends of the shaft into resultant forces and moments acting in the rotor's centre of mass in planes zx and zy respectively. It is important to note how the definition of the coordinate system of Fig. 6.1 implies a different sign convention for moments and rotations in the two planes.

To compute the transformation matrix between forces at the bearings and the forces and moments at the rotor's centre of mass, we apply two generic forces, F_{x_1} and F_{x_2}, at the supports and calculate the resulting force and moment at the rotor's centre of mass, obtaining:

$$\begin{aligned} F_x &= F_{x_1} + F_{x_2} \\ M_y &= -aF_{x_1} + bF_{x_2}. \end{aligned} \tag{6.1}$$

[1]This consideration is valid under the assumption of small lateral and rotational displacements.

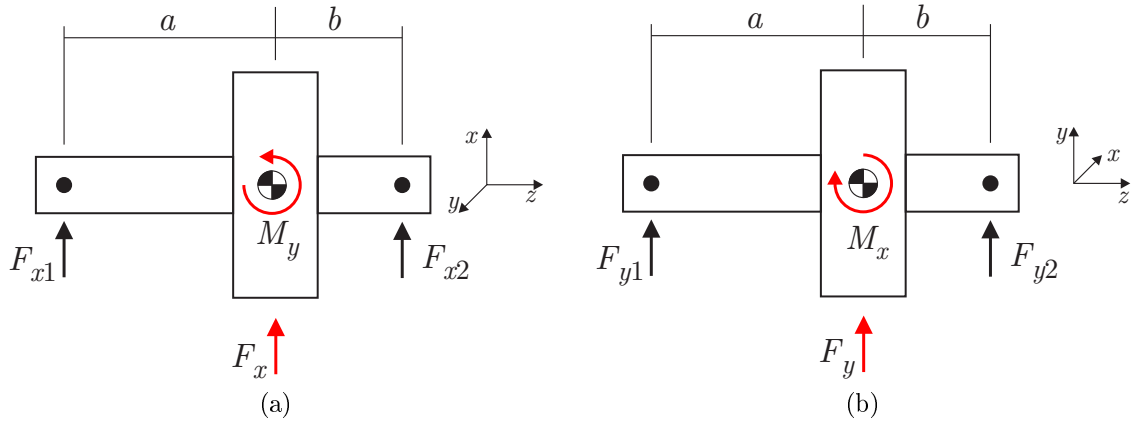

Figure 6.2. Definition of force exchange between the electrodynamic bearings and the centre of the rotor

Subsequently, the same procedure is performed in plane zy; forces F_{y_1} and F_{y_2} are applied at the supports and the resulting force and moment at the rotor's centre of mass are computed:

$$\begin{aligned} F_y &= F_{y_1} + F_{y_2} \\ M_x &= aF_{y_1} - bF_{y_2}. \end{aligned} \tag{6.2}$$

Condensing the operations in a transformation matrix we obtain:

$$\begin{Bmatrix} F_x \\ M_y \\ F_y \\ M_x \end{Bmatrix} = \mathbf{T} \begin{Bmatrix} F_{x_1} \\ F_{y_1} \\ F_{x_2} \\ F_{y_2} \end{Bmatrix}, \tag{6.3}$$

where $\mathbf{T}$ is:

$$\mathbf{T} = \begin{bmatrix} 1 & 0 & 1 & 0 \\ -a & 0 & b & 0 \\ 0 & 1 & 0 & 1 \\ 0 & a & 0 & -b \end{bmatrix}. \tag{6.4}$$

Using the complex notation:

$$\begin{aligned} F_q &= F_x + \mathrm{j}F_y \\ M_\phi &= M_y - \mathrm{j}M_x \end{aligned}, \tag{6.5}$$

it is easy to demonstrate how the transformation reduces to:

$$\mathbf{T} = \begin{bmatrix} 1 & 1 \\ -a & b \end{bmatrix}. \tag{6.6}$$

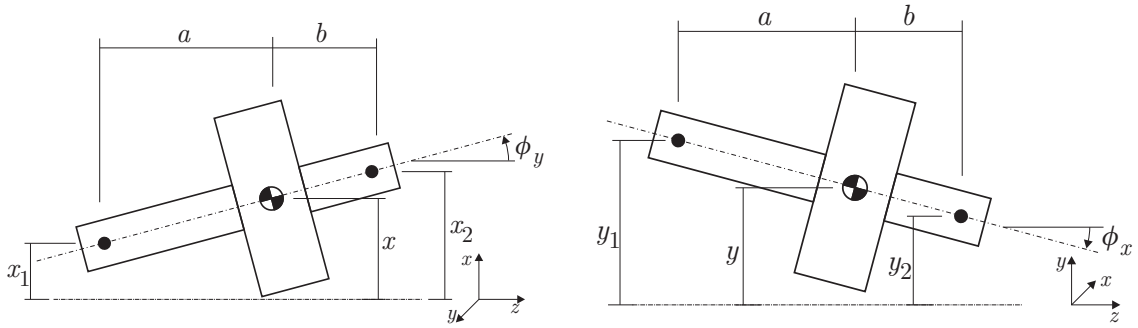

Figure 6.3. Definition of force exchange between the electrodynamic bearings and the centre of the rotor

A similar procedure is applied to compute the transformation between rotor's displacements and those in correspondence to the supports. For doing so the hypothesis of small lateral displacements and rotation angles must be considered.

We begin by considering the degrees of freedom on the zx shown in Fig. 6.3a. Virtual displacements are applyed to rotor's degrees of freedom x and ϕ_y, and the displacements in correspondence to the supports are computed:

$$\begin{aligned} x_1 &= x - a\phi_y \\ x_2 &= x + b\phi_y. \end{aligned} \tag{6.7}$$

Applying the same procedure to the degrees of freedom of plane zy we obtain:

$$\begin{aligned} y_1 &= y + a\phi_x \\ y_2 &= y - b\phi_x. \end{aligned} \tag{6.8}$$

As in the previous case, the operations can be condensed in a transformation matrix:

$$\begin{Bmatrix} x_1 \\ y_1 \\ x_2 \\ y_2 \end{Bmatrix} = \mathbf{T}^T \begin{Bmatrix} x \\ \phi_y \\ y \\ \phi_x \end{Bmatrix}, \tag{6.9}$$

where the transformation matrix in this case is the transpose of matrix $\mathbf{T}$ given by Eq. (6.4):

$$\mathbf{T}^T = \begin{bmatrix} 1 & -a & 0 & 0 \\ 0 & 0 & 1 & a \\ 1 & b & 0 & 0 \\ 0 & 0 & 1 & -b \end{bmatrix}. \tag{6.10}$$

Also in this case the complex notation is introduced. The complex variables in this case can be represented as:

$$\begin{aligned} q &= x + \mathrm{j}y \\ \phi &= \phi_y - \mathrm{j}\phi_x, \end{aligned} \tag{6.11}$$

and the transpose of the matrix of Eq. (6.6) represents this transformation as:

$$\begin{Bmatrix} q_1 \\ q_2 \end{Bmatrix} = \mathbf{T}^T \begin{Bmatrix} q \\ \phi \end{Bmatrix}. \tag{6.12}$$

The final shape of the transformation matrix is given by:

$$\mathbf{T}^T = \begin{bmatrix} 1 & -a \\ 1 & b \end{bmatrix} \tag{6.13}$$

6.1.2 Rotor's centre of mass beside the supports

Another case of interest for many possible applications is the case where both the bearings are located at the same side of the rotor's centre of mass. In this case the relation between forces generated at the bearings and those acting at the centre of mass are shown in Figs. 6.4a and 6.4b. The relation between the displacements of the rotor's centre of mass and the resulting displacements at the bearings is shown in Figs. 6.5a and 6.5b.

The procedure to obtain the transformation matrices is the same as presented in the previous case. The matrix representing the transformation between the forces generated at the bearings and those acting on the rotor is:

$$\mathbf{T} = \begin{bmatrix} 1 & 0 & 1 & 0 \\ -a & 0 & -b & 0 \\ 0 & 1 & 0 & 1 \\ 0 & a & 0 & b \end{bmatrix} \tag{6.14}$$

Using the complex notation the $\mathbf{T}$ reduces to:

$$\mathbf{T} = \begin{bmatrix} 1 & 1 \\ -a & -b \end{bmatrix} \tag{6.15}$$

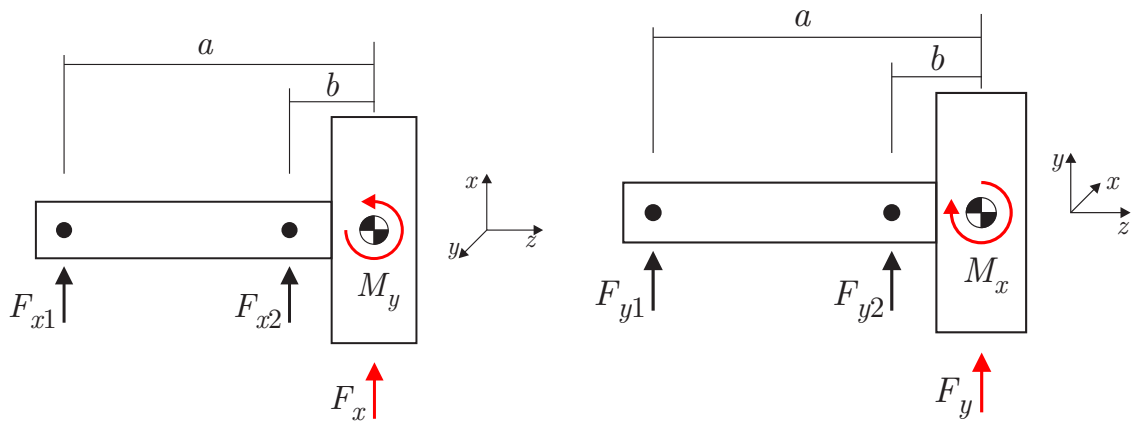

Figure 6.4. Definition of force exchange between the electrodynamic bearings and the centre of the rotor

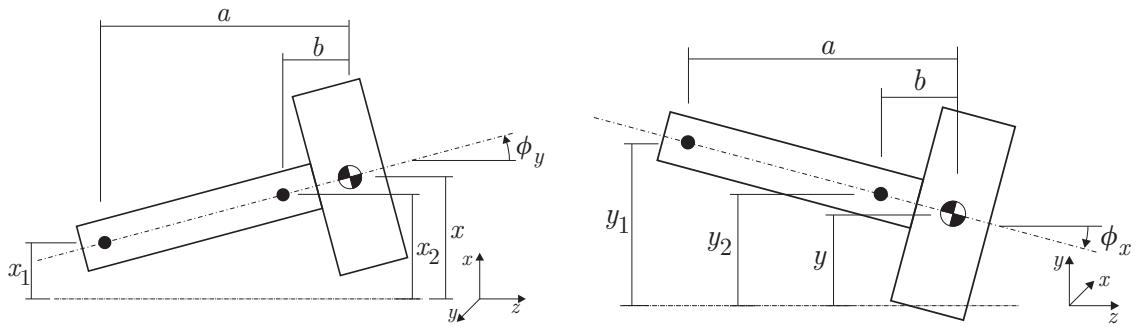

Figure 6.5. Definition of force exchange between the electrodynamic bearings and the centre of the rotor

Similarly, to the previous case, the transpose of $\mathbf{T}$ gives the transformation between displacements of the rotor's centre of mass and displacements at the bearings.

$$\mathbf{T}^T = \begin{bmatrix} 1 & -a & 0 & 0 \\ 0 & 0 & 1 & a \\ 1 & -b & 0 & 0 \\ 0 & 0 & 1 & b \end{bmatrix} \tag{6.16}$$

Also in this case the complex notation is introduced and the transpose of the matrix of Eq. (6.15) represents this transformation as:

$$\mathbf{T}^T = \begin{bmatrix} 1 & -a \\ 1 & -b \end{bmatrix} \tag{6.17}$$

6.2 State space model

In the introduction of this chapter it was stated that the whole system is composed by three subsystems that interact with each other by exchanging forces. At this point we define the equations of each system in order to build a state space model of the whole system describing its coupled dynamics. The equations are written in complex coordinates for compactness and clarity.

The equation of motion of the 4 degree of freedom rotor is [47]:

$$\begin{bmatrix} m & 0 \\ 0 & J_t \end{bmatrix} \begin{Bmatrix} \ddot{q} \\ \ddot{\phi} \end{Bmatrix} + \left(\begin{bmatrix} c & 0 \\ 0 & c_\phi \end{bmatrix} - \mathrm{j}\Omega \begin{bmatrix} 0 & 0 \\ 0 & J_p \end{bmatrix} \right) \begin{Bmatrix} \dot{q} \\ \dot{\phi} \end{Bmatrix} + \begin{Bmatrix} F_q \\ M_\phi \end{Bmatrix} = \begin{Bmatrix} F_{\text{ext}} \\ M_{\text{ext}} \end{Bmatrix} \tag{6.18}$$

The presence of non-rotating damping in this equation is considered in order to have a more general model where damping introduced directly between the rotor and the basing and damping introduced between the EDB's stator and the basing can be considered at the same time. Instead the force due to stiffness and rotating damping generated by the EDB are accounted for by means of F_q and M_ϕ, that depend on the EDB's states.

The EDB stator's equation of motion is the same as Eq. 5.14. For the sake of generality, each EDB and relative stator are considered to have different parameters, hence the stator equations are written as:

$$\begin{bmatrix} m_{s_1} & 0 \\ 0 & m_{s_2} \end{bmatrix} \begin{Bmatrix} \ddot{q}_{s_1} \\ \ddot{q}_{s_2} \end{Bmatrix} + \begin{bmatrix} c_{s_1} & 0 \\ 0 & c_{s_2} \end{bmatrix} \begin{Bmatrix} \dot{q}_{s_1} \\ \dot{q}_{s_2} \end{Bmatrix} + \begin{bmatrix} k_{s_1} & 0 \\ 0 & k_{s_2} \end{bmatrix} \begin{Bmatrix} q_{s_1} \\ q_{s_2} \end{Bmatrix} - \begin{Bmatrix} F_{q_1} \\ F_{q_2} \end{Bmatrix} = \begin{Bmatrix} 0 \\ 0 \end{Bmatrix} \tag{6.19}$$

The two electrodynamic bearings are represented by Eq. (3.48). The two bearings are thus described by the following set of equations:

$$\begin{aligned} \begin{Bmatrix} \dot{F}_{q_1} \\ \dot{F}_{q_2} \end{Bmatrix} = & \begin{bmatrix} \frac{\Lambda_{0_1}^2}{L_1} & 0 \\ 0 & \frac{\Lambda_{0_2}^2}{L_2} \end{bmatrix} \left(\begin{Bmatrix} \dot{q}_{c_1} \\ \dot{q}_{c_2} \end{Bmatrix} - \mathrm{j}\Omega \begin{Bmatrix} q_{c_1} \\ q_{c_2} \end{Bmatrix} \right) \\ & - \begin{bmatrix} \frac{R_1}{L_1} + \mathrm{j}(p_1 - 1)\Omega & 0 \\ 0 & \frac{R_2}{L_2} + \mathrm{j}(p_2 - 1)\Omega \end{bmatrix} \begin{Bmatrix} F_{q_1} \\ F_{q_2} \end{Bmatrix} \end{aligned} \tag{6.20}$$

In the previous equation (Eq. (6.20)) the displacements and speeds make reference to those given by Eq. (5.11).

The state-space model describing the dynamics of the overall system that couples Eqs. (6.18), (6.19), and (6.20), can be defined as:

$$\begin{Bmatrix} \ddot{q} \\ \ddot{\phi} \\ \ddot{q}_{s_1} \\ \ddot{q}_{s_2} \\ \dot{q} \\ \dot{\phi} \\ \dot{q}_{s_1} \\ \dot{q}_{s_2} \\ \dot{F}_{q_1} \\ \dot{F}_{q_2} \end{Bmatrix} = \mathbf{A} \begin{Bmatrix} \dot{q} \\ \dot{\phi} \\ \dot{q}_{s_1} \\ \dot{q}_{s_2} \\ q \\ \phi \\ q_{s_1} \\ q_{s_2} \\ F_{q_1} \\ F_{q_2} \end{Bmatrix} + \mathbf{B} \left\{ F_{\text{ext}} \right\}. \tag{6.21}$$

The dynamic matrix $\mathbf{A}$ of this system is:

$$\mathbf{A} = \begin{bmatrix} \mathbf{M}^{-1}(-\mathbf{C} + \mathrm{j}\Omega\mathbf{G}) & & [0]_{2\times6} & & -\mathbf{M}^{-1}\mathbf{T} \\ [0]_{2\times2} & -\mathbf{M}_s^{-1}\mathbf{C}_s & [0]_{2\times2} & -\mathbf{M}_s^{-1}\mathbf{K}_s & \mathbf{M}_s^{-1} \\ \mathbf{I}_{4\times4} & & & [0]_{4\times6} & \\ \mathbf{K}_{\text{EDB}}\,\mathbf{T}^T & -\mathbf{K}_{\text{EDB}} & \mathrm{j}\Omega\mathbf{K}_{\text{EDB}}\,\mathbf{T}^T & -\mathrm{j}\Omega\mathbf{K}_{\text{EDB}} & -\mathbf{D}_{\text{EDB}} \end{bmatrix} \tag{6.22}$$

where the submatrices that compose the model are defined as:

$$\mathbf{M} = \begin{bmatrix} m & 0 \\ 0 & J_t \end{bmatrix} \qquad \mathbf{C} = \begin{bmatrix} c & 0 \\ 0 & c_\phi \end{bmatrix} \qquad \mathbf{G} = \begin{bmatrix} 0 & 0 \\ 0 & J_p \end{bmatrix}$$

$$\mathbf{M}_s = \begin{bmatrix} m_s & 0 \\ 0 & m_s \end{bmatrix} \qquad \mathbf{C}_s = \begin{bmatrix} c_s & 0 \\ 0 & c_s \end{bmatrix} \qquad \mathbf{K}_s = \begin{bmatrix} k_s & 0 \\ 0 & k_s \end{bmatrix}$$

$$\mathbf{K}_{\text{EDB}} = \begin{bmatrix} (p_1 - 1)\frac{\Lambda_{0_1}^2}{L_1} & 0 \\ 0 & (p_2 - 1)\frac{\Lambda_{0_2}^2}{L_2} \end{bmatrix} \quad \mathbf{D}_{\text{EDB}} = \begin{bmatrix} \frac{R_1}{L_1} + \mathrm{j}(p_1 - 1)\Omega & 0 \\ 0 & \frac{R_2}{L_2} + \mathrm{j}(p_2 - 1)\Omega \end{bmatrix}.$$

6.2.1 Rotordynamic stability

The state space model of Eq. (6.21) considers the dynamic model derived in chapter 3 to represent the electromechanical interaction inside the electrodynamic bearing. For this reason, analogously to what presented in chapter 5, the rotor's stability can be analysed by means of a root loci plot. The difference in this case is the possibility of analysing the behaviour of conical modes and the influence of gyroscopic effect on the rotordynamic stability.

The root loci of Fig. 6.6 evidences the presence of three poles having positive real parts. The red and brown curves are related to poles that become stable at high rotational speeds, whereas the blue curve does not become stable even at higher speeds. Analysing the decay rate in Fig. 6.7 it is clear how the blue curve never

becomes stable. This influence of gyroscopic effect in the stability is a problem that has never been dealt with before in the literature of electrodynamic bearings. We can see on the Campbell diagram of the rotor's modes only, shown in Fig. 6.8, that the unstable mode is a conical forward mode.

The cause of this instability is the effect of rotating damping in supercritical regime. The rotating damping is destabilizing in this condition. Typically this phenomenon is demonstrated for the cylindrical modes using a Jeffcott rotor model [47], hence the effects on higher frequency rotor modes cannot studied. It is nevertheless interesting to notice how in the particular case under study (rotor - EDB - elastic base), the noticeable presence of rotating damping associated to the relatively low stiffness of the bearing itself leads to a condition where the conical mode of the 4DOF model is always unstable.

From the technical point of view it is natural that the unstable conical mode must be made stable to make the radial electrodynamic suspension feasible and useful. The stabilizing system using elastic connections between bearing's stator and case is very efficient to stabilize the cylindrical modes, but is ineffective on the conical mode. Given that, the simplest way to stabilize the conical mode is to use gyroscopic moments. Similar concept has proven useful with the Levitron toy [55], but in the present case the applicability can prove much more interesting as there is no upper boundary for the stability.

In this case, stability of the conical mode can be guaranteed if the conical mode is always subcritical, hence the rotating damping has a stabilizing effect on this mode. With reference to Fig. 6.8, this is achieved once the slope of the line $\omega = \Omega J_p/J_t$ is higher than that of the line $\omega = \Omega$. It cannot be neglected that this condition imposes heavy limitations on the possible applications of the electrodynamic suspensions. The conditions described to achieve stability with this method require the rotor to have the polar moment of inertia J_p greater than the transversal moment of inertia J_t which is a common condition for flywheels, but not for the majority of high speed applications.

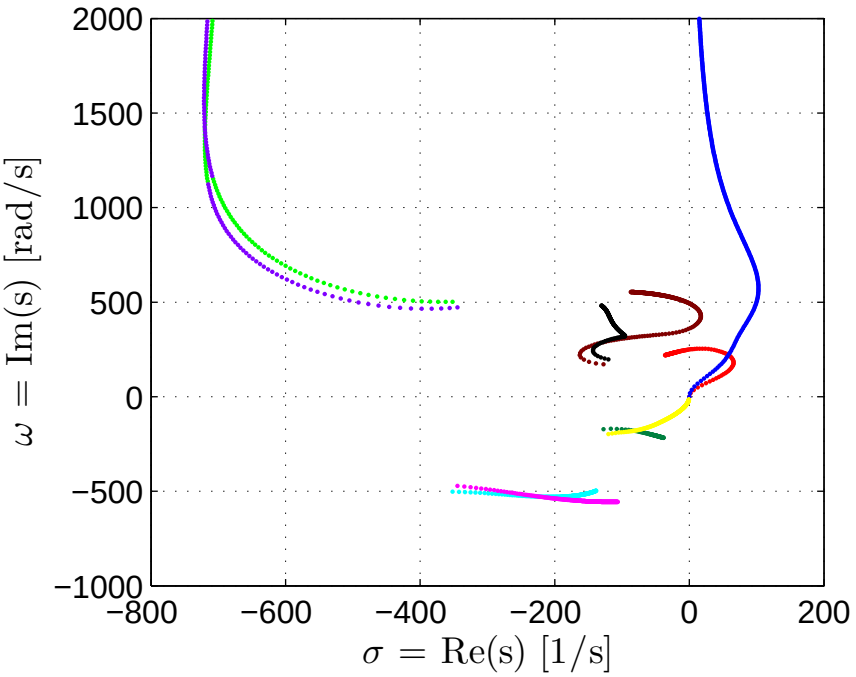

Figure 6.6. Root loci plot of the poles of a 4 degree of freedom rotor supported by homopolar electrodynamic bearings.

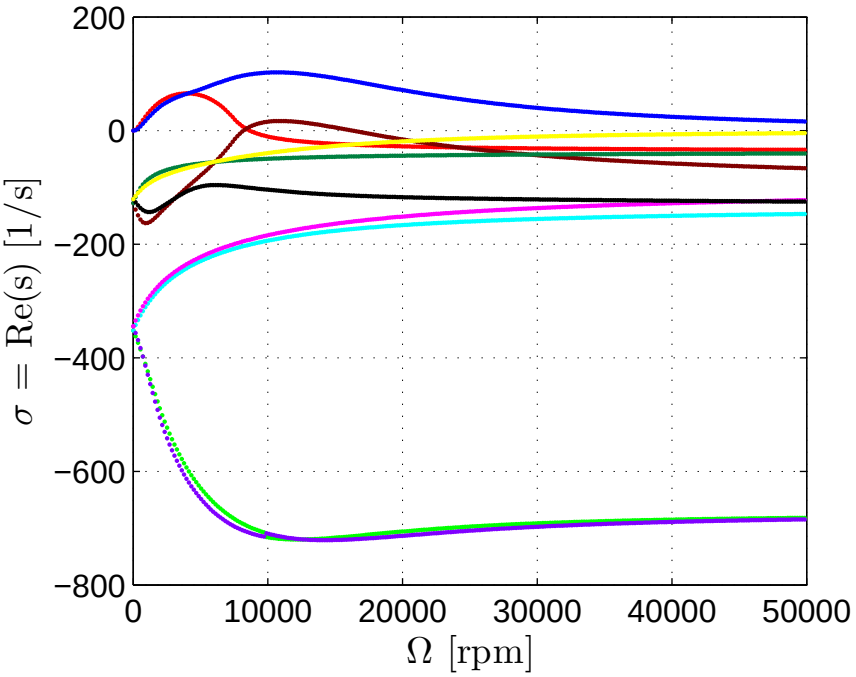

Figure 6.7. Decay rate plot of the poles of a 4 degree of freedom rotor supported by homopolar electrodynamic bearings.

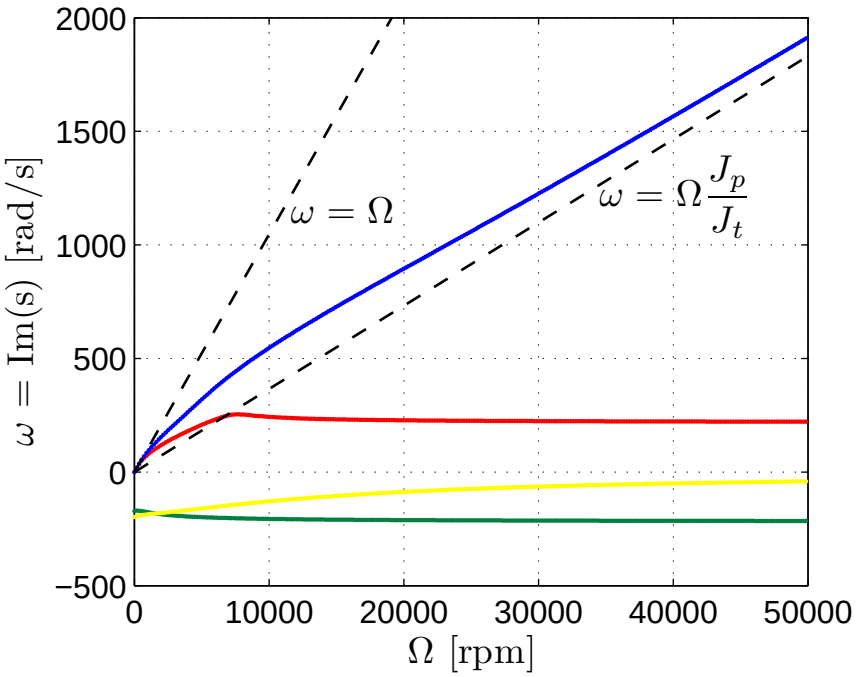

Figure 6.8. Campbell diagram of the rotor modes of a 4 degree of freedom rotor supported by homopolar electrodynamic bearings.

Part III

Test rig of a rotor on homopolar electrodynamic bearings

Chapter 7

Test rig design

Even though the working principle of electrodynamic bearings seem simple and straightforward, leading to promising characteristics, the design of a rotor running exclusively on electrodynamic radial bearings is a challenging task. As presented in the previous chapters, the electromagnetic interaction between rotor and stator gives place to intrinsically unstable rotor modes that must be dealt with.

Another difficulty introduced in the design phase is due to the strong coupling between the properties of all subsystems. Every subsystem, being either rotor, stator, or electrodynamic bearing, contribute substantially to the stability. Moreover, the passive nature of the suspension does not allow any correction of a parameter once the system is built. For this reason an accurate definition of each parameter is of major importance during the dimensioning and design phases.

The objective of this chapter is to present the design phases of a test rig implementing the concepts presented in the previous chapters. The test rig is devised to obtain stable radial levitation of a rotor using exclusively radial electrodynamic bearings. The design of the EDB is carried ou by means of finite element (FE) simulations of the electromagnetic field. The stabilization system implementing the concept presented in Sec. 5.3 is also presented. Experimental results are used to validate each phase of the design.

7.1 Electrodynamic Bearing

The design of the electrodynamic bearing is one fundamental part of the design of the suspension. As stated previously, it cannot be decoupled from the design of the rest of the system, therefore the final set of properties of the electrodynamic bearing can only be defined after an iterative process. Currently the first step of this process must be done in a trial and error basis without any clear guideline; an initial geometry that respects the mechanical constraints is chosen and FE analysis

is carried out to evaluate the properties. Refinements are performed subsequently after each iteration.

7.1.1 Finite element modelling

The design of the bearing is developed mainly by means of finite element simulations of the electromagnetic field generated by the motion of the conductor inside the stationary magnetic field. The equations governing this system can be solved by many commercial finite element codes; different numerical schemes to solve the formulation of the eddy current problem inside solid conductors are presented by Albertz *et al.* [36] and Rodger *et al.* [37] and won't be addressed here. Instead, a brief description of the simulation process is given, pointing out the steps taken in order to produce the results and what is expected from the finite element models.

An extensive discussion on the most important aspects to be taken into account when realizing this kind of finite element simulation can be found in the work of Lembke [30].

In particular for this application, COMSOL Multiphysics has been chosen for it is capable of solving the eddy currents in quasi-stationary conditions directly, without the necessity of time-stepping simulations. The main objective of the finite element simulations is to allow identifying the macroscopic electromechanical parameters describing the dynamics of the interaction between rotating conductor and stationary magnetic field. The identification of these parameters can be done with the help of the quasi stationary working condition. This particular operating condition has been described in chapter 3; as mentioned there, it can be reproduced easily both experimentally and numerically using finite element models.

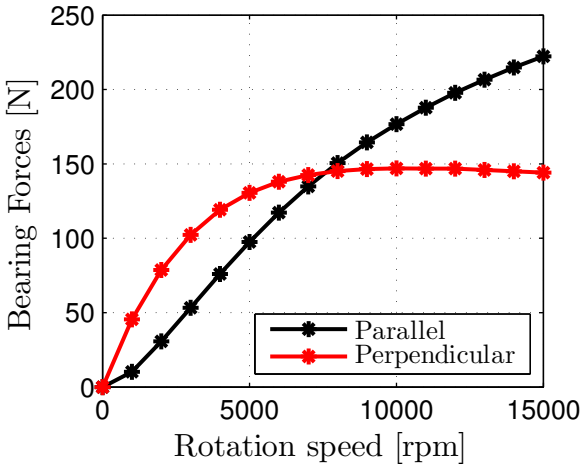

Figure 7.1. Quasi stationary force curves obtained using a finite element model.

The quasi stationary condition consists in fixing the rotor's spin speed and the position of the conductor's rotation axis with respect to the symmetry axis of the magnetic field. It is fundamental that the axis of rotation does not coincide with the axis of symmetry of the magnetic field. In this condition a force is developed between conductor and magnetic field. The finite element model allows calculating the value of the components of this force, and applying a curve fitting tool on Eq. (4.3) and FE results it is possible to identify the model's parameters. Because the homopolar bearing is realized using solid conductors and the concepts of resistance and inductance cannot be applied directly, we recall Eq. (4.1).

$$k = \frac{\Lambda_0^2}{L}$$
$$c = \frac{\Lambda_0^2}{R}.$$

This equation relates the flux constant, the inductance, and the resistance of the conductors allowing to express them in terms of two mechanical equivalent quantities [28] without any loss of validity of the modelling procedure presented previously.

From the simulation point of view, the definition of the models requires defining the velocity field of the rotating conductor. But, as mentioned previously, no real motion of the mesh is required. One simulation must be produced for each value of spin speed, and the forces acting in the rotating conductor are calculated using the Lorentz force formula. The results expected from the FE models are shown in Fig. 7.1.

To obtain good approximations of these results special attention must be given to the meshing of the conducting disc and air gap. First of all, as suggested by Lembke [30], tetrahedral and wedge elements should be avoided. These two types of elements introduce instabilities in the solution of the electric currents. Bondeson *et al.* [56] explains that 'eddy current calculations are more frequently carried out on hexahedral meshes than on tetrahedral ones. One reason for this is that eddy current problems often involve currents in thin layers, within the skin depth of conductor surfaces. The skin depth is typically in the millimetre to centimetre range, which is small compared to the global dimensions of a motor, generator, or transformer. Therefore, high resolution is required in the direction normal to the surface of a conductor, whereas the resolution requirement in the perpendicular direction can be much less demanding. This anisotropy is easier to achieve on a hexahedral mesh than a tetrahedral one'.

Although the electrodynamic bearing does not fall within the categories mentioned by Bondeson *et al.*, their analysis correctly apply also in this case. This can be noticed comparing the solutions of a model built using tetrahedral elements (Fig.

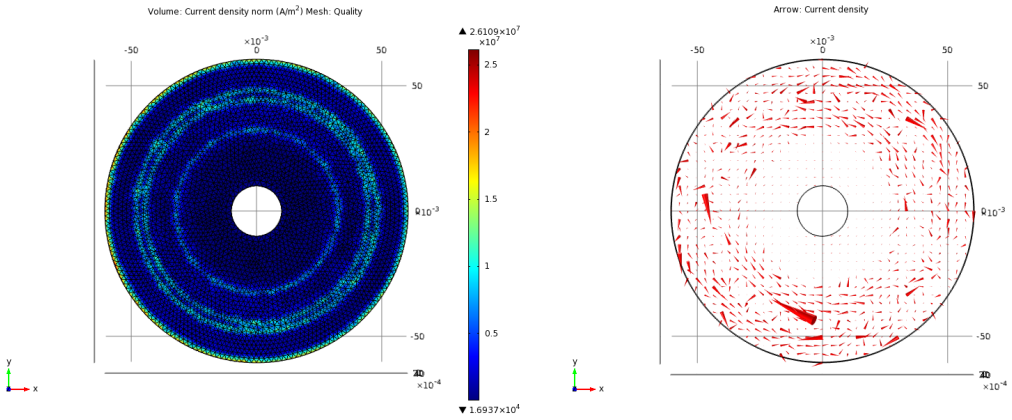

(a) (b)

Figure 7.2. Finite element solution using tetrahedral elements on conducting disc domain.

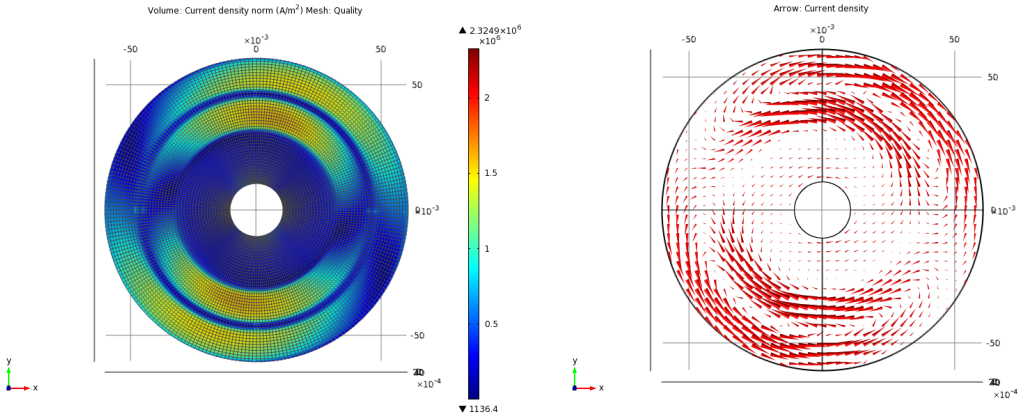

(a) (b)

Figure 7.3. Finite element solution using hexahedral elements on conducting disc domain.

7.2) and another using exclusively hexahedrons (Fig. 7.3) on the conductor domain. The arrow representation of the current density in both cases shows the main current path, but the solution produced by the tetrahedral mesh introduces undesired fake currents. These currents disturb the calculation of the forces with the finite element model giving place to unreal values of forces.

The models used on the analyses are obtained producing an accurate mesh of one section of the model and revolving it around the axis of symmetry, producing a mesh composed by hexahedral elements and some wedge elements in parts where accuracy requirements are less demanding. After the meshing is complete, a virtual

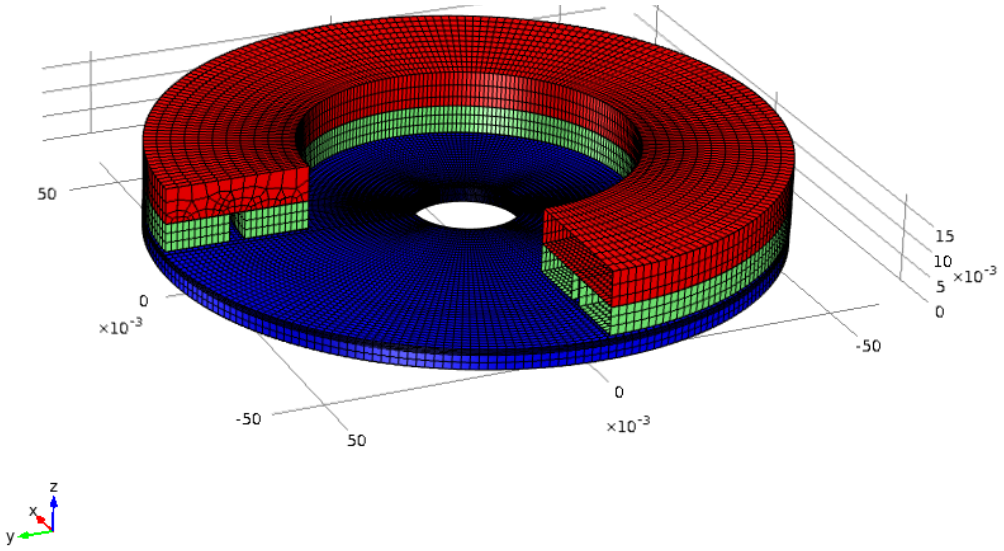

Figure 7.4. Finite element model of the double flux configuration of homopolar electrodynamic bearing.

displacement is imposed on all nodes of the conducting disc domain. It is also important to introduce eddy layers of elements in the upper part of the conducting disc to allow capturing the occurrence of skin effect accurately. Taking advantage of symmetry planes is also a relevant step; in this case study there is one anti-symmetry plane that can be considered. An example of mesh produced taking into account of the most important guidelines found in literature is shown in Fig. 7.4.

7.1.2 Sensitivity analysis and dimensioning of the bearing's components

To the present day there exists no reference for the initial dimensioning of a magnetic suspension using electrodynamic bearings. This means that there is no method to estimate the parameters of the bearing for a given geometry. For this reason the design phase requires a long sensitivity analysis where the finite element models are associated to the state-space model of the suspension given by Eq. (5.13). The overall influence of its parameters on the system can be understood and evaluated. This study of the whole system is also used to identify the properties of the elastic connection between EDB's stator and basing that optimize the suspension's behaviour in terms of stability.

To define the final geometry of the electrodynamic bearing, many analyses are carried out to find the most suitable configuration within feasible geometries. A reference model shown in Fig. 7.5 was defined to guide the analysis. The main

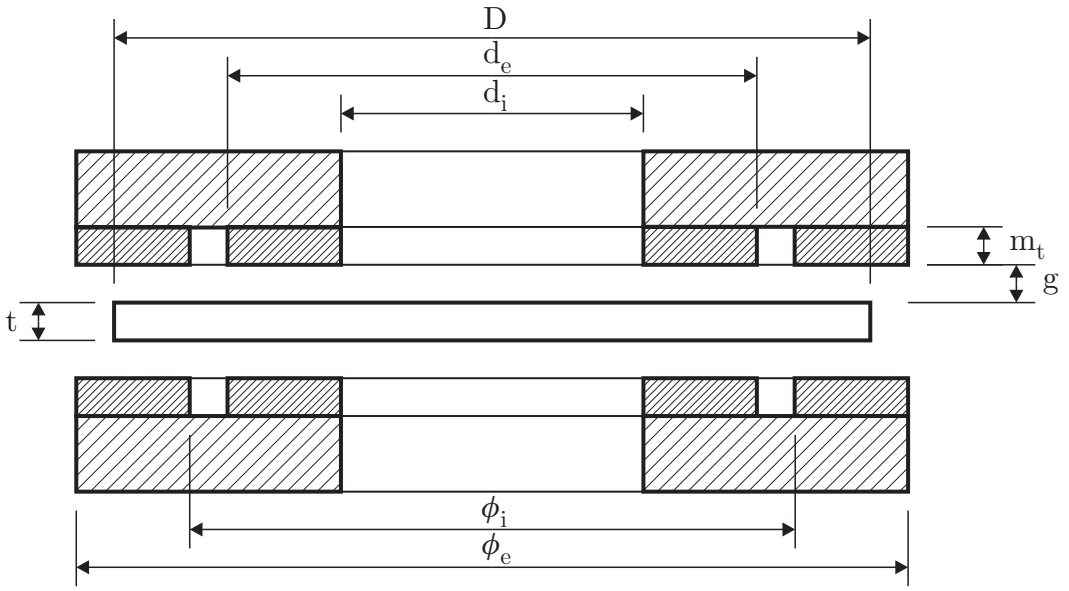

Figure 7.5. Reference model for design and sensitivity analysis of the mechanical properties of the electrodynamic bearing.

geometric parameters are shown in the quotations; a series of different configurations were tested varying one parameter each time. The geometrical values of the parameters of each configuration studied are summarized in the table below each figure from Fig. 7.6 to Fig. 7.21.

The dimensioning of the elastic connection is crucial because it works as stabilization system, as described in Sec. 5.3. For this reason the dimensioning of the parameters is difficult since for each different bearing configuration the rotor and stator masses must be updated and introduced in the model, and the characteristics of the stabilization system are calculated.

A simple strategy to devise the elastic connection of the stabilization system is to use a viscoelastic material. A relevant aspect in the dimensioning phase is that with the best technological solutions available, a loss factor ranging from 0.6 to 0.84 is achievable. Moreover, the mechanical characteristics of the material taken into consideration doesn't allow to consider a stiffness smaller than 200 kN m^{-1} because the stress on the material can cause excessive displacement due to the weight of the suspended mass and eventually rupture.

Given the above considerations, the eigenvalues of Eq. (5.14) can be obtained for different values of stiffness and damping of the elastic supports and the stabilization speed calculated as the minimal speed for which all roots have negative real parts. The value of stabilization speed threshold can thus be plotted with respect to the characteristic of the stabilization system in a contour map. This kind of map is shown beside the finite element result curves in Fig. 7.6b to Fig. 7.21b. The

different colour regions evidence a region where the stabilization speed threshold is within the values evidenced by the contours. In the figures there is one contour every 5000 rpm. In the same plot the values of the loss factor are also evidenced. The loss factor is approximated with the classical representation for mass-spring-damper oscillating systems as:

$$\eta = \frac{c_s}{\sqrt{k_s m_s}} \tag{7.1}$$

All results from these design and dimensioning phases are shown in the following figures. The final configuration of the prototype is chosen to be configuration 16, whose properties and characteristics are shown in Fig. 7.21. This configuration is chosen because it represents the best compromise between stabilization speed threshold, loss factor and stiffness of the elastic elements, and the electrodynamic bearing's properties. Also the mechanical feasibility of the bearing has been taken into account for this choice.

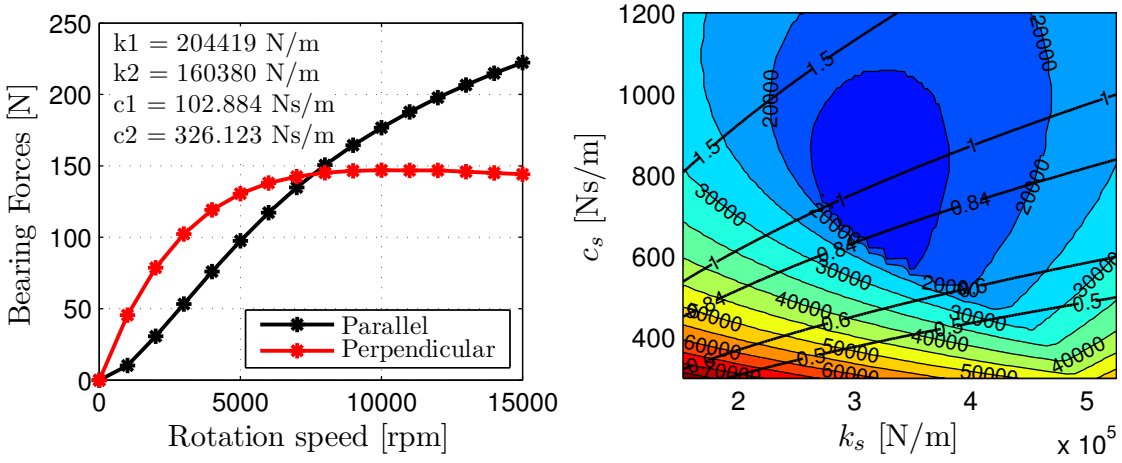

(a) (b)

D	d_e	d_i	ϕ_e	ϕ_i	m_t	t	g
120	92	64	120	92	5.5	6	0.5

Figure 7.6. Electrodynamic bearing in configuration 1.

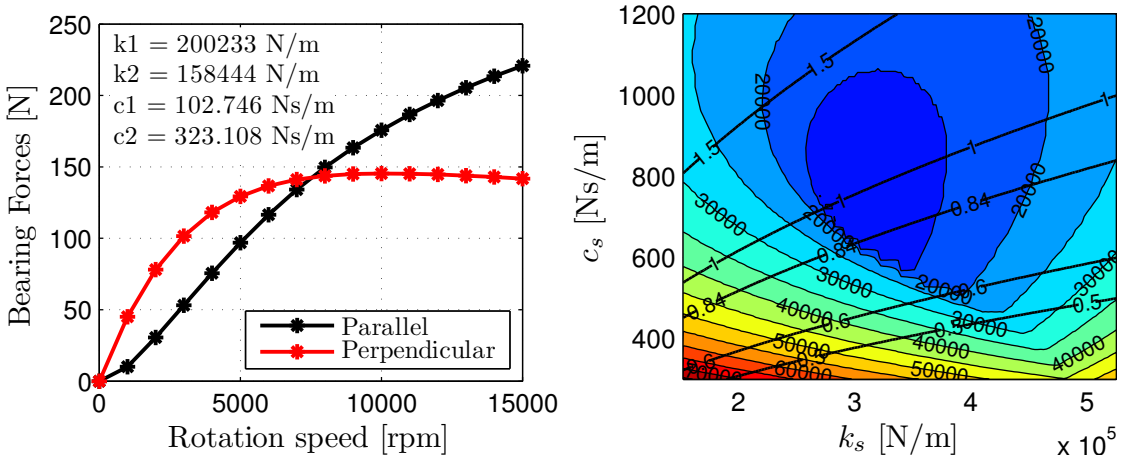

(a) (b)

D	d_e	d_i	ϕ_e	ϕ_i	m_t	t	g
120	91	64	120	93	5.5	6	0.5

Figure 7.7. Electrodynamic bearing in configuration 2.

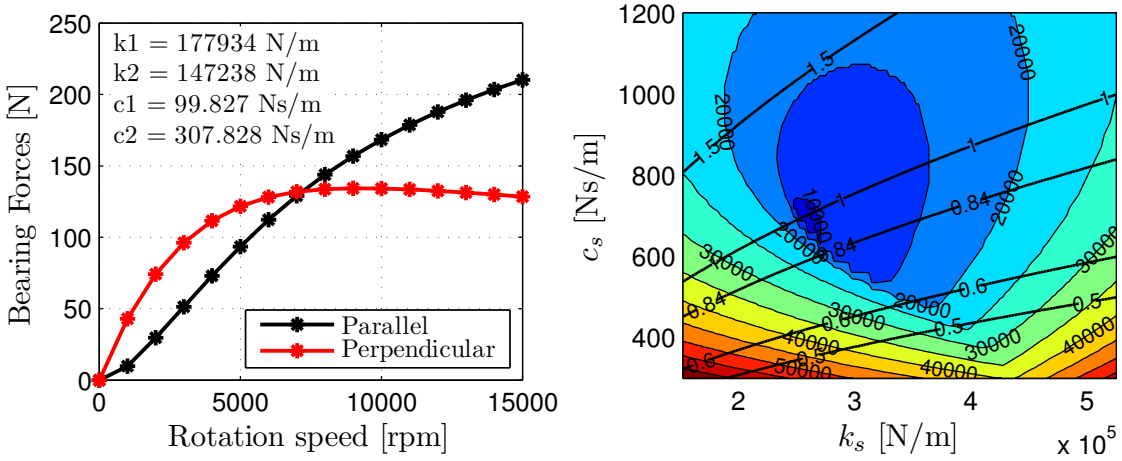

(a) (b)

D	d_e	d_i	ϕ_e	ϕ_i	m_t	t	g
120	89	64	120	95	5.5	6	0.5

Figure 7.8. Electrodynamic bearing in configuration 3.

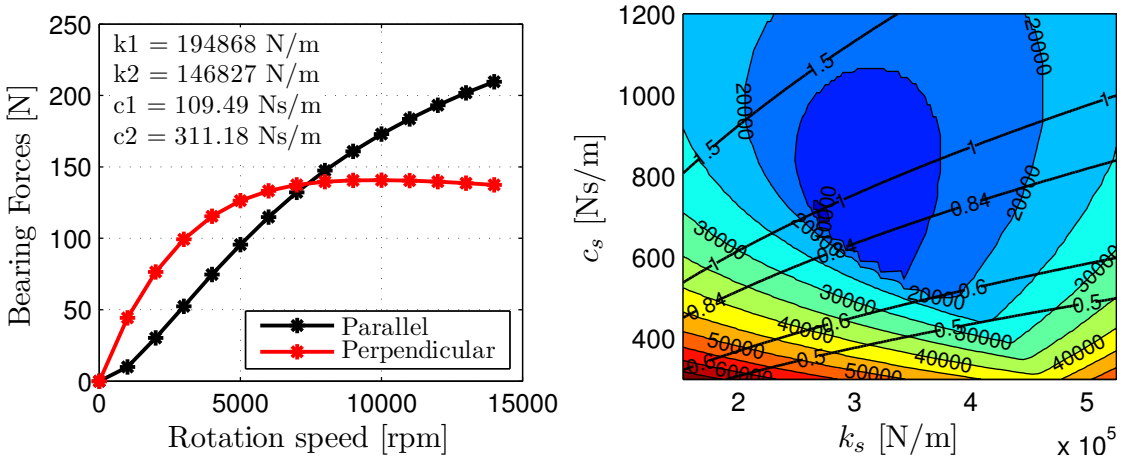

(a) (b)

D	d_e	d_i	ϕ_e	ϕ_i	m_t	t	g
120	90	64	120	94	5.5	6	0.5

Figure 7.9. Electrodynamic bearing in configuration 4.

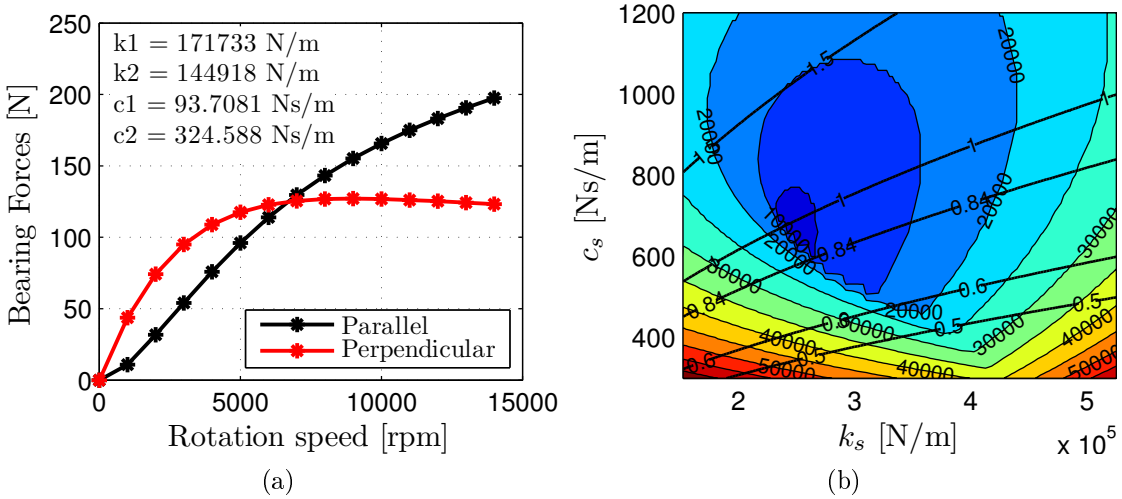

(a) (b)

D	d_e	d_i	ϕ_e	ϕ_i	m_t	t	g
120	90	64	120	94	5.5	7	0.5

Figure 7.10. Electrodynamic bearing in configuration 5.

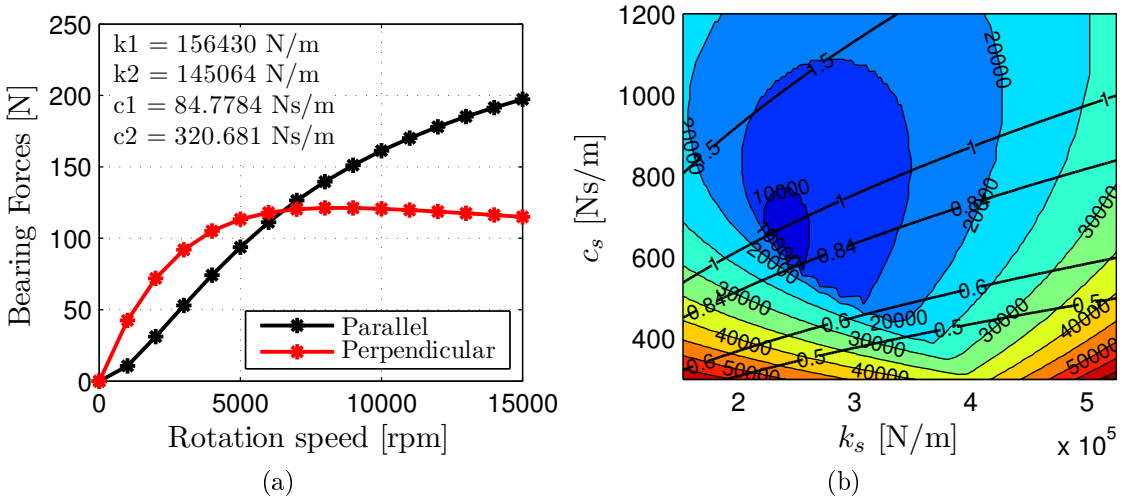

(a) (b)

D	d_e	d_i	ϕ_e	ϕ_i	m_t	t	g
120	89	64	120	95	5.5	7	0.5

Figure 7.11. Electrodynamic bearing in configuration 6.

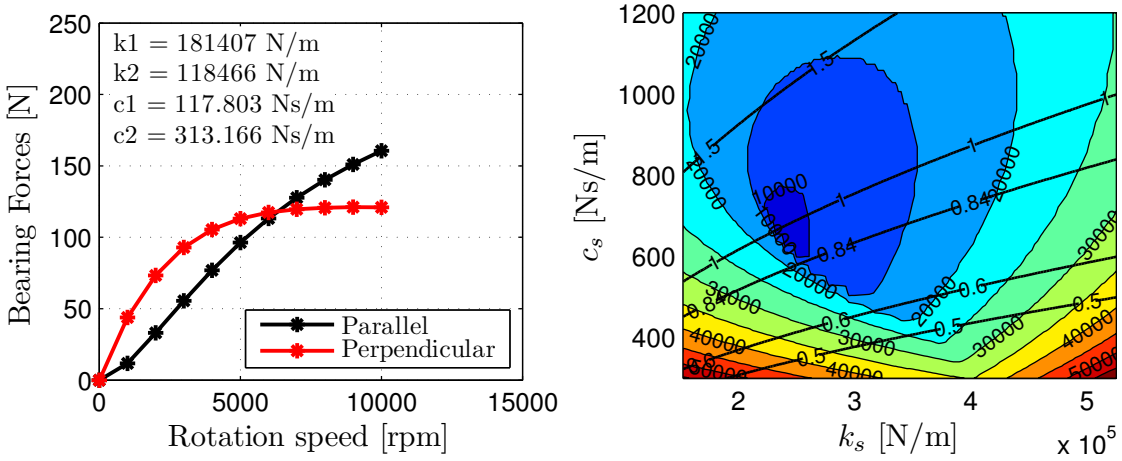

(a) (b)

D	d_e	d_i	ϕ_e	ϕ_i	m_t	t	g
120	92	64	120	92	5.5	8	0.5

Figure 7.12. Electrodynamic bearing in configuration 7.

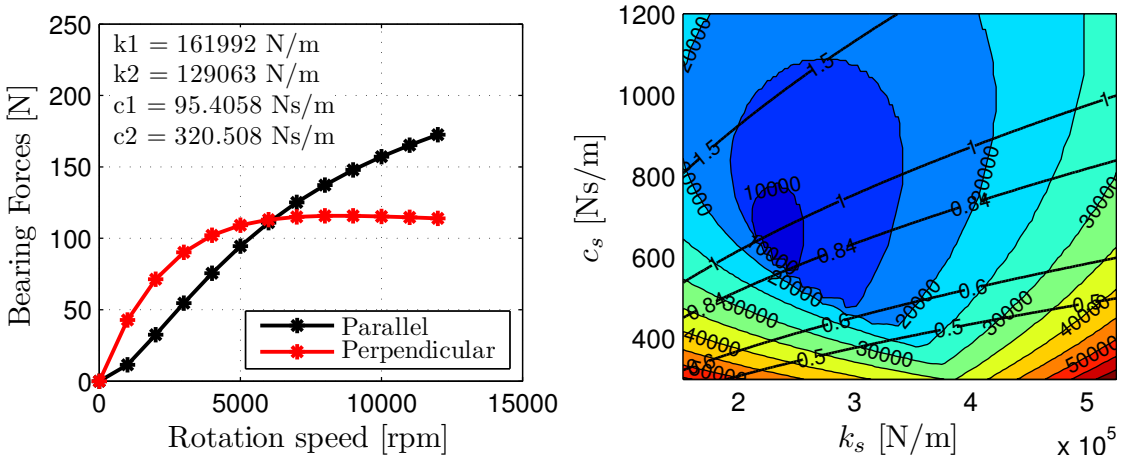

(a) (b)

D	d_e	d_i	ϕ_e	ϕ_i	m_t	t	g
120	90	64	120	94	5.5	8	0.5

Figure 7.13. Electrodynamic bearing in configuration 8.

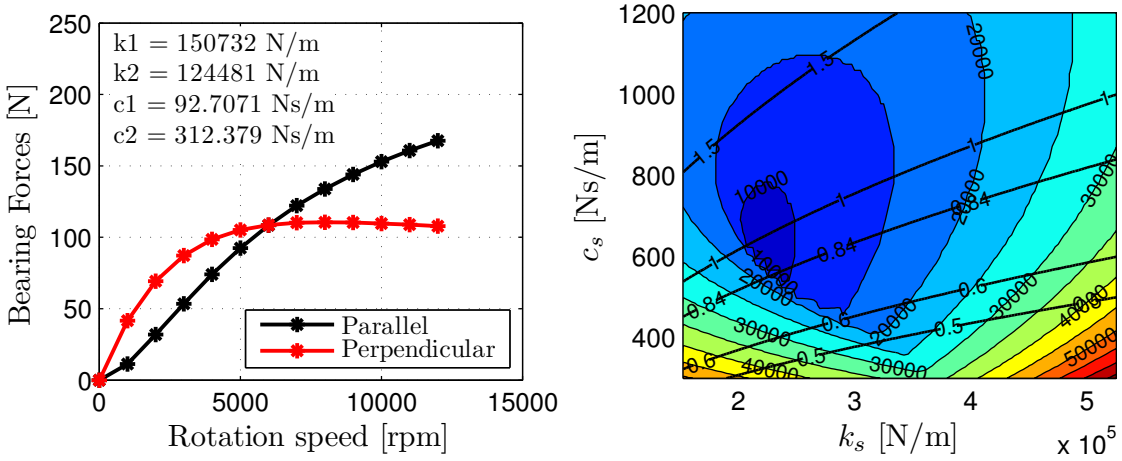

(a) (b)

D	d_e	d_i	ϕ_e	ϕ_i	m_t	t	g
120	89	64	120	95	5.5	8	0.5

Figure 7.14. Electrodynamic bearing in configuration 9.

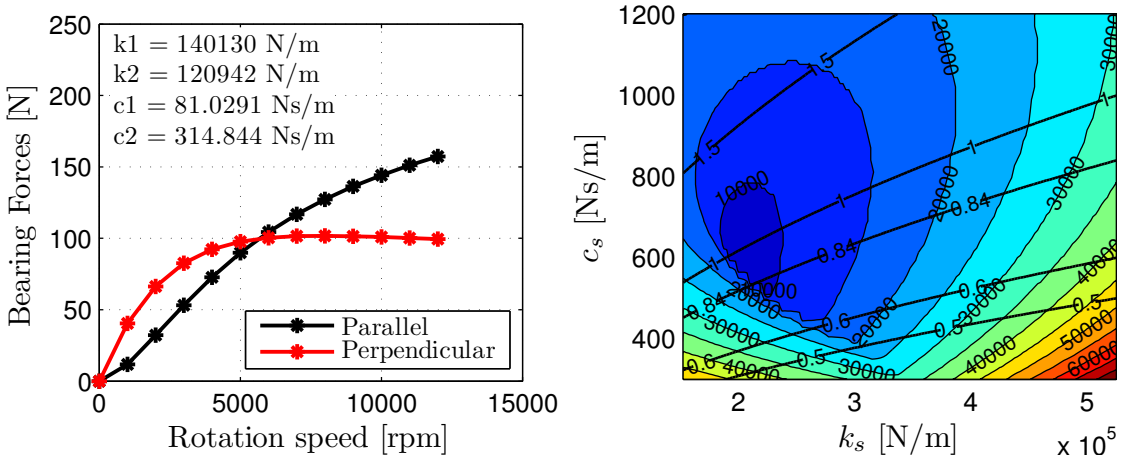

(a) (b)

D	d_e	d_i	ϕ_e	ϕ_i	m_t	t	g
120	89	64	120	95	5.5	9	0.5

Figure 7.15. Electrodynamic bearing in configuration 10.

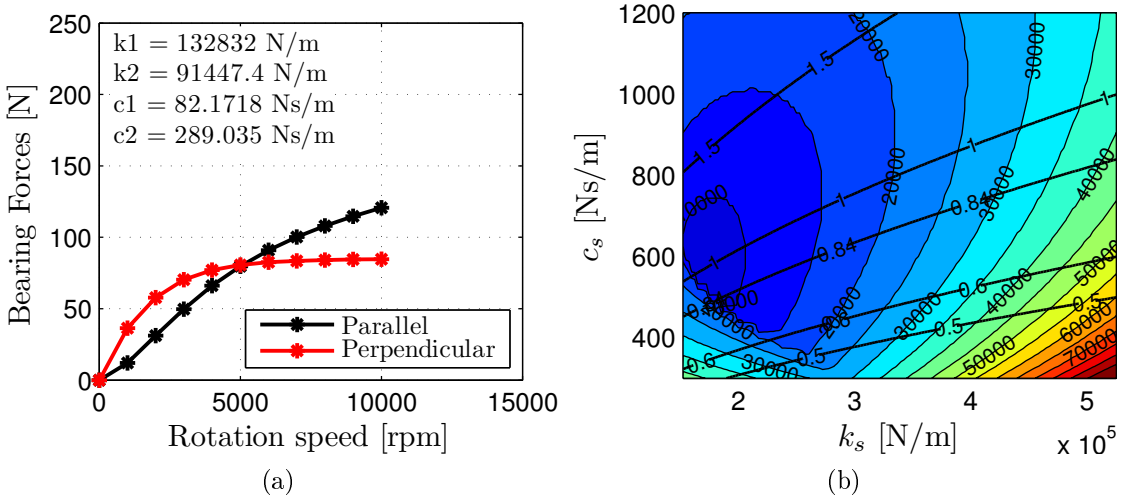

(a) (b)

D	d_e	d_i	ϕ_e	ϕ_i	m_t	t	g
120	89	64	120	95	5.5	12	0.5

Figure 7.16. Electrodynamic bearing in configuration 11.

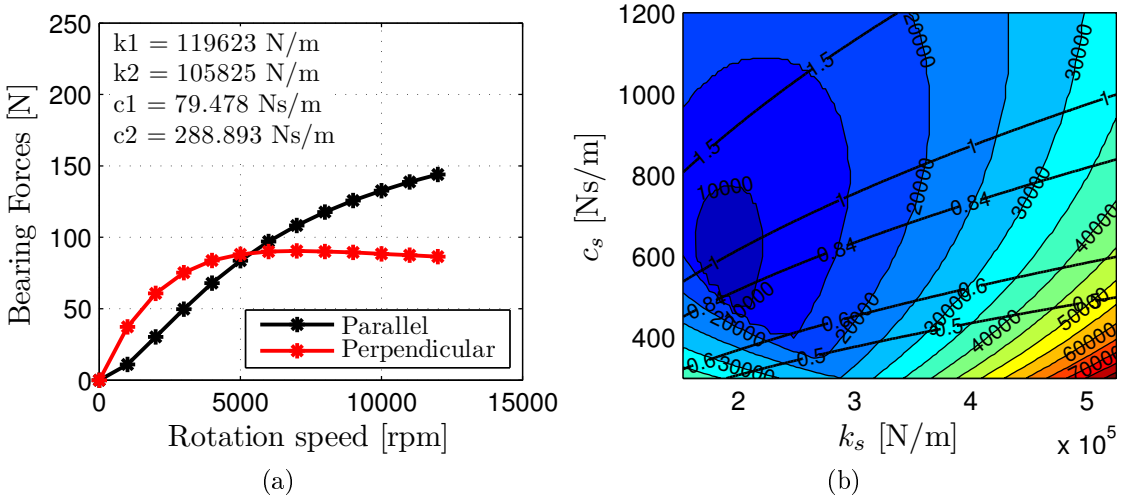

(a) (b)

D	d_e	d_i	ϕ_e	ϕ_i	m_t	t	g
120	87	64	120	97	5.5	9	0.5

Figure 7.17. Electrodynamic bearing in configuration 12.

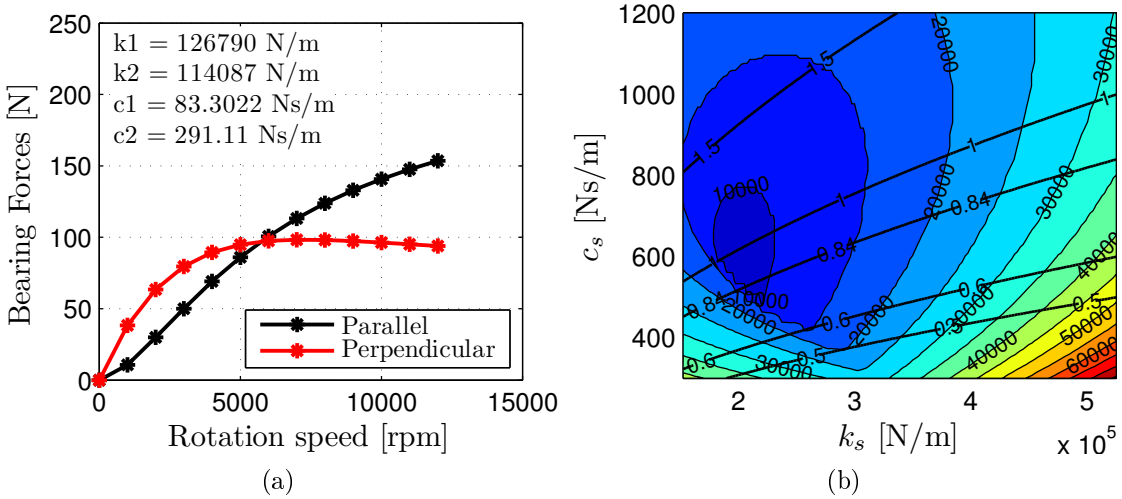

(a) (b)

D	d_e	d_i	ϕ_e	ϕ_i	m_t	t	g
120	87	64	120	97	5.5	8	0.5

Figure 7.18. Electrodynamic bearing in configuration 13.

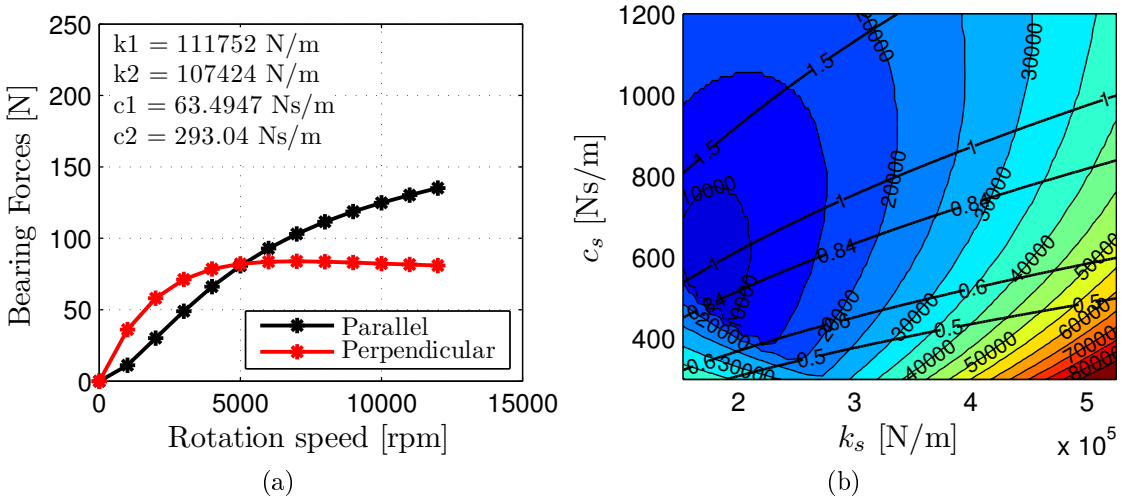

(a) (b)

D	d_e	d_i	ϕ_e	ϕ_i	m_t	t	g
120	87	64	120	97	5.5	10	0.5

Figure 7.19. Electrodynamic bearing in configuration 10.

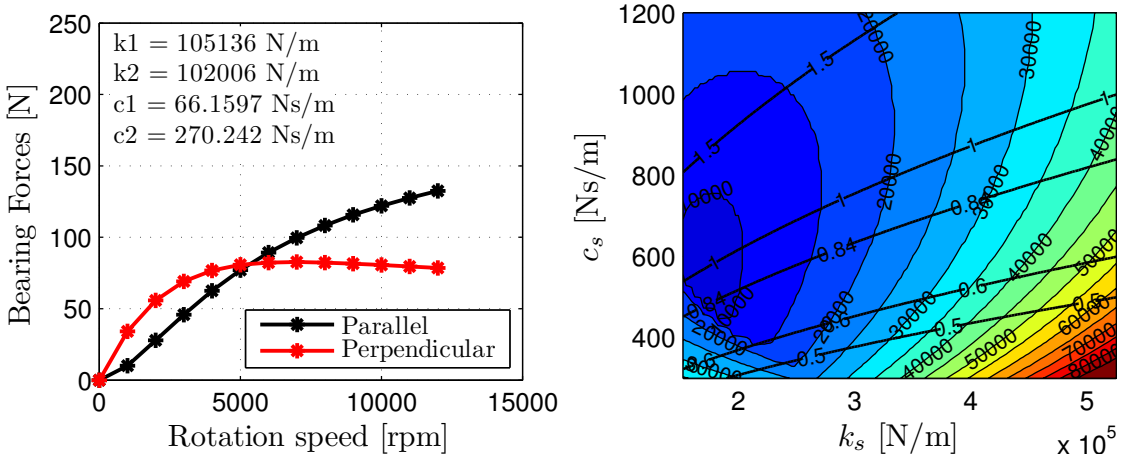

(a) (b)

D	d_e	d_i	ϕ_e	ϕ_i	m_t	t	g
120	87	64	120	97	5.5	10	0.5

Figure 7.20. Electrodynamic bearing in configuration 15.

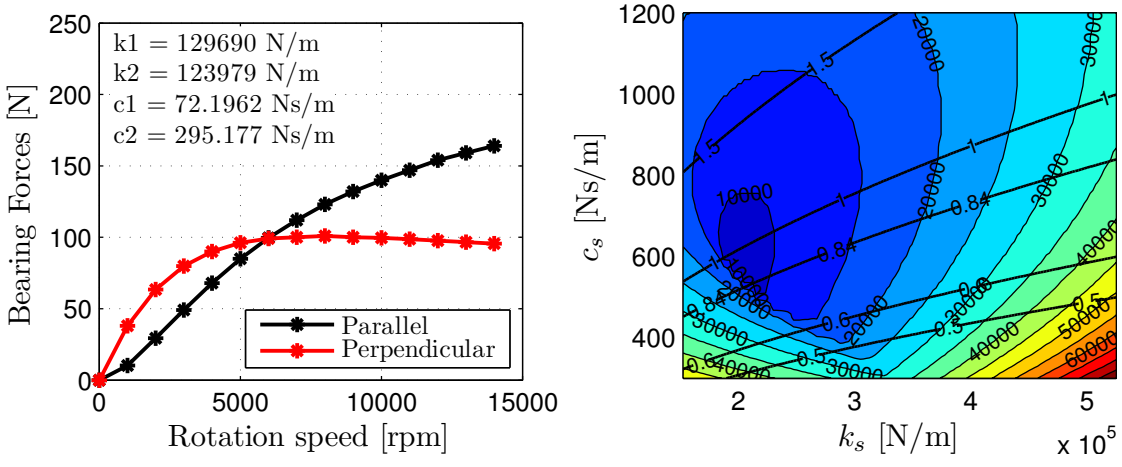

(a) (b)

D	d_e	d_i	ϕ_e	ϕ_i	m_t	t	g
120	89	64	120	95	5.5	8	0.75

Figure 7.21. Electrodynamic bearing in configuration 16.

7.1.3 Flexibility of the rotor

To guarantee the validity of the analyses developed previously it is necessary ensure that the shaft behaves as a rigid body inside the working range of speed. To this end a finite element rotordynamic analysis of the shaft taking into account the masses of the bearing's and motor's discs can be performed. The Dynrot 8.3 Matlab toolbox for rotordynamics developed at Politecnico di Torino has been used to perform the analysis. The analysis is performed considering a rotor that is already the result of the mechanical feasibility study that is presented in sec. 7.3. Assuming that the motor's disc, EDB's disc, and washers, do not contribute substantially to the mechanical stiffness of the shaft, but strongly affect the mass properties, they are

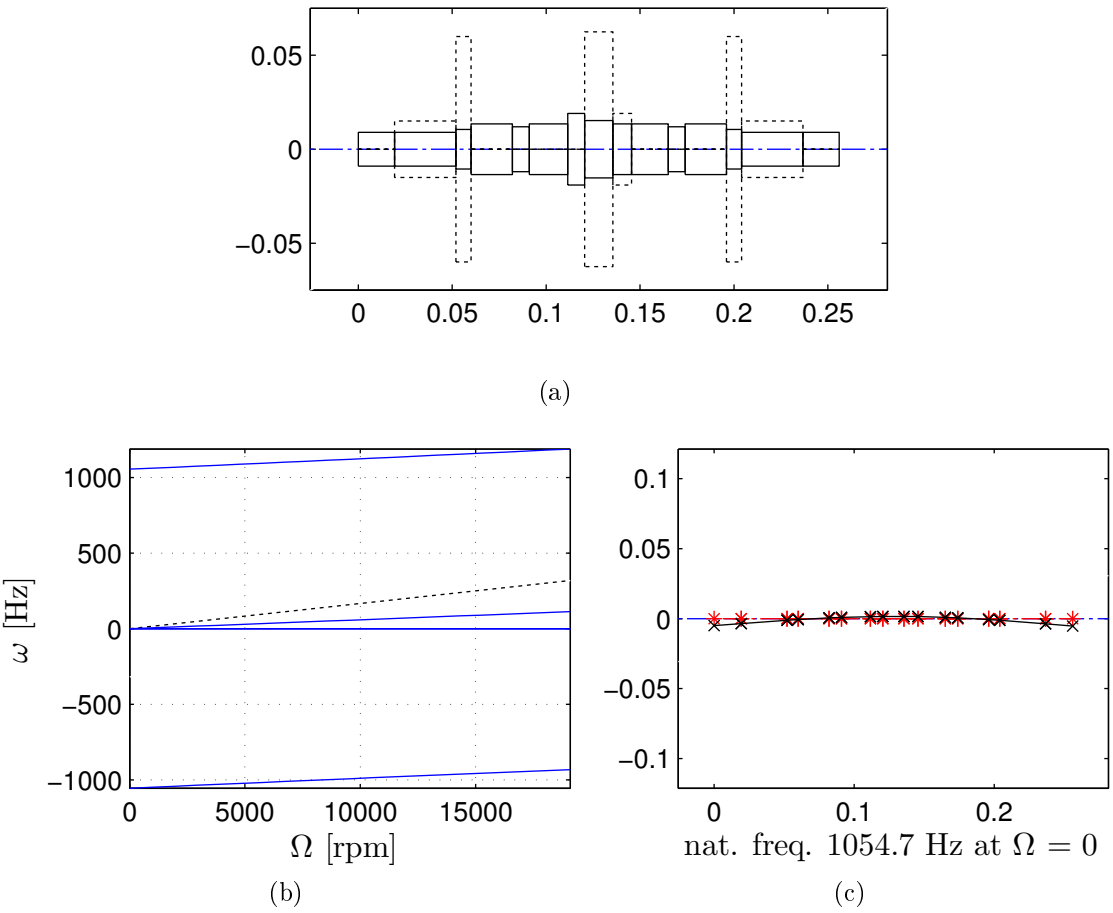

Figure 7.22. Finite element rotordynamic analysis of the shaft. a) FE model of the shaft; b) Campbell diagram of the first 3 natural frequencies; c) modal shape of the first bending mode of the shaft.

modelled as non-structural elements. This assumption is nevertheless conservative as it should reduce the values of the natural frequencies. Figure 7.22a shows the FE model evidencing the structural elements with bold lines and non-structural ones with dashed lines.

The Campbell diagram presented in Fig. 7.22b evidences that the natural frequency of the first bending mode of the shaft is 1054.7 Hz, and is well above the line $\omega = \Omega$; the relative mode shape is displayed in Fig. 7.22c. Since the operating speed of this shaft ranges from 15000 to 20000 rpm, any flexural behaviour of the shaft during operation is excluded, thus confirming the validity of the models used in the previous analyses.

7.2 Stabilization system

In past research on electrodynamic bearings the rotordynamic stability has been of great concern. A stabilization system is an important part of the test rig. It is the structure responsible for introducing the non-rotating damping that stabilizes the lateral dynamics of the shaft.

The structure is designed relying on viscoelastic materials to introduce the stiffness and damping needed. The use of viscoelastic materials in this case reduces the complexity of the system because damping and stiffness are associated with one single mechanical component of simple manufacturing, thus convenient for a prototype. An alternative is to use fluid film dampers or electromagnetic dampers associated with mechanical springs, but in both cases the system gains in complexity.

To build the test rig a material commercially available under the name An-Vi was chosen. This material presents outstanding damping characteristics, having a rather robust structure. A qualitative comparison of its properties with respect to those of other common viscoelastic materials is shown in Figs. 7.23a and 7.23b. In Fig. 7.23c the real pieces of the AN-VI material are shown. Cube shaped samples with shore hardness ranging from 36 to 65 are available. Bearing in mind the physical properties of the material while analysing the stabilization speed maps presented in sec. 7.2, it is possible to define a region of physically feasible systems within those studied. In Fig. 7.24 this region is evidenced by the white ellipse.

In order to have a preliminary evaluation of the damping properties of this material, an impact test was conducted. During the test a known mass connected to the basing using the very same method intended for the test rig is hit with an instrumented hammer, and the accelerations of the mass are measured. The results were compared to those of an analytical model of a simple mass-spring-damper, where stiffness and damping were identified in order to fit the experimental results. This method for characterizing the material represents an oversimplification as the test sample is not subject to a sinusoidal excitation, but, for this design phase is an

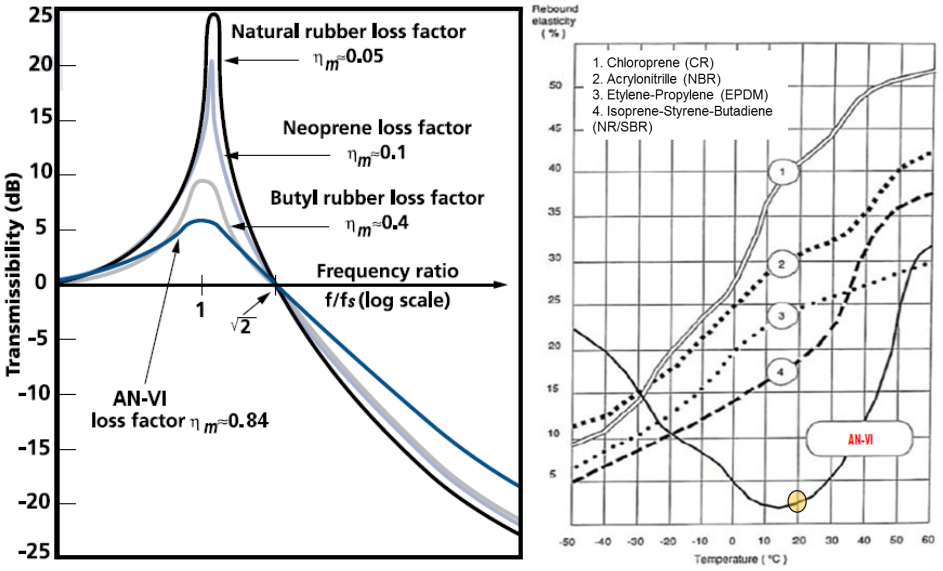

(a) (b)

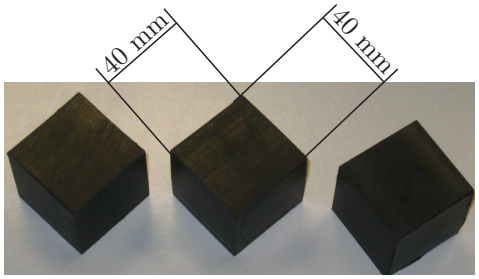

(c)

Figure 7.23. Characteristics of AN-VI material. a) and b) Qualitative comparison of the damping properties of AN-VI material with respect to other common viscoelastic materials; c) Presentation of the material in cubes.

acceptable method. Figure 7.25 shows the comparison between experimental and analytical results.

One important aspect to be considered when using viscoelastic dampers is that the material usually works better when working under shear loads. For this reason a configuration where the elastic connections between stator of electrodynamic bearing and casing of the machine work manly under shear stress is designed.

At this point, this data can be used to define the geometry of the element connecting the stator of the electrodynamic bearing to the case of the machine. The stiffness of the elastic connections is calculated considering that the material is submitted to pure shear as:

$$k_{\text{stab}} = \frac{AG}{l}, \tag{7.2}$$

where A and l are the cross section area and length of the connecting element, respectively, and G is the shear modulus of the material.

The final layout of the electrodynamic bearing implementing the solution of Fig. 7.21 and the stabilization system described is shown in Fig. 7.26.

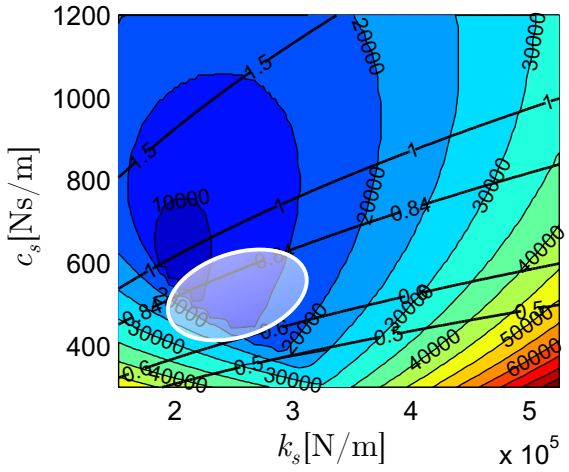

Figure 7.24. Stabilization speed map. The area beneath the white ellipse represents the points of interest that are physically feasible with the current technology.

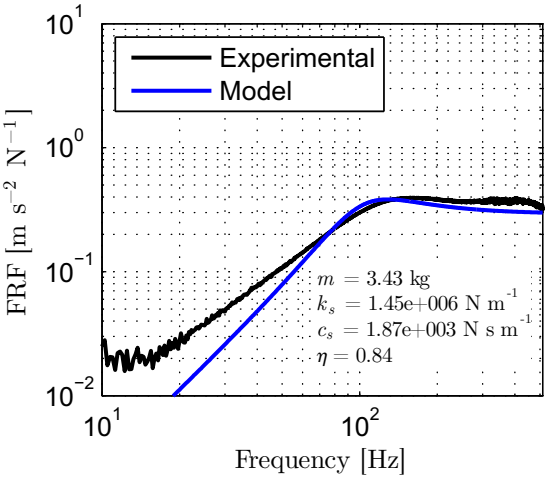

Figure 7.25. Experimental measurement and comparison with a simplified model of the dynamic characteristics of a support using An-Vi material.

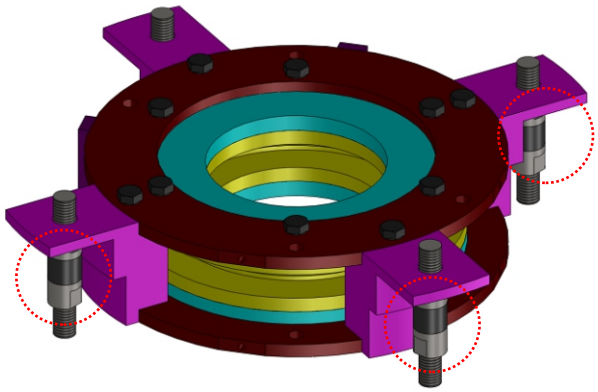

Figure 7.26. Final mechanical layout of the stator of the electrodynamic bearing and the elements of viscoelastic material of the stabilization system.

7.3 Mechanical layout

In the previous sections of this chapter the properties and mechanical layout of the main components of the electrodynamic suspension have been defined. This section presents the mechanical layout of the whole test rig designed to test the feasibility of passive radial electrodynamic levitation. The mechanical layout is defined trying to keep it close to that of a real application specially concerning the dimensions and mass of the rotating part.

The main characteristics expected from this prototype are:

- Realize passive radial levitation relying exclusively on electrodynamic bearings.
- Operating speed range 15000 to 20000 rpm.
- Stabilization system based on the use of elastic connections between bearing's stator and machine case.
- Non rotating damping introduced by means of a viscoelastic element.
- Possibility of monitoring the rotordynamics with position probes.
- Possibility of monitoring the electrodynamic bearing's stator with accelerometers.

Since the EDB system cannot provide levitation forces at zero spin speed, a disengaging mechanical system using regular ball bearings supports the rotor until operating speed is reached. Above this speed the system is stable and can run virtually at any speed within the constraints imposed by the material's mechanical

Table 7.1. Main parameters of the electrodynamic bearing test rig.

Parameter	Symbol	Value	Unit
Mass	m	4.05	kg
Polar moment of inertia	J_p	$5.69e-3$	kg m^2
Transversal moment of inertia	J_t	$16.26e-3$	kg m^2
Electrodynamic bearing stator's mass	m_s	1.90	kg
Distance between bearing and centre of mass	a	72	mm
Distance between bearing and centre of mass	b	72	mm
Elastic connection approximated stiffness	k_s	$240e3$	N m^{-1}
Elastic connection approximated damping	c_s	510	N s m^{-1}

strength limits. For this application the maximum speed is limited to 20000 rpm for safety reasons.

Within these constraints, the electric motor used to drive to rotor was designed exclusively for this application. The axial flux configuration was chosen for its reduced axial dimension and reduced introduction of lateral forces that can disturb the dynamic operation. The designed motor is an ironless, dual stator, permanent magnet motor. During the design phase the possibility of using it as an axial self-bearing motor to provide axial levitation was also considered. The design of the motor will not be addressed any further here, but it's important to notice that the inertia properties of the motor disc were taken into account during the design of the electrodynamic suspension and stabilization system.

The test rig is composed of three main parts: (a) the structure, (b) the magnetic circuit that forms the stator of the electrodynamic bearing and (c) the rotating shaft. In Fig. 7.27 the main components of the system are identified, and an overview of the final structure can be obtained looking at the isometric section on Fig. 7.28.

Each part contains a different number of subsystems. The structural part is composed by four stainless steel columns clamped to three aluminium layers (6) (one central and two end plates) that ensure a stiff construction. The connection of this structure to a seismic base is done by means of two steel profiles (7). One structural part dedicated to the housing of radial position probes is screwed to each of the two end plates (5). The two housing of the position probes serve also as support for the movable housings (4) of the two ball bearings that allow supporting the shaft during the acceleration phase.

The stator of the electrodynamic bearing (2) contains four NdFeB N42 permanent magnets oriented in attraction. The magnetic circuit closure is done using two plates of soft iron that are kept separated by an aluminium structure. This part is connected to the test rig's structure using a viscoelastic element (3), whose design is described in Sec. 7.2.

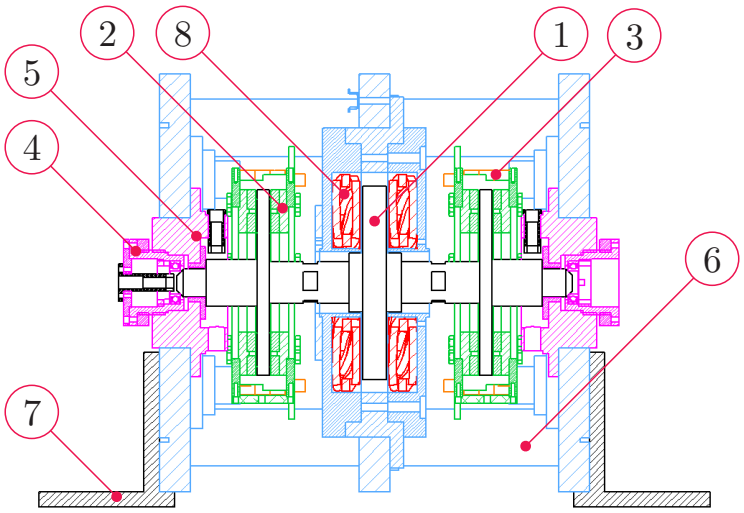

Figure 7.27. Cross section of the test rig model.

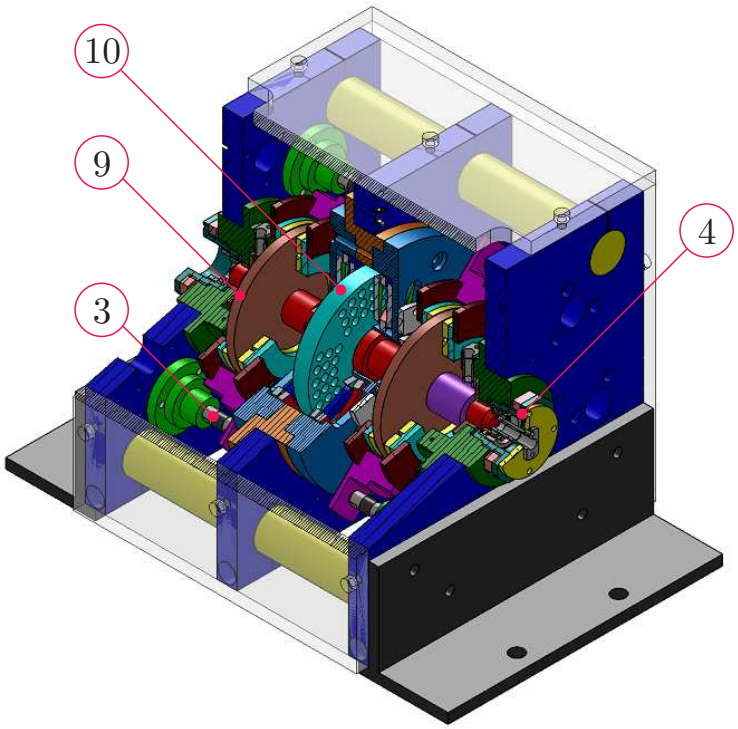

Figure 7.28. Isometric section of the test rig model.

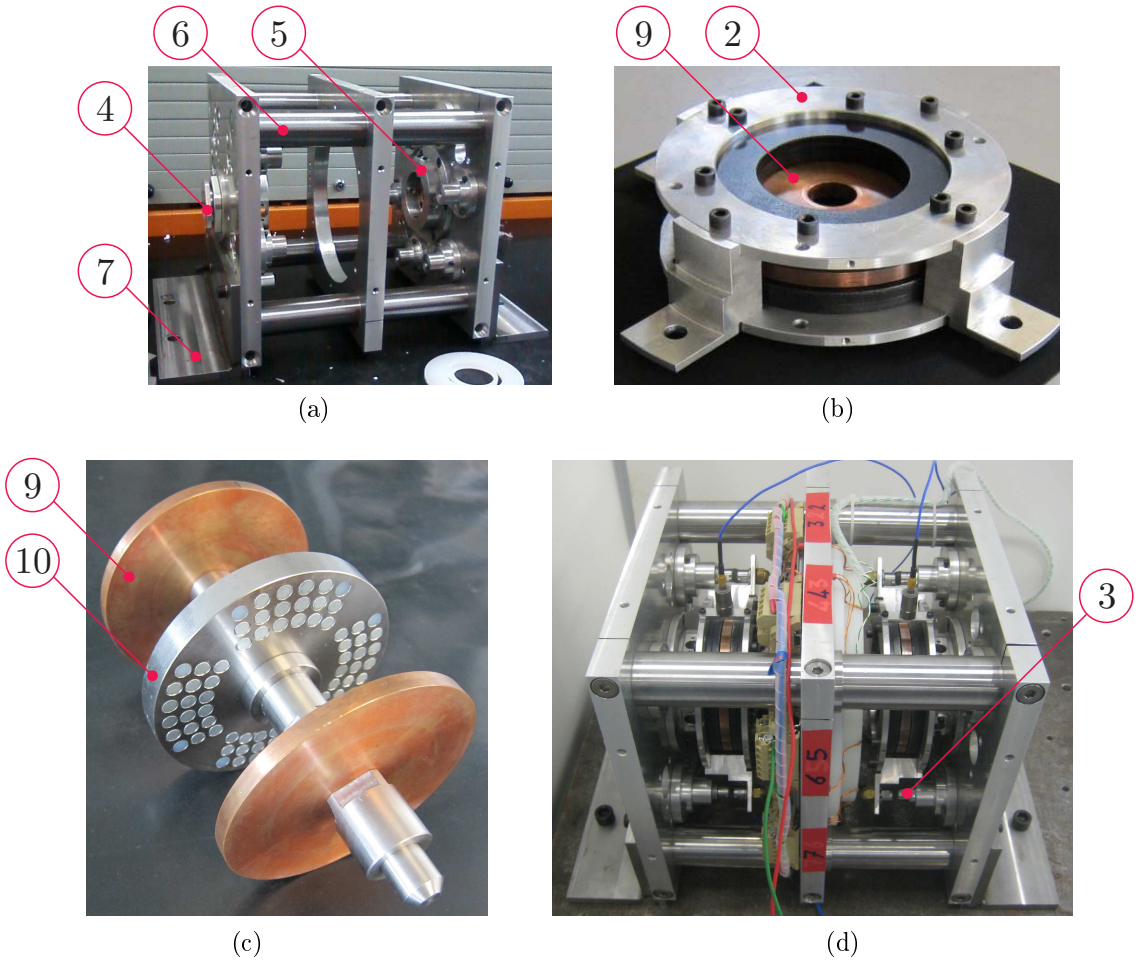

Figure 7.29. Picture of subsystems composing the test rig. a) Outer structure, b) electrodynamic bearing, c) rotor, and d) assembled test rig.

The rotating parts (1) of the test rig contain a stainless steel shaft to which are attached the copper discs of the electrodynamic bearings (9) and the disc of the motor (10).

Another important part for the working of the test rig is the stator of the electric motor (8). In this part are located the coils of the motor together with three Hall effect sensors used to control the commutations of the phase currents.

The main parts of the real system are shown singularly in Figs. 7.29a, 7.29b and 7.29c, and the assembled test rig is presented in Fig. 7.29d. The bullets indicate the number of the part with respect to the description given above.

Chapter 8

Conclusions

This dissertation presented the analysis of electrodynamic suspensions for high speed rotors. A study of the electromechanical interactions generated between rotor and bearing is presented being strongly based on previous works of a number of researchers. The work was designed to be a step towards the final goal of demonstrating the feasibility of radial electrodynamic bearings as contactless supports for high rotational speed applications. The main aspects covered in the work were:

1. A relatively wide bibliographic review is carried out aiming to cover the majority of journal and conference papers, doctoral and master theses, and technical reports available.

2. A general electromechanical model of electrodynamic bearings is derived from the analytical solution of the magnetic field in the air surrounding the rotating conductor.

3. The bearing's model is validated with experimental results obtained under quasi stationary conditions.

4. A study of the dynamics of rotors on electrodynamic bearings is conducted devoting special attention to the study of stability.

5. The design of a prototype of an electric spindle on full electrodynamic radial suspension is presented addressing many of the problems arising during the design phase.

The main findings obtained with the research conducted on electrodynamic bearings and that were presented in this dissertation are summarized as:

1. The unification of the modelling of electrodynamic bearings that allows analysing the differences and similarities between homopolar and heteropolar electrodynamic bearings.

2. The demonstration of the intrinsic filtering capabilities of homopolar electrodynamic bearings, evidencing the notch filter effect for vibrations introduced by rotor's unbalance.

3. The demonstration of the occurrence of instability on rotors supported by EDBs due to the conical rotor mode.

4. A stabilization method for the unstable conical mode relying on gyroscopic effect is identified and described.

The technology of electrodynamic levitation of rotors is still some steps away from the industrial application because the damping technologies available are still very difficult to be dealt with. In order to keep the research on this field in the direction of industrialization of the technology it is necessary to improve the accuracy of the modelling of the viscoelastic elements used to stabilize the rotordynamics. Otherwise it is necessary to use an alternative approach that can be modelled using simpler methods. Considering one of the main contributions of this work, that is the presentation of how the design of the suspension can be approached, it is necessary to confirm the correctness of the approach by performing experimental verification. To verify the validity of the design approach it is necessary to test every step done in the design phase of rotor, electrodynamic suspension, and stabilization system. This work would require the following activities:

1. Performing an experimental modal analysis of the rotor.

2. Measuring the EDB's properties using the procedure presented in this dissertation.

3. Measuring the vibrating response of the EDB's stator with constrained rotor at different values of spin speed of the rotor to verify the modelling of the viscoelastic stabilizing element.

The research requires following these steps before stable radial suspension provided by electrodynamic bearings can be demonstrated, but the way for this technology is wide open and to the current level of knowledge the possibilities for it in industrial applications are very encouraging.

Bibliography

[1] P. A. Basore. Passive stabilization of flywheel magnetic bearings. Master's thesis, Massachusetts Institute of Technology, 1980.

[2] J. L. Nikolajsen. Experimental investigation of an eddy current bearing. In *Proceedings of the 1st International Symposium on Magnetic Bearings*, Zurich, Switzerland, June 1988.

[3] J. L. Nikolajsen. A magnetic bearing based on eddy current repulsion. In *Proceedings of the 4th Workshop on Rotordynamic Instability Problems in High Performance Turbomachinery*, Texas A&M University, USA, June 1986.

[4] L. Ting and J. Tichy. Stiffness and damping of an eddy current magnetic bearing. *ASME Journal of Tribology*, 114:600 – 605, 1992.

[5] J. L. Nikolajsen. An ac electromagnetic bearing for flywheel energy storage in space. In *NASA Langley Research Center Magnetic Suspension Technology Workshop*, Hampton, Virginia, USA, January 1993.

[6] K. A. Connor and J. A. Tichy. Analysis of an eddy current journal bearing. *ASME Journal of Tribology*, 110:320 – 326, 1988.

[7] J. A. Tichy and K. A. Connor. Geometric effects on eddy current bearing performance. *ASME Journal of Tribology*, 111:209 – 214, 1989.

[8] M. Simone and J. Tichy. Forces due to a magnetic dipole near a sliding conductor: applications to magnetic levitation and bearings. *ASME Journal of Tribology*, 116:720 – 725, 1994.

[9] R. Y. Siegwart, P. Buhler, and D. Baumann. Eddy current bearings for microstructure levitation. In *Proceedings of the 4th International Symposium on Magnetic Bearings*, pages 359 – 363, Zurich, Switzerland, August 1994.

[10] R. F Post, D. D. Ryutov, J. R. Smith, and L. S. Tung. Research on ambient-temperature passive magnetic bearings at the lawrence livermore national laboratory. In *Proceedings of the MAG' 97 Industrial Conference and Exhibition on Magnetic Bearings*, August 1997.

[11] R. F. Post and D. D. Ryutov. Ambient-temperature passive magnetic bearings: Theory and design equations. In *Proceedings of the 6th International Symposium on Magnetic Bearings*, Cambrige, Massachusetts, USA, August 1998.

[12] R. F. Post. Stability issues in ambient-temperature passive magnetic bearing systems. *NASA STI/Recon Technical Report N*, 3, February 2000.

[13] D. C. Karnopp, D. L. Margolis, and R. C. Rosenberg. *System dynamics: modeling and simulation of mechatronic systems*. John Wiley & Sons, 2000.

[14] R. F. Post and D. A. Bender. Ambient-temperature passive magnetic bearings for flywheel energy storage systems. In *Proceedings of the 7th International Symposium on Magnetic Bearings*, Zurich, Switzerland, August 2000.

[15] D. J. Eichenberg, C. A. Gallo, and W. K. Thompson. Development and testing of a radial halbach array magnetic bearing. Technical Report NASA/TM 2006-214447, NASA - Glenn Research Center, Cleveland, Ohio, USA, 2006.

[16] C. Murakami and I. Satoh. Experiments of a very simple radial-passive bearing based on eddy currents. In *Proceedings of the 7th International Symposium on Magnetic Bearings*, pages 141 – 146, Zurich, Switzerland, August 2000.

[17] J. L. Bermudez, S. Zanolli, J. Sandtner, H. Bleuler, and C. Benabderrahmane. Preliminary experiments on an eddy currents bearing. In *Proceedings of the 7th International Symposium on Magnetic Bearings*, pages 135 – 139, Zurich, Switzerland, August 2000.

[18] A. V. Filatov and E. H. Maslen. Passive magnetic bearing for flywheel energy storage systems. *IEEE Transactions on Magnetics*, 37(6), 2001.

[19] A. V. Filatov. *"Null-E" Magnetic Bearings*. PhD thesis, University of Virginia, 2002.

[20] A. V. Filatov and E. H. Maslen. High speed, high efficiency magnetic bearings. In *Proceedings of the 6th International Symposium on Magnetic Suspension Technology*, pages 58–63, 2001.

[21] A. V. Filatov, E. H. Maslen, and G. T. Gilles. A method of noncontact suspension of rotating bodies using electromagnetic forces. *Journal of Applied Physics*, 91(4), 2002.

[22] A. V. Filatov, E. H. Maslen, and G. T. Gillies. Stability of an electrodynamic suspension. *Journal of Applied Physics*, 92(6), 2002.

[23] K. Davey, A. V. Filatov, and R. Thompson. Design and analysis of passive homopolar null flux bearings. *IEEE Transactions on Magnetics*, 41(3), 2005.

[24] A. V. Filatov, P. McMullen, K. Davey, and R. Thompson. Flywheel energy storage system with homopolar electrodynamic magnetic bearing. In *Proceedings of the 10th International Symposium on Magnetic Bearings*, 2006.

[25] V. Kluyskens, B. Dehez, and H. Ben Ahmed. Dynamical electromechanical model for magnetic bearings. *IEEE Transactions on Magnetics*, 43(7), 2007.

[26] V. Kluyskens and B. Dehez. Parameterized electromechanical model for magnetic bearings with induced currents. *Journal of System Design and Dynamics*, 3(4), 2009.

[27] V. Kluyskens and B. Dehez. Comparison between models predicting the evolution of the electrical impedance with frequency. *International Journal of Circuit Theory and Applications*, 39(9):973 – 982, 2011.

[28] N. Amati, X. De Lepine, and A. Tonoli. Modeling of electrodynamic bearings. *ASME Journal of Vibration and Acoustics*, 130, 2008.

[29] A. Tonoli, N. Amati, F. Impinna, and J. G. Detoni. A solution for the stabilization of electrodynamic bearings: Modeling and experimental validation. *ASME Journal of Vibration and Acoustics*, 133, 2011.

[30] T. A. Lembke. *Design and analysis of a novel low loss homopolar electrodynamic bearing*. PhD thesis, Royal Institute of Technology, Stockholm, Sweden, 2005.

[31] V. Kluyskens and B. Dehez. Computation of the forces acting on a magnetic bearing due to eddy currents. In *Proceedings of the COMSOL Users Conference*, Grenoble, France, 2007.

[32] S. Iskierka. Analysis of an induction bearing by the finite element method. *Archiv fur Elektrotechnik*, 6:375 – 380, 1984.

[33] T. A. Lembke. 3d-fem analysis of a low loss homopolar induction bearing. In *Proceedings of the 9th International Symposium on Magnetic Bearings*, August 2004.

[34] G. Genta, X. De Lepine, F. Impinna, J. G. Detoni, N. Amati, and A. Tonoli. Sensitivity analysis of the design parameters in electrodynamic bearings. In *IUTAM Symposium on Emerging Trends in Rotor Dynamics*, pages 287 – 296, New Delhi, India, 2009.

[35] N. Amati, A. Tonoli, E. Zenerino, J. G. Detoni, and F. Impinna. Design methodology of electrodynamic bearings. In *Proceedings of the XXXVIII National Meeting of the Italian Society of Mechanical Engineers (AIAS)*, Torino, Italy, 2009.

[36] D. Albertz, G. Arians, and G. Hennenberger. Comparison between transient and quasi-stationary calculations of eddy current field problems with moving conductors. *COMPEL: The International Journal for Computation and Mathematics in Electrical and Electronic Engineering*, 19(2), 2000.

[37] D. Rodger, H. C. Lai, and P.J. Leonard. A comparison of finite-element models for 3d rotating conductors. *IEEE Transactions on Magnetics*, 38(2), 2002.

[38] J. R. Powell and G. R. Danby. High speed transport by magnetically suspended trains. In *ASME Publ. 66 WA/RR5*, December 1966.

[39] K. R. Davey and T. Morris. Passive null-flux coil magnetic bearing system for translation or rotation. US. Patent 5 481 146, January 2 1996.

[40] J. Sandtner and H. Bleuler. Electrodynamic passive magnetic bearings with planar halbach arrays. In *Proceedings of the 9th International Symposium on Magnetic Bearings*, August 2004.

[41] J. Sandtner and H. Bleuler. Passive electrodynamic magnetic thrust bearing especially designed for constant speed applications. In *Proceedings of the 10th International Symposium on Magnetic Bearings*, pages 483 – 487, Martigny, Switzerland, August 2006.

[42] D. J. Eichenberg, C. A. Gallo, and W. K. Thompson. Development and testing of an axial halbach array magnetic bearing. Technical report, NASA - Glenn Research Center, Cleveland, Ohio, USA, 2006.

[43] W. K. Thompson. Three dimensional field solutions for multi-pole cylindrical halbach arrays in an axial orientation. Technical Report NASA/TM 2006-214359, NASA - Glenn Research Center, Cleveland, Ohio, USA, 2006.

[44] M. Storm. The application of electrodynamic levitation in magnetic bearings. Master's thesis, North-West University, Potchefstroom, South Africa, 2006.

[45] A. Tonoli, N. Amati, F. Impinna, J. G. Detoni, H. Bleuler, and J. Sandtner. Dynamic modeling and experimental validation of axial electrodynamic bearings. In *Proceedings of the 12th International Symposium on Magnetic Bearings*, pages 68 – 80, Wuhan, China, August 2010.

[46] F. Impinna, J. G. Detoni, N. Amati, and A. Tonoli. Passive magnetic levitation of rotors on axial electrodynamic bearings. Submitted to Journal of Sound and Vibration, January 2012.

[47] G. Genta. *Dynamics of Rotating Systems*. Springer, New York, 2005.

[48] A. Tonoli. Dynamic characteristics of eddy current dampers and couplers. *Elsevier Journal of Sound and Vibration*, 301, 2007.

[49] D. J. Griffiths and R. College. *Introduction to Electrodynamics*. Prentice Hall, New Jersey, 1999.

[50] A. Tonoli and N. Amati. Dynamic modeling and experimental validation of eddy current dampers and couplers. *ASME Journal of Vibration and Acoustics*, 130, 2008.

[51] A. Canova and B. Vusini. Design of axial eddy-current couplers. *IEEE Transactions on Industry Applications*, 39(3), 2003.

[52] R. C. Dorf and R. H Bishop. *Modern Control Systems*. Prentice Hall, 2010.

[53] R. Herzog, P. Buhler, C. Gahler, and R. Larsonneur. Unbalance compensation using generalized notch filters in the multivariable feedback. *IEEE Transactions on Control Systems Technolocy*, 4(5), 1996.

[54] R. Markert, N. Skircka, and X. Zhang. Unbalance compensation on flexible rotors by magnetic bearings using transfer functions. In *Proceedings of the 8th International Symposium on Magnetic Bearings*, Mito, Japan, August 2002.

[55] G. Genta, C. Delprete, and D. Rondano. Gyroscopic stabilization of passive magnetic levitation. *Meccanica*, 34:411–424, 1999.

[56] A. Bondeson, T. Rylander, and P. Ingelstrom. *Computational electromagnetics*. Springer, 2005.

List of Figures

List of Tables